Crystal engineering of mixed-ligand metal-organic frameworks based on simple carboxylate and bipyridyl ligands

UNIVERSITÀ DI PARMA

MSc Student: Marcello Mutti

Supervisor: Dr. Clive Oliver

Co-Supervisor: Prof. Paolo Pelagatti

University of Cape Town

University of Parma

Academic Year 2016/2017

Acknowledgements

First of all, I would like to thank my supervisor, Dr Clive Oliver for his supervision, direction and teaching. I'm grateful to him for having followed me during all this project and for making me a better chemist. A special thanks to my co-supervisor Professor Paolo Pelagatti for his support and encouragement.

I would like to thank all the members of the Centre for Supramolecular Chemistry Research group for all the advice and friendship given to me during this six months. In particular, Dr Nabanita Chatterjee for constantly helping and supporting me.

A special thanks to Mrs. Deirdre Brooks for her fundamental help in all the bureaucratic issues.

Many thanks to all my friends, old and new, with a mention to the other Italian guys that shared with me this experience.

Last but not least I would like to thank my parents for their continuous support.

Abbreviations:

- 1D = one dimensional
- 2D = two dimensional
- 3D = three dimensional
- ASU = asymmetric unit
- 3NDC/nipa = 5-nitro-1,3-benzenedicarboxylic acid / 5-nitroisophthalic acid
- BET = Brunauer-Emmett-Teller
- bipy = 4,4'-bipyridine
- CCDC = Cambridge Crystallographic Data Centre
- CP = coordination polymer(s)
- CSD = Cambridge Structural Database
- DMA = dimethylacetamide
- DMF = dimethylformamide
- DPBD = 2,3-Di(4-pyridyl)-2,3-butanediol
- DSC = differential scanning calorimetry
- H_3BTC/TMA = 1,3,5-benzenetricarboxylic acid/trimesic acid
- HSM = hot stage microscopy
- MEG = monoethylene glycol
- MOF = metal-organic framework
- PXRD = powder X-ray diffraction
- RT = room temperature
- SBU = secondary building unit
- SCXRD = single crystal X-ray diffraction
- SOF = site occupancy factor
- TGA = thermogravimetric analysis
- VT-PXRD = variable-temperature powder X-ray diffraction

Abstract

Over the last few decades research in supramolecular chemistry and crystal engineering have seen an exponential growth. The synthesis of metal-organic frameworks (MOFs) has attracted much interest worldwide due to the possibility of obtaining a large variety of structures with a wide range of applications in fields pertaining to storage, separation and catalysis. This work focuses on the crystal engineering of MOFs based on mixed ligands which may ultimately be used in the gas storage of pollutants, greenhouse gases or fuel.

Two novel 2D mixed-ligand MOFs, both based on manganese, 4,4'-bipyridine and 1,3,5-benzenetricarboxylic acid, have been prepared and fully characterized. The employment of dimethylformamide or dimethylacetamide, as the solvent, results in two isostructural MOFs. Another novel MOF, similar in structure to the previous two, with 5-nitroisophthalic acid instead of 1,3,5-benzenetricarboxylic acid has been also prepared and characterized. This MOF has the same metal and ligand combination as, and is largely isostructural to, a literature example, but differs in method of preparation and solvent content. These Mn-based MOFs have potential voids in the structure making them candidates for gas sorption experiments.

A novel 2D mixed-ligand MOF based on cobalt, 4,4'-bipyridine and 5-nitroisophthalic acid has been synthesized and fully characterized. Its structure is the same as that of another MOF, based on manganese, present in this work and like its manganese analogue it exhibits potential void spaces in the framework that make it a candidate for gas sorption experiments.

Finally, a novel 2D MOF based on 1,3,5-benzenetricarboxylic acid and cadmium bromide has been synthesized and fully characterized. Dehydration and rehydration studies performed by combining powder X-ray diffraction with thermogravimetric analysis show that it can lose coordinated water, that comes from the reaction solvent, upon heating, and reabsorb water from the atmosphere, ultimately regaining its original structure.

All MOFs were synthesized via the solvothermal method and characterized with X-ray diffraction (single crystal and powder) and thermal analyses (hot stage microscopy, differential scanning calorimetry and thermogravimetric analysis).

Table of Contents

Chapter 1: Introduction

Chapter 2: Experimental

Chapter 3: Manganese and Cobalt Mixed-Ligand Metal-Organic Frameworks

Chapter 4: Cadmium Coordination Polymer

Chapter 5: Conclusion

Chapter 1: Introduction

This chapter introduces the most important topics and terms related to the field of metal-organic frameworks (MOFs), e.g. supramolecular chemistry, crystal engineering and coordination polymers. Special attention is also given to porosity, mixed-ligand design and to water vapour and gas sorption applications.

1.1 Supramolecular chemistry

Until 50 years ago chemistry, in particular organic chemistry, was largely a molecule-centric subject because molecules were considered to be the ultimate determinants of all significant properties of substances. Since 1948, the year in which H.M. Powell described hydroquinone clathrates, the interest in supramolecular structures has grown and today supramolecular chemistry is one of the major themes in chemical research. Supramolecular chemistry, coined by Jean-Marie Lehn in his Nobel prize lecture in which he also described it as "chemistry beyond the molecule",[1] is focused on the intermolecular bonds such as van der Waals interactions and hydrogen bonds, which are considerably weaker than covalent intramolecular bonds. An important principle of this kind of chemistry is the mutual recognition of molecules that leads to self-assembly. In supramolecular chemistry the whole is greater than the sum of its parts, so the properties of an assembly or collection of molecules are more than the sum of the properties of its constituent molecules.[1,2]

1.2 Crystal engineering

G.R Desiraju stated that: "Crystal engineering is concerned with the understanding of intermolecular interactions in crystal packing and applying this understanding in the design of solids characterized by specific, and desired, physical and chemical properties".[3] The term crystal engineering was first used in 1955 by R. Pepinsky in a meeting abstract of the American Physical Society (*Phys. Rev.*,1955, **100**, 952) but is usually associated with the work of G. M. J. Schmidt[4] and A. I. Kitaigorodskii.[5] A first rigorous definition of molecular crystal was given by A. I. Kitaigorodskii, where he stated that, "within a molecular crystal, it is possible to identify groups of atoms such that for every atom in a group, at least one interatomic distance within this group is significantly shorter than the smallest interatomic distance to an atom in another group".[5] This definition, even if suitable, is purely based on

geometry and cannot be considered a “chemical” definition. A chemical definition of molecular crystals should be based on bond energies, ”If the energies of covalent bonds, the interactions that hold atoms together in molecules, are in the range of 75-125 kcal mol^{-1}, the energies that hold molecules together in molecular crystals are much less, by more than an order of magnitude”.[2] The aim of crystal engineering is to produce crystals, constructed molecule by molecule, with specific functions. R. Feynmann stated that no fundamental laws of physics are violated if a molecule is assembled atom by atom, thus in an analogous manner no physical laws are violated if supramolecular entities are constructed molecule by molecule. Many molecular crystals are organic solids and, thus in its infancy crystal engineering focused on crystals of organic compounds. However, in the last few decades many materials constructed of both metal and organic components appeared in the field of crystal engineering.[2]

1.3 Coordination Polymers (CPs)

The term “coordination polymer” refers to the class of compounds that consist of coordination bonds which build an infinite, polymeric structure in at least one direction. It was first used in the scientific literature in 1916 but without a single crystal structure it was not possible to unequivocally demonstrate that the coordination was infinite. In 1893, Werner suggested that a coordination compound consists of a central metal ion surrounded by an array of molecules or anions called ligands, or complexing agents. Typical coordination compounds are discrete units, or 0-dimensional, with all ligands coordinated at the same metal ion. In coordination polymers ligands are polytopic, i.e. the ligands bridge different metal centres giving rise to an infinite array in which the coordinated units are repeated. Coordination polymers perfectly fit Kitaigoroskii’s definition of molecular crystals, as they are an infinite repetition of a defined group of atoms, and present many properties that chemists can tune, which justifies their inclusion in the subject of crystal engineering.

1.4 Metal-Organic Crystal Engineering

Coordination polymers arise from solid state, inorganic and coordination chemistry, therefore knowledge gained from all of these fields has been successfully applied in this interdisciplinary subject. A.F. Wells simplified the topological description of crystal structures of inorganic compounds by reducing them to a collection of nodes of a defined geometry, connected to each other by node connections (also called linkers or rods)[6]. From this arose the idea of network structures, which can be 1D, 2D or 3D. R. Robson,[7,8] extended this idea to coordination compounds, where polycoordinated metal ions with polydentate ligands build up polymeric structures in which the inorganic vertices act as nodes while the organic linkers represent the node connections. The metal-ligand bond strengths are approximately 40-120 kcal mol^{-1},[9] which are strong enough to give structural stabilization, whilst being weak enough to be easily broken under ambient conditions in solution. This allows for self-correction of the self-assembly process during crystallization. In 1995, Yaghi et al. proposed that ions located in open pores of coordination polymers could be exchanged once the solvent of crystallization was removed. Compounds with these characteristics were called metal-organic frameworks (MOFs).[10] Yaghi et al. demonstrated this for a 3D interpenetrated, cationic MOF, prepared *via* hydrothermal synthesis, with the starting materials being 4,4'-bipyridine (bpy) and copper(II) nitrate, the final compound having the formula $[Cu(4,4'\text{-}bpy)_{1.5}\cdot(NO_3)(H_2O)_{1.5}]$.[10] Ligands such as bpy impart flexibility to the resulting MOFs but is not strongly coordinated. In order to increase the structural strength of MOFs, Yaghi et al., from 1998, focussed on the use of ligands with carboxylate functionality.[11,12,13] This yielded a tremendous boost to research aimed at producing porous MOFs which are stable enough to be successfully used in various applications.[10,14]

CPs have been defined by Rowsell and Yaghi as extended connections of metal-ligand monomers through coordination bonds.[15] A solid eligible to be classified as a MOF should possess certain characteristics such as a geometrically well-defined structure and strong bonding that provide robustness with linking units that could be modified by organic synthesis. It is clear that accepting this definition excludes all systems based on bipyridyl ligands. This definition was contradicted in the same publication in which it was proposed when the authors distinguished between pyridyl-based and carboxylate-based MOFs, marking them as two individual groups but both under the MOF family. This exemplifies the ambiguity in MOF terminology at the time.[15] O'Keeffe proposed a distinction between CPs

and MOFs based on coordination bond strength, suggesting that these are weaker in CPs than in MOFs. The most recent, accepted definitions of coordination polymers and metal-organic frameworks, respectively, follow the IUPAC recommendations which refers to a CP as, “A coordination compound with repeating coordination entities extending in 1, 2 or 3 dimensions” and states that “A metal-organic framework, abbreviated to MOF, is a coordination network with organic ligands containing potential voids”.[16] According to these definitions, this dissertation will present four MOFs and one CP.

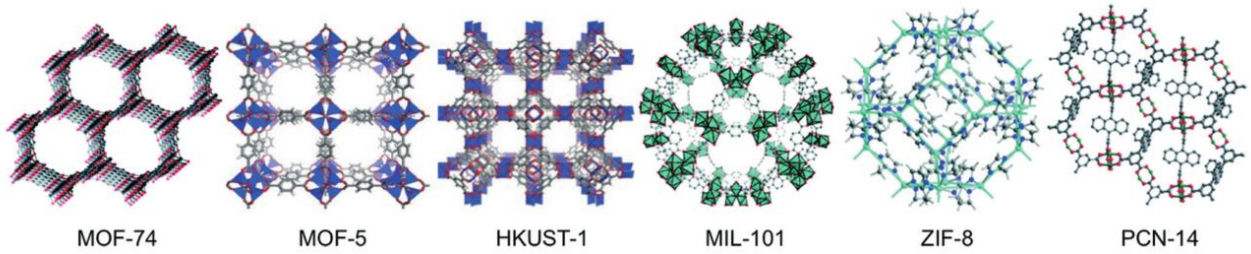

Figure 1.1 Crystal structures of common MOFs published in the CSD database[17] Reproduced from Ref.18 with permission of The Royal Society of Chemistry

1.5 Metal-Organic Framework Synthesis

The term “design” is often associated with MOF synthesis. M. O’Keeffe presented an interesting personal view,[18] even if the rigorous definition of design, which implies “to create, fashion, execute or construct according to plan” (Webster Dictionary) is generally not applicable to MOF synthesis.[19] O’Keeffe stated that it is appropriate to associate the term to the experiment itself as it can be “designed” to produce materials with desired characteristics. The aim of most researchers involved in MOF synthesis is to establish the conditions that lead to defined structures without decomposition of the organic linkers. Several synthetic strategies based on the “node-and-spacer” or “secondary building unit” (SBU) approaches have been successfully developed. Both approaches start from the idea that molecular precursors can be conceptualized as abstract objects such as points, lines, etc. making CPs and MOFs nothing more than periodic and complementary assemblies of geometric motifs.[20] The “node-and-spacer” approach allows many complicated crystal lattices to be simplified by grouping parts of the structure as node or spacer (rod) sets, i.e. points connected by lines.[20,21,22] Nodes correspond to points in the structure where the

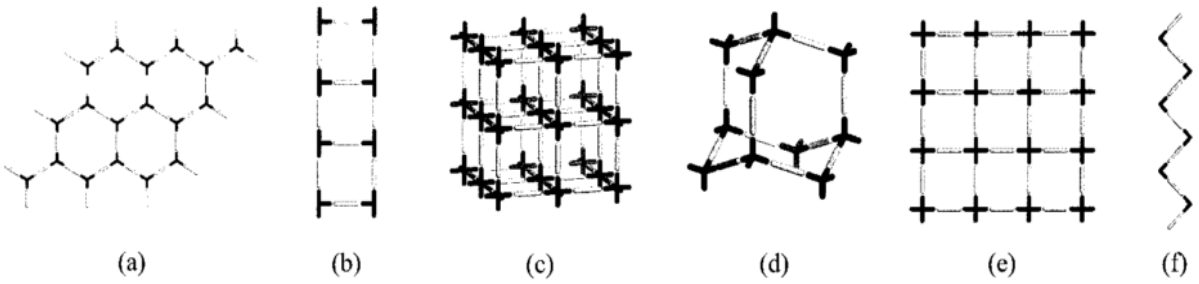

Figure 1.2 Schematic representation of a few simple network architectures of MOFs structurally characterized by nodes and rods: (a) 2D Honeycomb, (b) 1D Ladder, (c) 3D Octahedral, (d) 3D Hexagonal Diamondoid, (e) 2D Square Grid, and (f) 1D Zigzag Chain[23] Reprinted (adapted) with permission from (B. Moulton and M. J. Zaworotko, Chem. Rev., 2001, **101**, 1629–1658). Copyright (2001) American Chemical Society

polymeric connectivity is repeated or changes direction. In this regard, nodes can be placed at metal ions (or at the centroids of metal ion clusters), as well as at centroids of the organic ligands where their functional groups indicate a change in direction of ligation. For example, in terms of the latter, a node would not be placed at the centroid of a linear ligand such as 1,4-benzenedicarboxylate but would be placed at the centroid of a trigonal ligand such as 1,3,5-benzenetricarboxylate. Rods represent the linkages between the nodes and are often aligned with the axis of a ligand. Figure 1.2 presents a few simple architectures that can be produced using commonly available metal ions and organic linkers. Voids are often present in these kinds of networks as an intrinsic characteristic of their architectures.[23]

Yaghi et al. introduced the “secondary-building-unit” approach where MOF design can be rationalized in terms of isolating directional metal-oxygen-carbon clusters in the structure and treating these as SBUs from which the structure is constructed (Figures 1.3 and 1.5). Since the carbon and oxygen atoms belong to the organic component but are also defined as part of the SBU the rational design aspect of this approach was that the rest of the organic ligand can be varied. This leads to structures with varying distances between the SBUs (and thus effecting pore size) but with the same network topology. Yaghi et al. demonstrated the success of this approach for many structures, with MOF-2 and MOF-5 being amongst the first examples.[10,14]

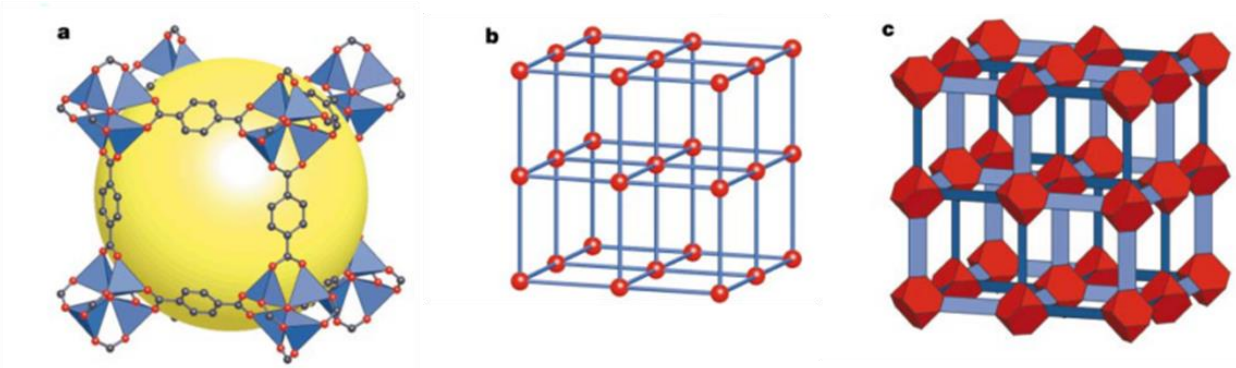

Figure 1.3 The MOF-5 structure and its topology. a, The MOF-5 structure shown as ZnO_4 tetrahedra (blue polyhedra) joined by benzene dicarboxylate linkers (O, red and C, black) to give an extended 3D cubic framework with interconnected pores of 8 Å aperture width and 12 Å pore (yellow sphere) diameter. (Yellow sphere represents the largest sphere that can occupy the pores without coming within the van der Waals size of the framework). b, The topology of the structure (primitive cubic net) shown as a ball-and-stick model. c, The structure shown as the envelopes of the $(OZn_4)O_{12}$ cluster (red truncated tetrahedron) and benzene dicarboxylate (bdc) ion (blue slat). Note that opposing slats are all at 90° [14]

In attempts to speed-up the discovery of new MOFs, high-throughput methods have been borrowed from pharmaceutical research (Figure 1.4). The number of synthetic methods has increased vastly, leading to the possibility that many different MOFs can be produced from the same starting materials. However, despite the introduction of these much newer techniques such as microwave-assisted heating, mechano- and sonochemistry, the more traditional method of solvothermal synthesis is still responsible for most of the new MOFs produced today. One of the most accepted definitions for solvothermal reactions was given by Rabenau who defined these as, “reactions that take place in closed vessels under autogenous pressure above the boiling point of the solvent”.[24] Mechanochemistry, where the starting materials are physically ground together, has long since been known and used in a wide range of fields, especially in inorganic and pharmaceutical chemistry. Recently, this technique has seen an incredible growth in MOF synthesis. It provides a fast and efficient method, which, with minimal solvent (as in liquid-assisted grinding, LAG) or in its absence, can produce products which are not necessarily accessible via the solvothermal method. Braga and Friščić have conducted extensive research in this field which has been classified as one of four sub-disciplines of chemistry alongside thermochemistry, electrochemistry and photochemistry.[25,26]

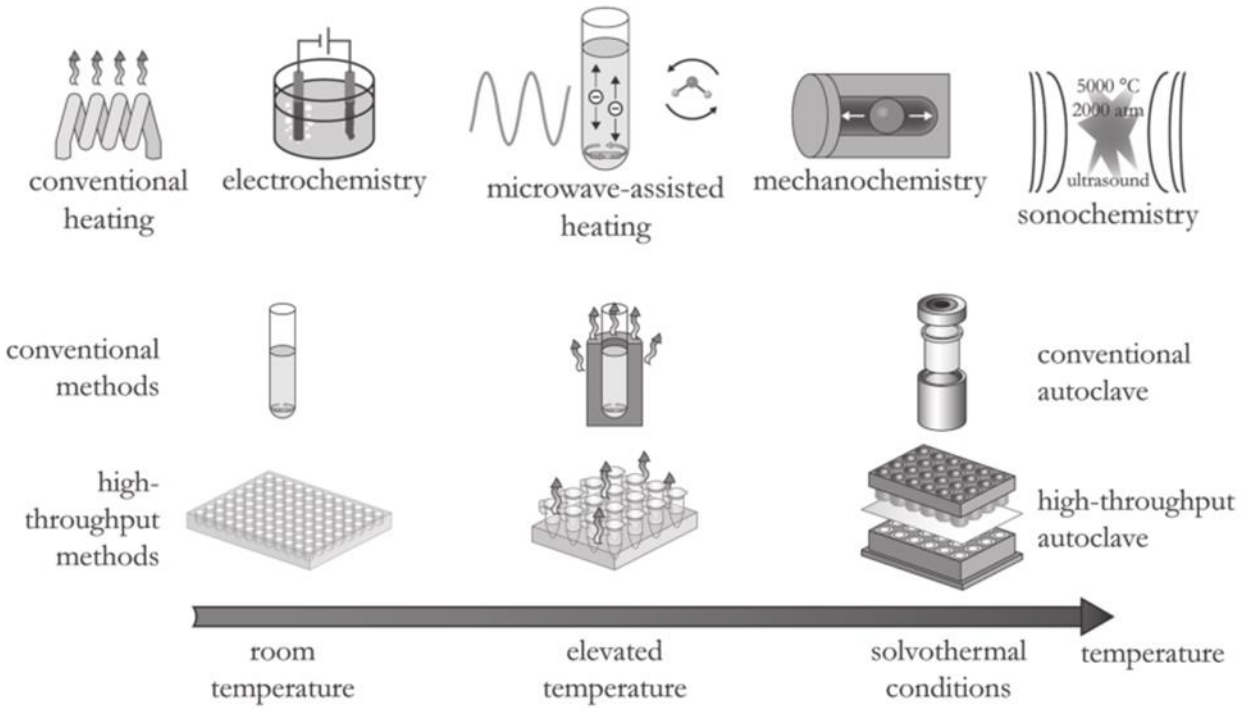

Figure 1.4 Overview of different synthetic methodologies which may be used in MOF synthesis [13]
Adapted from Ref .13 with permission of The Royal Society of Chemistry (RSC) on behalf of the European Society for Photobiology, the European Photochemistry Association and the RSC

1.6 Porosity

Porosity refers to the property where a material's host framework has 'holes' or channels which may be vacant or occupied by suitably-sized molecules.[27] Porosity is the characteristic that distinguishes MOFs from generic coordination polymers which have also, alternatively, been referred to as "porous coordination polymers" or PCPs. The property of porosity is the basis of many MOF applications, from gas storage and heterogeneous catalysis to drug delivery and sensing. The crystal packing features of PCP networks determine whether voids or channels are generated. Kitagawa et al. classified PCPs into three distinct categories depending upon their "kind" of porosity.[28] In the first type, also referred to as first generation or type I, the porosity is crucially dependent on the presence of guest molecules, i.e. the framework structure collapses if the guest is removed. In the second generation, or type II, the framework structure is preserved upon guest removal, thus allowing the cyclic uptake/removal of guest molecules. In the third generation (type III), the frameworks are flexible and dynamic, responding to external stimuli such as the presence of guest molecules, light or electric fields. This allows for the reversible modulation of channel diameters and pore volumes sizes.[2] The most common MOFs are first and second generation with only those belonging to the second and third generations being suitable for

applications related to porosity. Barbour argued that porosity can only be ascribed to a material if it can be demonstrated.[22] In this regard, he introduced the term “virtual porosity” referring to cases where researchers simply delete atoms from the crystal structure and claim porosity based on the resulting voids. Barbour argues that this involves a biased opinion on what may be defined as “guest” entities in the crystal structure without knowledge of whether these entities can diffuse throughout the crystal structure or what their structural roles are. The demonstrated porosity argument is bolstered by his introduction of the term “porosity without pores” which refers to structures where no clear pathways for the exit or entry of guest entities are obvious, yet it has been demonstrated that molecules can exit and enter these materials. This necessitates complex dynamic changes in the host structure in order to allow for movement of these entities.

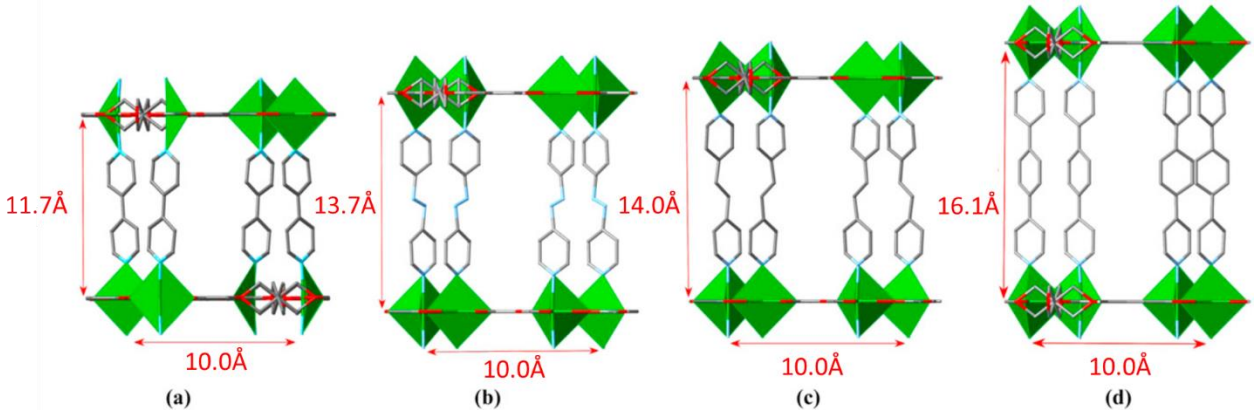

Figure 1.5 Schematic illustration showing the frameworks with different pillars: (a) 4,4’-bipyridine, (b) 4,4’-azopyrdine, (c) 1,2-di(4-pyridyl)ethane, and (d) 2-[4-(4-pyridinyl)phenyl]pyridine [20]. Adapted from M. Du, C. P. Li, C. Sen Liu and S. M. Fang, Design and construction of coordination polymers with mixed-ligand synthetic strategy, *Coord. Chem. Rev.*, 2013, **257**, 1282–1305, with permission from Elsevier

The control of pore sizes in porosity studies of MOFs is a major goal in order to ‘tune’ their uses in different applications. A suitable way to control pore size may be via controlling linker length, this allows tuning of the pore size along a preferential direction (if different ligands are used in the same MOF) as shown in Fig. 1.5 or in all three directions as in Fig.1.6. This possibility is clearly shown by the IRMOF series (Fig 1.6), where IR stand for isoreticular, in which the same SBU is connected by different ligands giving rise to MOFs with the same geometry but different dimension of pore size.[29] However, an increase in linker length, and thus pore size, also increases the chance of interpenetration, i.e. where two or more entangled frameworks exist in the same crystal structure. Interpenetrated structures may have small pores or narrow channels between frameworks, resulting in increased surface areas, and may thus be advantageous in sorption applications of small molecules such as hydrogen.[30]

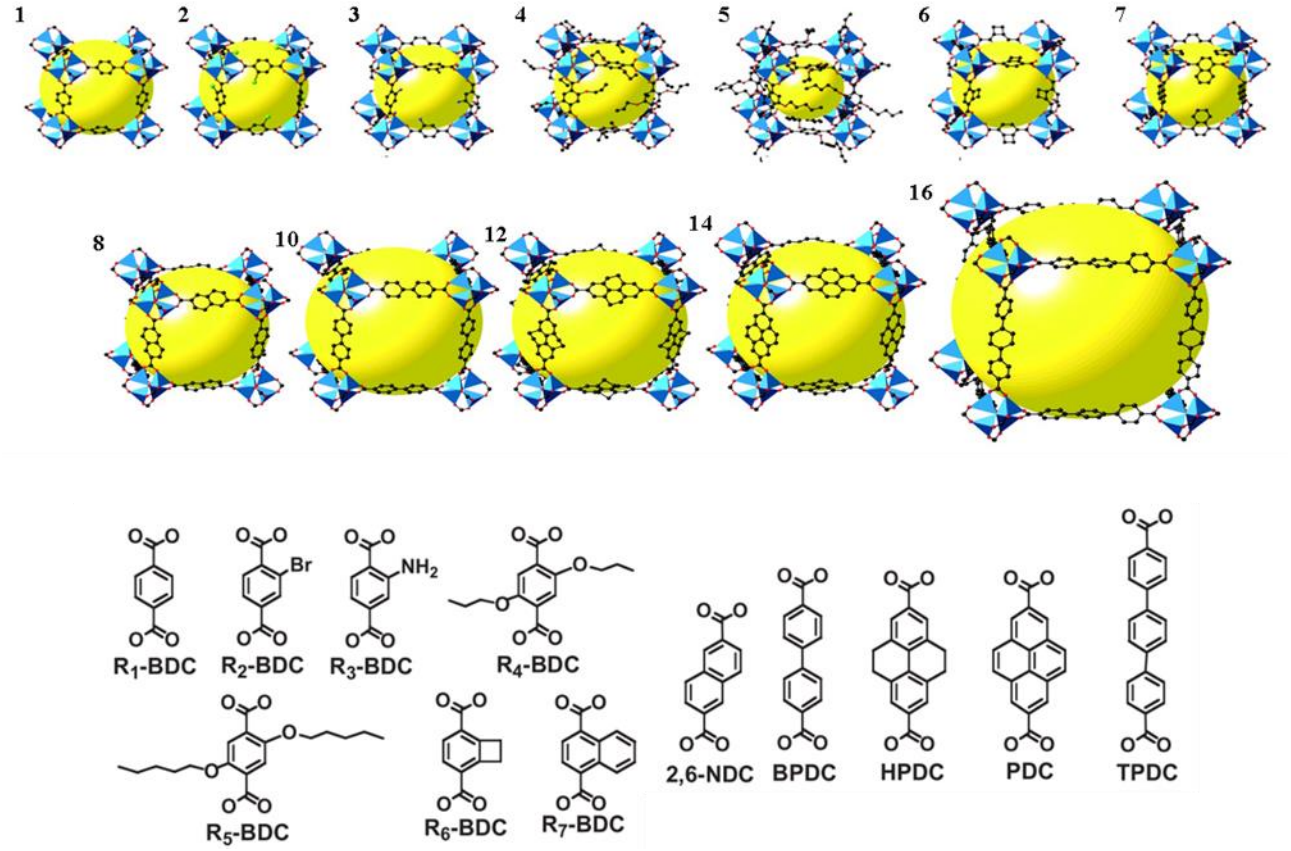

Figure 1.6 Single crystal x-ray structures of IRMOF-n (n = 1 through 7, 8, 10, 12, 14, and 16), labelled respectively. Colour scheme is as follows: Zn (blue polyhedron), O (red spheres), C (black spheres), Br (green spheres in 2), amino-groups (blue spheres in 3). Below is reported the scheme with ligand that connect the SBUs. Ligands R_1 to R_7 are involved in the compound from 1 to 7. The others are associated as follow: 2,6-NDC (2,6-Naphthalenedicarboxylic acid)-IRMOF-8, BPDC (Biphenyl-4,4′-dicarboxylic acid) - IRMOF-10, HPDC (4,5,9,10-tetrahydropyrene-2,7-dicarboxylic acid) – IRMOF-12, PDC (pyrene-2,7-dicarboxylic acid) – IRMOF-14, TPDC (p-Terphenyl-4,4″-dicarboxylic acid) – IRMOF-16. From M. Eddaoudi, J. Kim, N. Rosi, D. Vodak, J. Wachter, M. O. Keeffe, O. M. Yaghi, M. Eddaoudi, J. Kimrn, N. Rosi and O. M. Yaghil, Systematic Design of Pore Size and Functionality in Isoreticular MOFs and Their Application in Methane Storage Published by : American Association for the Advancement of Science Linked references are available on JSTOR for this article : Systematic Design, 2002, **295,** 469–472Reprinted with permission from AAAS

1.7 The Role of the Metal Ion

Metal ions play a key role in MOF structure due to their influence on the geometry of the coordination environment and thus the extended framework structure. The coordination number of transition metals can range from 2 to 7 with oxidation states usually ranging between +1 and +3. These differences give rise to a wide range of possible geometries. MOFs present in this work are based on manganese, cobalt and cadmium which are from groups 7, 9 and 12, respectively, in the periodic table. Group 7 and 9 metals are transition metals; however, group 12 elements do not, strictly-speaking, belong to this class as IUPAC nomenclature states that a transition element is "an element whose atom has a partially filled *d* sub-shell, or which can give rise to a cation with an incomplete *d* sub-shell"[31]. Thus, group 12 elements are considered as post-transition elements.[21] The metals employed in this work are common metals used in MOF synthesis and can be found with different coordination numbers and, consequently coordination geometries, and oxidation states. Manganese and cobalt have nearly equal atomic radii of 127 pm and 125 pm,[32] respectively, and have oxidation states in common. Thus, it is unsurprising that these can give rise to isostructural MOFs when the same or closely-related ligands are employed, as is reported in this dissertation.

1.8 The Role of the Ligand

The choice of ligands, equal to that of metal ions, plays a significant role in MOF design. Adjustments to linker geometry, length, ratio between ligands, and functional groups can tune the size, shape, and internal surface of a MOF for a targeted application.[33] The most common ligands used are pyridine- and carboxylate-based, as shown in Figure 1.7.[17] The role that the linker length may play is illustrated previously in Figure 1.6.[33]

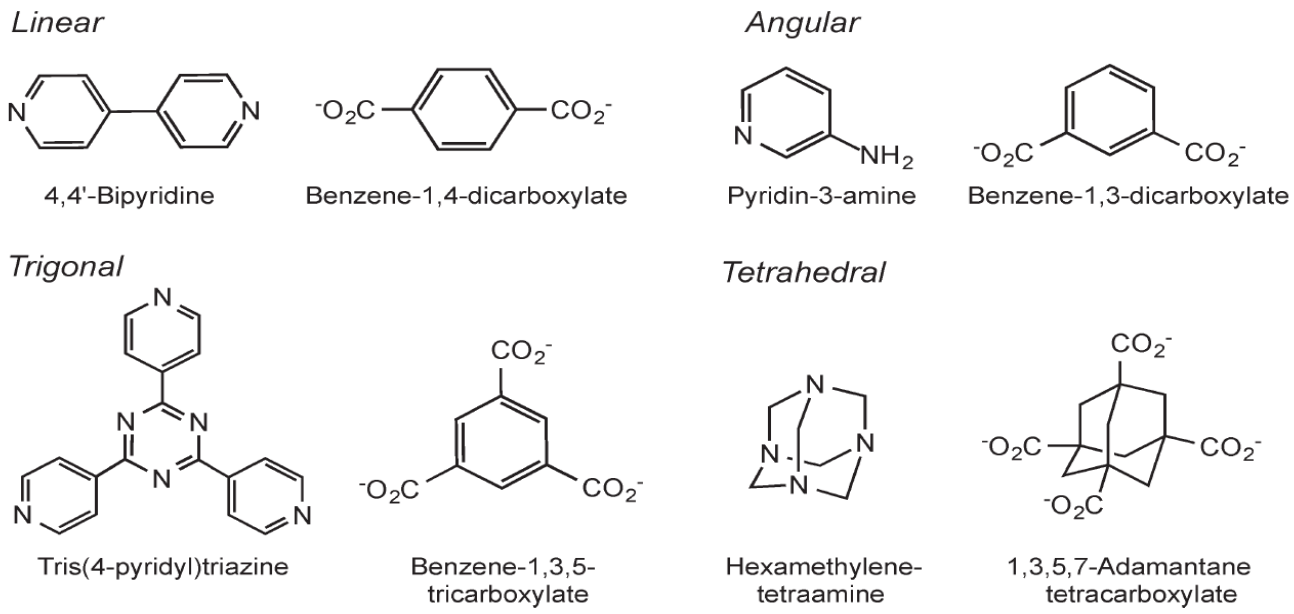

Figure 1.7 Representative examples of pyridine- and carboxylate-based linear, angular, trigonal and tetrahedral linkers used to assemble MOF structures. Reproduced from Ref. 33 with permission of The Royal Society of Chemistry

1.9 Mixed-Ligand MOF Strategy

Recently, research in CPs field has focussed on mixed-ligand frameworks where two different ligands can be simultaneously incorporated into MOFs, leading to a wide range of frameworks. The first examples of these, reported by Kitagawa et al., were $[Mn(bpe)_2(NCS)_2]$, $[Cd(dpds)_2(H_2O)_2]\bullet 2NO_3\bullet 2EtOH\bullet 2(H_2O)$ and $[Cd(pzdc)(azpy)]\bullet 2(H_2O)$, where bpe = 4,40-bipyridylethane, dpds = 4,4'-dipyridyldisulfide, EtOH = ethanol, pzdc = pyrazine-2,3-dicarboxylate and azpy = 4,4'-azopyrdine. [34,35] Selecting organic ligands with specific structural features has a fundamental role in MOF design due to the varying properties that these features may impart. MOFs have the unique possibility to modulate their structures in terms of dimensionality and pore volume, in the pursuit of desired networks for targeted applications. Mixed-ligand MOFs facilitate reaching this goal in that two different

ligands allow further tailoring or 'fine-tuning' of their structures and thus properties. These MOFs can be divided into three major categories based on the classification of their ligands prior to MOF synthesis, namely acid-acid, base-base and acid-base mixed-ligand MOFs.[20] Acid-base mixed-ligand MOFs are by far the most common with the acid and base ligands complementing each other by compensating for charge balance, coordination deficiency, whilst being weakly interacting.[20] Bipyridyl and polycarboxylate groups seems to be the most suitable combination for producing mixed-ligand MOFs as these complement each other well in terms of the above factors. Bipyridyl ligands act as pillars providing pore expansion, whilst carboxylate linkers provide structural rigidity. Examples of acid-acid and base-base MOFs are not as prevalent, with few examples reported in the literature being $[Cd_2(2,3\text{-pydc})_2(bix)_3 \cdot 2(H_2O)]$[36] (where 2,3-pydc = pyridine-2,3-dicarboxylic acid and bix = 1,4-bis(imidazolyl-1-methyl)-benzene), UMCM-1[37] and $Co(bimb)(4,4'\text{-bpy})(SCN)_2$ (where bimb = 1,4-bis(4-pyridineethynyl)benzene and bpy = 4,4-bipyridine).[38] Most of the MOFs presented in this dissertation were synthesised using the mixed-ligand approach. The aim of this project was to synthesise mixed-ligand MOFs with commercially available ligands which are relatively simple from a molecular structure point of view. However, synthesis of these frameworks can still be challenging due to the different reactivities of the ligands, which may lead to the incorporation of only one ligand in the MOF framework, as occurred for the reported cadmium-based MOF.

1.9.1 Carboxylate ligands

Coordination bonds between the oxygen atoms of carboxylate groups and metal ions have high thermal and chemical stabilities, increasing structural rigidity of MOFs where these functional groups are employed. Most carboxylate ligands also have aromatic rings which afford additional rigidity due to their fewer degrees of freedom when compared to using aliphatic chains as linkers. In the case of multicarboxylate ligands, different states of deprotonation can influence metal:ligand ratios and thus influence connectivities of the resulting MOFs, whilst variation in denticity (e.g., monodentate vs bidentate ligation) further adds to structural complexity.[39] Examples of common ligands incorporating these features are 1,4-benzenedicarboxylic and 1,3,5-benzenetricarboxylic acid.[40,41] Non-coordinating functional groups can also influence the ligation of other groups as in the case of 5-nitro-1,3-benzenedicarboxylic acid, where the usually, non-coordinating nitro group ($-NO_2$), which

may through hydrogen bonding with other components of the framework provide additional strength to it, may also act as electron withdrawing group and thus promote coordination.[56]

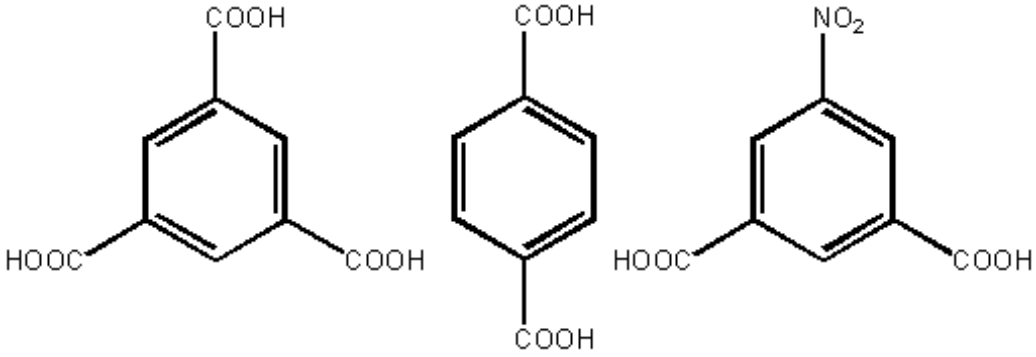

Figure 1.8 From left to right: 1,3,5-benzenetricarboxylic acid (H_3btc), 1,4-benzenedicarboxylic acid (H_2bdc) and 5-nitro-1,3-benzenedicarboxylic acid (H_2nipa)

1.9.2 Bipyridyl ligands (co-ligands)

Ligands functionalized with two 4-pyridyl nitrogen donor atoms have played a significant role in MOF design.[42] The voids of the framework can be obtained and tuned, by the employment of elongated, pyridyl-based linkers that tend to extend the diameter of the voids. Three common N-donor ligands employed in MOF synthesis, from 'short' to 'long', are 1,4-diazabicyclo[2.2.2]octane (DABCO), 4,4'-bipyridine (bpy) and 1,2-bis(4-pyridyl)ethane (bpe) illustrated in Figure 1.9. These ligands, as well as their derivatives, can be found in numerous publications in the scientific literature[43,44,45,46] One example of derivatization of bpe is the co-ligand 2,3-di(4-pyridyl)-2,3-butanediol presented in Figure 1.9, an example of a MOF with this ligand was been reported in 2007.[47]

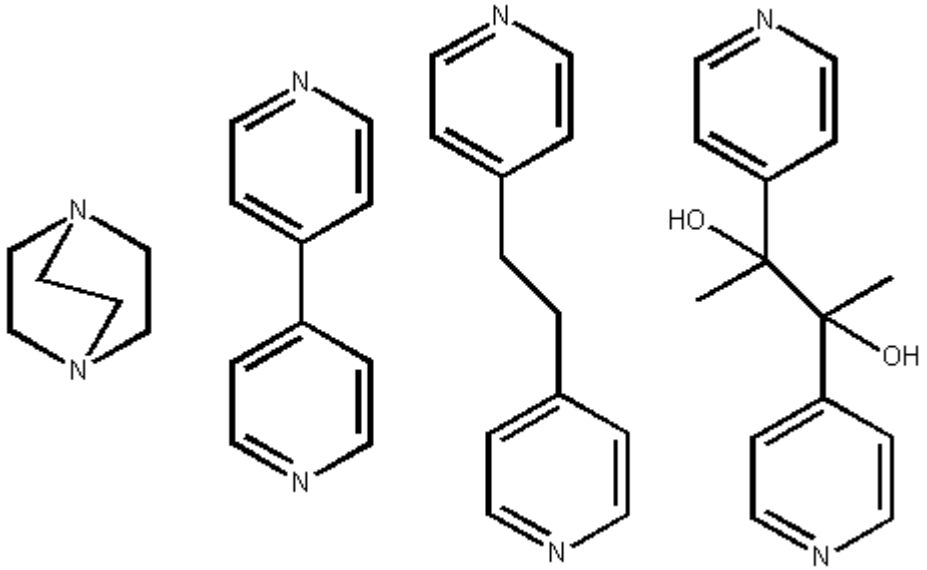

Figure 1.9 From left to right: DABCO, bpy, bpe and 2,3-di(4-pyridyl)-2,3-butanediol

1.10 Gas sorption

In the last decade metal-organic frameworks have been widely synthesised, characterized and studied for their properties due to the large versatility in applications their porous frameworks provide. They combine both the possibilities of metal-organic coordination chemistry and an incredible choice of organic linkers which may be functionalised. The broad array of possibilities with respect to structure geometry and connectivity lead to never before seen scope in tailoring materials properties, such as pore sizes. MOFs can be created with exceptionally large pore sizes, whilst remaining crystalline. Tunable pore size, geometry, topology and internal pore chemistry make MOFs the best choice for gas sorption and separation over other crystalline, porous solids such as zeolites, mesoporous materials (e.g. MCM-41[48]) and activated carbon materials. This is the reason that gas sorption is the aim of so many research projects, even though many of these materials have not yet been tested for gas sorption compared to the number of synthesized materials due to the relative youth of this research field. The process of adsorption of small gas molecules in most materials follows a simple path that is common in other nanoporous materials. Fluid separation in MOFs, zeolites and activated carbon materials adhere to common principles, for example the physical principles of correlation of molecular size and shape of the adsorbed molecules with that of the nanopores, and the chemical principles governing competitive interactions of adsorbed molecules onto the pore surface. MOFs and zeolites could be quite similar in design and they are also eligible for common applications, but the former have the potential for larger pore sizes and greater access to these pores due to the higher tunability in terms of ligand and metal choice. On the other hand, ligand hydrolysis and structure collapse upon solvent removal can occur in MOFs. Zeolites offer a limited choice in terms of possible structures as their frameworks must be formed by Si and Al but they are characterized by well-defined pore shapes, narrow pore-size distributions and high stabilities. This, associated with the possibility to find them in natural deposits, make zeolites one of the earliest, most successful and widely used porous materials for industrial applications. MOFs with pore sizes at the lower end of the spectrum present impressive separation properties, due to the high tunability of these properties, when compared to other porous solids such as the previously mentioned zeolites. Gas sorption is usually related to specific surface area and MOFs have of the highest values for this property. Examples of MOFs with high surface areas are MOF-177[49] and UMCM-2[50] with impressive values of 4500 and 5200 $m^2 g^{-1}$, respectively. UMCM-2 synthesis starts from the same SBU as that of

MOF-5, i.e. a Zn_4O cluster. As shown in Figure 1.10 these clusters are connected to each other by carboxylate linkers, bdc for MOF-5 and $t_2$dc (thieno[3,2-b]thiopene-2,5-dicarboxylic acid) and btb (4-[3,5-bis(4-carboxyphenyl)phenyl]benzoic acid) for UMCM-2.

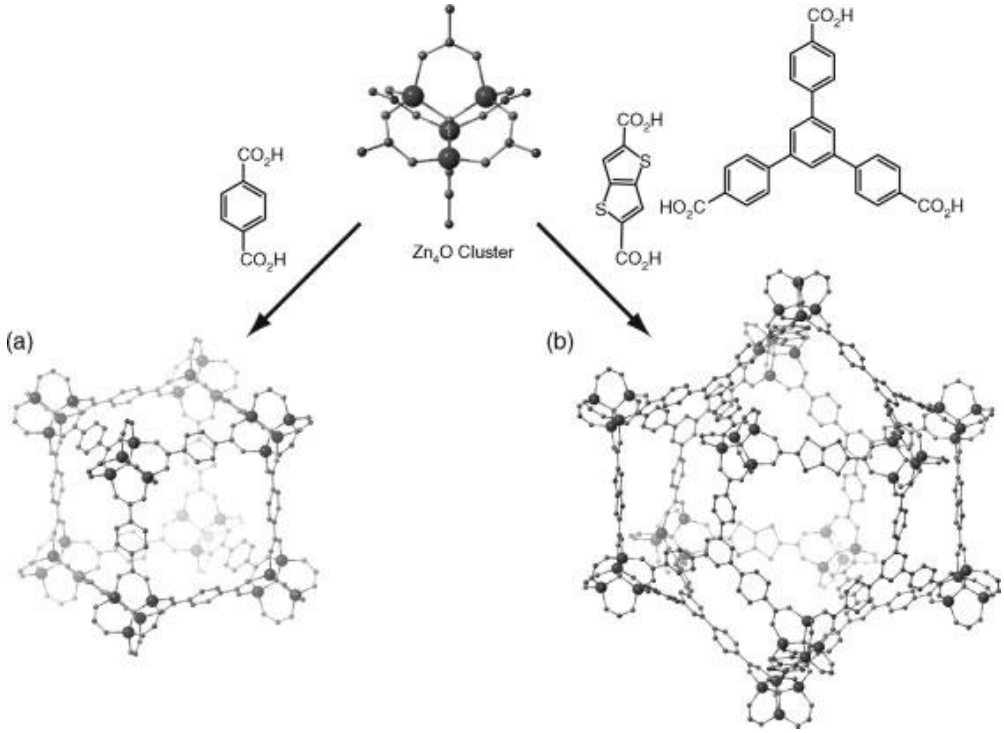

Figure 1.10 Partial crystal structures of (a) $[Zn_4O(bdc)_3]$ (MOF-5) and (b) $Zn_4O(t_2dc)(btb)_{4/3}$ (UMCM-2) constructed from Zn_4O clusters. Reprinted (adapted) with permission from K. Koh, A. G. Wong-Foy and A. J. Matzger, A porous coordination copolymer with over 5000 m^2/g BET surface area., J. Am. Chem. Soc., 2009, **131**, 4184–5. Copyright (2009) American Chemical Society

The surface area of powders and porous materials are evaluated experimentally using nitrogen gas (at 77 K) with the Brunauer-Emmett-Teller (BET) model being the most widely used. The surface area of the solid is calculated at the point at which monolayer coverage occurs (according to the BET model), with knowledge of the amount of nitrogen adsorbed and the molecule's cross-sectional area. In the case of nitrogen, the cross-sectional area is taken as 16.2 $Å^2$ $molecule^{-1}$.[51]

Yaghi's research group investigated and compared nine compounds with different structures and porosities (Figure 1.11): MOF-2 with square channels, MOF-505 and $Cu_3(BTC)_2$ with open metal sites, MOF-74 with packed, cylindrical channels, interpenetrated IRMOF-11, IRMOF-3 and IRMOF-6 with alkyl and amino functionalised pores, ultra-high porous IRMOF-1 and MOF-177. Amongst these MOF-177 was shown to have the highest surface area of 4508 m^2 g^{-1}.[52] CO_2 uptake for these materials (Figure 1.12), indicate that MOF-177 has an

incredible CO_2 capacity of 33.5 mmol g^{-1} at 35 bar, which is more than the traditional benchmark physisorptive materials at the time, namely zeolite 13X (7.4 mmol g^{-1}at 32 bar) and MAXSORB (25 mmol g^{-1} at 35 bar). [53,54,55]

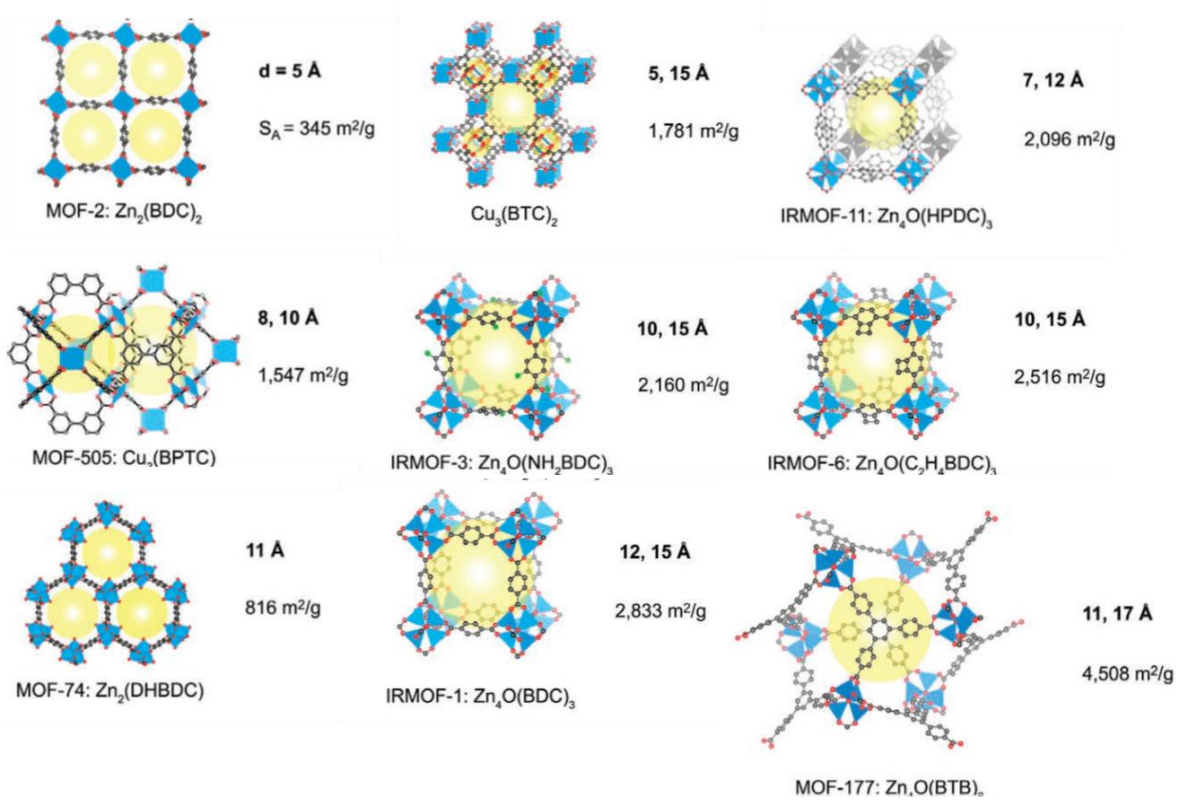

Figure 1.11 Crystal structures of MOFs examined for CO_2 storage capacity at room temperature. For each MOF, the framework formula, pore size, and surface area are given. Figure adapted from A. R. Millward and O. M. Yaghi, Metal-organic frameworks with exceptionally high capacity for storage of carbon dioxide at room temperature, J. Am. Chem. Soc., 2005, **127**, 17998–17999. Reprinted (adapted) with permission from (A. R. Millward and O. M.Yaghi, J. Am. Chem. Soc., 2005, **127**, 17998–17999). Copyright (2010) American Chemical Society.

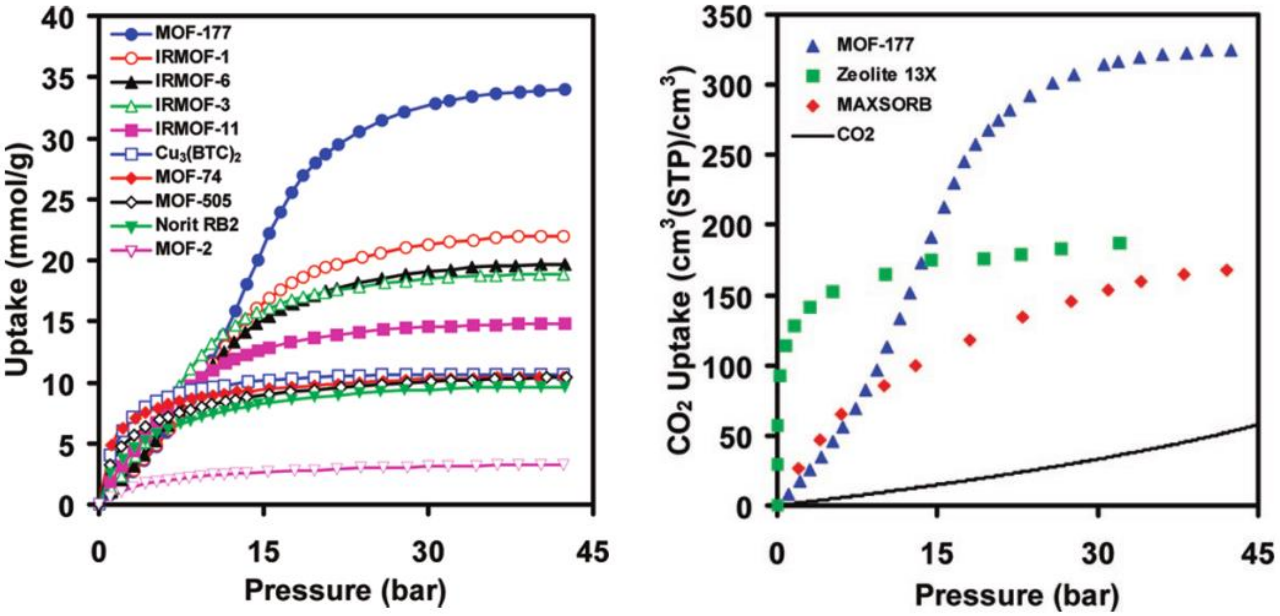

Figure 1.12 (Left) Comparison of gravimetric CO_2 capacities for several MOFs (and an activated carbon, Norit RB2, as a reference) determined at ambient temperature and pressures up to 42 bar and (Right) comparison of the volumetric CO_2 capacity of crystalline MOF-177 relative to zeolite 13X pellets, MAXSORB carbon powder, and pressurized CO_2. Reprinted (adapted) with permission from (A. R. Millward and O. M.Yaghi, J. Am. Chem. Soc., 2005, **127**, 17998–17999). Copyright (2010) American Chemical Society

1.11 Objectives

The main objectives of this thesis work were the preparation and characterization of mixed-ligand metal-organic frameworks:

1. The preparation of mixed-ligand metal-organic frameworks based on simple carboxylate and biprydyl ligands adopting various synthetic techniques typical in crystal engineering;

2. The characterization, both structural and thermal, of the prepared compounds using X-ray diffraction studies (powder X-ray diffraction, single crystal X-ray diffraction and variable-temperature powder X-ray diffraction) and thermal analysis (thermogravimetric analysis, differential scanning calorimetry, and hot stage microscopy).

1.12 References:

1 J. M. Lehn, Supramolecular chemistry - Scope and perspectives: Molecules - Supermolecules - Molecular devices, *J. Incl. Phenom.*, 1988, **6**, 351–396.

2 D. Braga, Crystal Engineering. A Textbook By Gautam R. Desiraju, Jagadese J. Vittal and Arunachalam Ramanan., *Angew. Chemie Int. Ed.*, 2012, **51**, 3516.

3 G. R. Desiraju, Chemical crystallography and crystal engineering, *IUCrJ*, 2014, **1**, 380–381.

4 M. D. Cohen and G. M. J. Schmidt, 383. Topochemistry. Part I. A survey, *J. Chem. Soc.*, 1964, 1996–2000.

5 A. I. Kitaigorodskii, *Molecular crystals and molecules [by] A. I. Kitaigorodsky*, Academic Press New York, 1973.

6 A. F. Wells, The geometrical basis of crystal chemistry. Part 2, *Acta Crystallogr.*, 1954, **7**, 545–554.

7 S. R. Batten and R. Robson, Interpenetrating Nets: Ordered, Periodic Entanglement, *Angew. Chemie Int. Ed.*, 1998, **37**, 1460–1494.

8 R. Robson, A net-based approach to coordination polymers†, *J. Chem. Soc. Dalt. Trans.*, 2000, 3735–3744.

9 M. T. Rodgers and P. B. Armentrout, Noncovalent metal-ligand bond energies AS studied by threshold collision-induced dissociation, *Mass Spectrom. Rev.*, 2000, **19**, 215–247.

10 O. M. Yaghi and H. Li, Hydrothermal Synthesis of a Metal-Organic Framework Containing Large Rectangular Channels, *J. Am. Chem. Soc.*, 1995, **117**, 10401–10402.

11 H. Li, M. Eddaoudi, M. O'Keeffe and O. M. Yaghi, Design and synthesis of an exceptionally stable and highly porous metal-organic framework, *Nature*, 1999, **402**, 276–279.

12 M. E. Braun, C. D. Steffek, J. Kim, P. G. Rasmussen and O. M. Yaghi, 1,4-Benzenedicarboxylate derivatives as links in the design of paddle-wheel units and metal – organic frameworks, *Chem. Commun. (Camb).*, 2001, **2**, 2532–2533.

13 M. Eddaoudi, D. Moler, H. Li, B. Chen, T. Reineke, M. O'Keeffe and O. Yaghi, Modular Chemistry: Secondary Building Units as a Basis for the Design of Highly Porous and Robust Metal− Organic Carboxylate Frameworks, *Acc. Chem. Res.*, 2001, **34**, 319–330.

14 O. M. Yaghi, M. O'Keeffe, N. W. Ockwig, H. K. Chae, M. Eddaoudi and J. Kim, Reticular synthesis and the design of new materials, *Nature*, 2003, **423**, 705–714.

15 J. L. C. Rowsell and O. M. Yaghi, Metal-organic frameworks: A new class of porous materials, *Microporous Mesoporous Mater.*, 2004, **73**, 3–14.

16 S. R. Batten, N. R. Champness, X.-M. Chen, J. Garcia-Martinez, S. Kitagawa, L. Öhrström, M. O'Keeffe, M. P. Suh and J. Reedijk, Coordination polymers, metal–organic frameworks and the need for terminology guidelines, *CrystEngComm*, 2012, **14**, 3001.

17 M. D. Allendorf and V. Stavila, Crystal engineering, structure–function relationships, and the future of metal–organic frameworks, *CrystEngComm*, 2015, **17**, 229–246.

18 M. O'Keeffe, Design of MOFs and intellectual content in reticular chemistry: a personal view, *Chem. Soc. Rev.*, 2009, **38**, 1215.

19 N. Stock and S. Biswas, Synthesis of metal-organic frameworks (MOFs): Routes to various MOF topologies, morphologies, and composites, *Chem. Rev.*, 2012, **112**, 933–969.

20 M. Du, C. P. Li, C. Sen Liu and S. M. Fang, Design and construction of coordination polymers with mixed-ligand synthetic strategy, *Coord. Chem. Rev.*, 2013, **257**, 1282–1305.

21 L. Öhrström, Let's Talk about MOFs—Topology and Terminology of Metal-Organic

Frameworks and Why We Need Them, *Crystals*, 2015, **5**, 154–162.

22 L. J. Barbour, Crystal porosity and the burden of proof, *Chem. Commun.*, 2006, 1163.

23 B. Moulton and M. J. Zaworotko, From molecules to crystal engineering: Supramolecular isomerism and polymorphism in network solids, *Chem. Rev.*, 2001, **101**, 1629–1658.

24 A. Rabenau, The Role of Hydrothermal Synthesis in Preparative Chemistry, *Angew. Chemie Int. Ed. English*, 1985, **24**, 1026–1040.

25 S. L. James, C. J. Adams, C. Bolm, D. Braga, P. Collier, T. Friščić, F. Grepioni, K. D. M. Harris, G. Hyett, W. Jones, A. Krebs, J. Mack, L. Maini, A. G. Orpen, I. P. Parkin, W. C. Shearouse, J. W. Steed and D. C. Waddell, Mechanochemistry: opportunities for new and cleaner synthesis, *Chem. Soc. Rev.*, 2012, **41**, 413–447.

26 V. Strukil, L. Fábián, D. G. Reid, M. J. Duer, G. J. Jackson, M. Eckert-Maksić and T. Friščić, Towards an environmentally-friendly laboratory: dimensionality and reactivity in the mechanosynthesis of metal-organic compounds., *Chem. Commun.*, 2010, **46**, 9191–9193.

27 D. Farrusseng, *Metal-Organic Frameworks*, 2011.

28 K. Susumu and K. Mitsuru, Functional Micropore Chemistry of Crystalline Metal Complex-Assembled Compounds, *Bull. Chem. Soc. Jpn.*, 1998, **71**, 1739–1753.

29 M. Eddaoudi, J. Kim, N. Rosi, D. Vodak, J. Wachter, M. O. Keeffe, O. M. Yaghi, M. Eddaoudi, J. Kimrn, N. Rosi and O. M. Yaghil, Systematic Design of Pore Size and Functionality in Isoreticular MOFs and Their Application in Methane Storage Published by : American Association for the Advancement of Science Linked references are available on JSTOR for this article : Systematic Design, 2002, **295**, 469–472.

30 B. Kesanli, Y. Cui, M. R. Smith, E. W. Bittner, B. C. Bockrath and W. Lin, Highly interpenetrated metal-organic frameworks for hydrogen storage, *Angew. Chemie - Int. Ed.*, 2004, **44**, 72–75.

31 IUPAC, Compendium of Chemical Terminology 2nd ed. (the 'Gold Book'), *Blackwell Sci. Publ. Oxford*, 2014, 1670.

32 N. N. (Norman N. Greenwood and A. (Alan) Earnshaw, *Chemistry of the elements*, Butterworth-Heinemann, 1997.

33 W. Lu, Z. Wei, Z.-Y. Gu, T.-F. Liu, J. J. Park, J. J. Park, J. Tian, M. Zhang, Q. Zhang, T. Gentle III, M. Bosch and H.-C. Zhou, Tuning the structure and function of metal–organic frameworks via linker design, *Chem. Soc. Rev.*, 2014, **43**, 5561–5593.

34 M. Kondo, M. Shimamura, S. I. Noro, Y. Kimura, K. Uemura and S. Kitagawa, Synthesis and structures of coordination polymers with 4,4'-dipyridyldisulfide, *J. Solid State Chem.*, 2000, **152**, 113–119.

35 T. K. Maji, K. Uemura, H. C. Chang, R. Matsuda and S. Kitagawa, Expanding and shrinking porous modulation based on pillared-layer coordination polymers showing selective guest adsorption, *Angew. Chemie - Int. Ed.*, 2004, **43**, 3269–3272.

36 L. Wen, Y. Li, Z. Lu, J. Lin, C. Duan and Q. Meng, Syntheses and structures of four d10metal-organic frameworks assembled with aromatic polycarboxylate and bix [bix = 1,4-bis(imidazol-1- ylmethyl)benzene], *Cryst. Growth Des.*, 2006, **6**, 530–537.

37 K. Koh, A. G. Wong-Foy and A. J. Matzger, A crystalline mesoporous coordination copolymer with high microporosity, *Angew. Chemie - Int. Ed.*, 2008, **47**, 677–680.

38 Y. Qi, Y.-X. Che, S. R. Batten and J.-M. Zheng, Unprecedented trinodal 4-connected metal–organic frameworks (MOFs) with 2-fold interpenetration, *CrystEngComm*, 2008, **10**, 1027.

39 X. Zhu, P. P. Sun, J. G. Ding, B. L. Li and H. Y. Li, Tuning cobalt coordination architectures by bis(1,2,4-triazol-1-ylmethyl) benzene position isomers and 5-nitroisophthalate, *Cryst. Growth Des.*, 2012, **12**, 3992–3997.

40 P. S. Mukherjee, D. Ghoshal, E. Zangrando, T. Mallah and N. R. Chaudhuri, Use of different unsaturated dicarboxylates toward the design of new 3D and 2D networks of copper(II), *Eur. J. Inorg. Chem.*, 2004, 4675–4680.

41 H. Y. Bai, J. F. Ma, J. Yang, L. P. Zhang, J. C. Ma and Y. Y. Liu, Eight two-dimensional and three-simensional metal-organic frameworks based on a flexible tetrakis(imidazole) ligand: Synthesis, topological structures, and photoluminescent properties, *Cryst. Growth Des.*, 2010, **10**, 1946–1959.

42 D. L. Long, a J. Blake, N. R. Champness and M. Schroder, Can 4,4 '-bipyridine N,N '-dioxide play the same important role as 4,4 '-bipyridine in the construction of metal coordination networks and crystal engineering?, *Chem. Commun.*, 2000, 2273–2274.

43 L. Luan, W. Zhang, K. Wang, Z. Lin and H. Huang, Two open-framework zinc phosphites constructed from different secondary building units, *Inorg. Chem. Commun.*, 2016, **72**, 96–99.

44 S. Barman, A. Khutia, R. Koitz, O. Blacque, H. Furukawa, M. Iannuzzi, O. M. Yaghi, C. Janiak, J. Hutter and H. Berke, Synthesis and hydrogen adsorption properties of internally polarized 2,6-azulenedicarboxylate based metal–organic frameworks, *J. Mater. Chem. A*, 2014, **2**, 18823–18830.

45 J. Gu, Y. Cui, X. Liang, J. Wu, D. Lv and A. M. Kirillov, Structurally Distinct Metal-Organic and H-Bonded Networks Derived from 5-(6-Carboxypyridin-3-yl)isophthalic Acid: Coordination and Template Effect of 4,4′-Bipyridine, *Cryst. Growth Des.*, 2016, **16**, 4658–4670.

46 X. Li, R. Cao, D. Sun, W. Bi, Y. Wang, X. Li and M. Hong, Syntheses and characterizations of zinc(II) compounds containing three-dimensional interpenetrating diamondoid networks constructed by mixed ligands, *Cryst. Growth Des.*, 2004, **4**, 775–780.

47 S. M. Neville, B. Moubaraki, K. S. Murray and C. J. Kepert, A thermal spin transition in a nanoporous iron(II) coordination framework material, *Angew. Chemie - Int. Ed.*, 2007, **46**, 2059–2062.

48 D. Kumar, K. Schumacher, C. Du Fresne von Hohenesche, M. Grün and K. K. Unger, MCM-41, MCM-48 and related mesoporous adsorbents: their synthesis and characterisation, *Colloids Surfaces A Physicochem. Eng. Asp.*, 2001, **187**–**188**, 109–116.

49 R. F. Bruinsma, P. G. De Gennes, J. B. Freund and D. Levine, Letters To Nature, *Nature*, 2004, **427**, 523–527.

50 K. Koh, A. G. Wong-Foy and A. J. Matzger, A porous coordination copolymer with over 5000 m2/g BET surface area., *J. Am. Chem. Soc.*, 2009, **131**, 4184–5.

51 J. M. Zielinski and L. Kettle, Physical Characterization: Surface Area and Porosity, *no. April*, 2013, 1–7.

52 Y. Li and R. T. Yang, Gas Adsorption and Storage in Metal-Organic Framework MOF-177 on and Storage in Metal-Organic Framework MOF-177, *Langmuir*, 2007, **23**, 12937–12944.

53 A. R. Millward and O. M. Yaghi, Metal-organic frameworks with exceptionally high capacity for storage of carbon dioxide at room temperature, *J. Am. Chem. Soc.*, 2005, **127**, 17998–17999.

54 J.-P. Zhang, P.-Q. Liao, H.-L. Zhou, R.-B. Lin and X.-M. Chen, Single-crystal X-ray diffraction studies on structural transformations of porous coordination polymers, *Chem. Soc. Rev.*, 2014, **43**, 5789–5814.

55 J. Hyo Park, K. Min Choi, H. Joon Jeon, Y. Jung Choi and J. Ku Kang, In-situ observation for growth of hierarchical metal-organic frameworks and their self-sequestering mechanism for gas storage, *Sci. Rep.*, 2015, **5**, 12045.

56 X.-L. Wang, B. Mu, H.-Y. Lin, G.-C. Liu, A.-X. Tian and S. Yang, Assembly and property of four 2D layer-like coordination polymers with different structural features derived from bis(3-pyridylformyl)piperazineligand and aromatic dicarboxylic acids with nitro group, CrystEngComm, 2012, 14, 1001–1009.

Chapter 2: Experimental and Analytical Methods

2.1 Starting Materials

All metal salts, organic linkers and solvents were purchased from commercial sources and used without any further purification.

2.1.1 Organic Linkers

The organic linkers used can be divided into two groups, i.e. multicarboxylic acid and bipyridyl ligands.

2.1.1.1 Multicarboxylic acids

Ligands belonging to this class are common choices in MOF synthesis due to the stability of the carboxylate-metal coordination bond and to the multiple coordination modes which may yield a diversity of structures. In mixed-ligands MOFs, these ligands are often responsible for extending the coordination in two dimensions. Linkers chosen for this project were:

- benzene-1,3,5-tricarboxylic acid (abbreviated as H_3BTC; common name is trimesic acid)
- 5-nitro-1,3-benzenedicarboxylic acid (abbreviated as H_2nipa; common name is 5-nitroisophthalic acid)

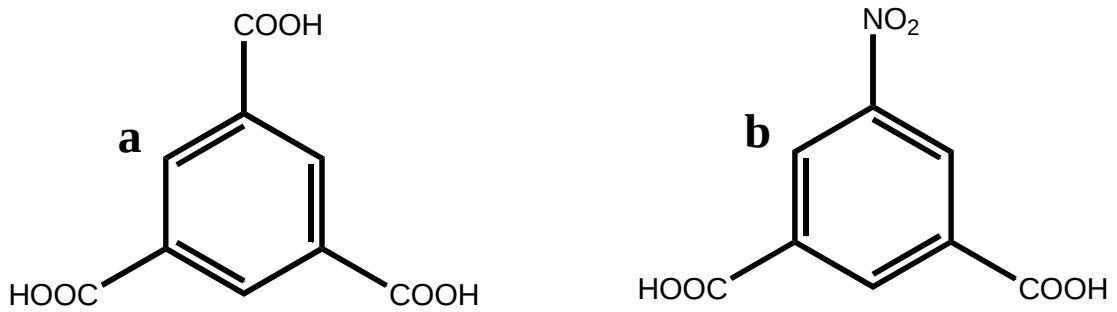

Figure 2.1 Molecular structures of (a) benzene-1,3,5-tricarboxylic acid and (b) 5-nitro-1,3-benzenedicarboxylic acid

2.1.1.2 Bipyridyl ligands (co-ligands)

This class of neutral ligands are often used in the synthesis of mixed-ligands MOFs acting as pillars connecting 2D sheets consisting of carboxylate ligands and metal ions. Bipyridyl ligands employed in this project were:

- 4,4'-bipyridine (abbreviated as bipy)
- 1,2-di(4-pyridyl)ethane (abbreviated as bpe)
- 2,3-di(4-pyridyl)-2,3-butanediol (abbreviated as dpdb)

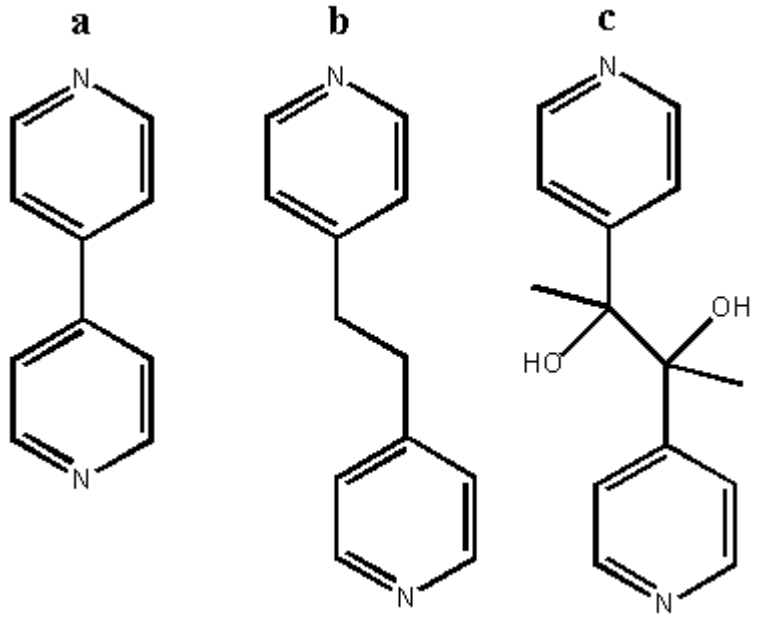

Figure 2.1 Molecular structures of (a) 4,4'-bipyridine (bipy), (b)1,2-di(4-pyridyl)ethane (bpe) and (c) 2,3-di(4-pyridyl)-2,3-butanediol (dpdb)

2.1.2 Metal Salts

Metal ions with nitrates as counterions were preferentially employed due to the high solubilities of these salts, the poor coordinating capability and the absent basic behaviour of the nitrate anion. The metal salts used in the syntheses of the MOFs in this project were:

- $Mn(NO_3)\cdot 4H_2O$
- $Co(NO_3)\cdot 6H_2O$
- $CdBr_2$

2.1.3 Solvent

The choice of solvent plays an important role in MOF synthesis since solvents directly or indirectly influence the coordination behaviour of metals and ligands. Although the effect of the solvent choice for each synthesis is not always clear, a number of examples of MOF synthesis show that each solvent system has a role in regulating the formation of different coordination environments.[1,2,3] The solvents used in the assembly process may participate in coordination with metal ions or can also act as guest molecules in the final lattice structure.[4,5] In this project, the most common solvents used in MOF synthesis are water and *N*,*N*-dimethylformamide (DMF), used separately or in combination. Other solvents used were methanol (MeOH), ethanol (EtOH), monoethylene glycol (MEG) and *N*,*N*-dimethylacetamide (DMA).

2.2 Synthetic Methods

Three different synthetic methods have been used in attempted MOF synthesis, namely, slow diffusion by layering,[6,7] solvothermal synthesis[8] and liquid-assisted grinding (LAG).[9,10] Hundreds of syntheses were attempted with these methods, especially using solvothermal conditions where different parameters such as molar ratios, solvents, temperature and time were varied. Crystals were only produced in a small subset of these attempts.

2.2.1 Slow Diffusion by Layering Metal salts were dissolved in a small amount of water (e.g. 1-2 ml) while the ligands were dissolved in a certain amount (e.g., double the volume of water) of organic solvents which are miscible with water but have a slow mixing rate. The two solutions are stirred separately and the solution containing the ligand is carefully layered on top of the aqueous metal salt solution. This procedure has a fast preparation but requires a lot of attention by the operator with crystal growth taking place over weeks to months in this project.

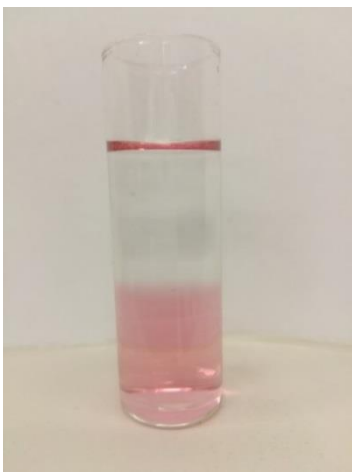

Figure 2.2 Picture of a methanolic solution layered on top of an aqueous solution of $Co(NO_3)_2 \cdot 6H_2O$

2.2.2 **Solvothermal Synthesis** Metal salts and ligands were dissolved in various solvents which were either placed in an autoclave or vials at temperatures ranging from 80 to 170 °C. Autoclaves are needed when the operating temperature exceeds 100 °C because vial caps could pop out due to autogenous pressure. Temperature, time and cooling rates were varied for different attempts. This is the most common method used for the synthesis of MOFs because the preparation is relatively simple, multiple samples can be set up simultaneously and crystals are usually produced when the reaction solutions are cooled. In this project, on occasion, crystals only appeared when the heated solutions were kept at room temperature for extended periods or/and when vials were left uncapped to allow partial solvent evaporation for the promotion of crystal growth.

Figure 2.3 Multiple vials placed in an oven for a solvothermal experiment

2.2.3 **Liquid Assisted Grinding** Metal salts and ligands were ground together using an agate mortar and pestle. This could be done without solvent, called “dry grinding”, or with a few drops of solvent added, called liquid-assisted grinding (LAG). In some instances, auxiliary templating agents can be added to the reaction mixture which is then known as Inorganic-Liquid-Assisted-Grinding (ILAG)[9]. LAG was the method in this project. LAG has the advantage of fast, efficient preparation of products with high yields, however, suffers from the preclusion of producing large-enough crystals for single crystal X-ray diffraction due to the destructive (in terms of crystals) nature of the method.

2.3 X-Ray Diffraction

X-ray diffraction (XRD) involves the irradiation of a crystalline sample with X-rays which are then scattered (diffracted) in particular directions with particular intensities as result of the internal, periodic arrangement of the sample's atoms. The ability of a crystal to diffract X-rays was first demonstrated by Max van Laue in 1912, after which W.L. Bragg in 1913 proposed his famous Bragg law which simplified the interpretation of the diffracted X-rays.

2.3.1 Single Crystal X-ray Diffraction

Single crystal X-ray diffraction (SCXRD) is a technique that allows the determination of accurate 3D coordinates of atoms within a crystal. Initial unit cell parameters can be determined from the collection of a few frames, however, a complete collection of diffracted X-ray intensities (typically several hundred to thousands of frames) is required to successfully solve and refine a typical MOF crystal structure. Crystals were removed from the mother liquor and immediately placed under Paratone N oil in order to avoid desolvation. A polarizing microscope was used to select a suitable, single crystal after which it was mounted on a nylon loop and submerged in a cold nitrogen stream shrouded by dry air. At lower temperatures the Paratone N oil, besides being cryoprotectant, also acts to glue the crystal in a fixed position. Single crystal X-ray data collections were carried out on a Bruker APEX II Duo diffractometer utilizing graphite monochromated MoKα X-rays (λ = 0.71073 Å). Temperatures were regulated using an Oxford Cryostream-700 with a constant stream of nitrogen gas at a flow rate of 20 cm^3 min^{-1}. Unit cell refinement and data reduction were carried out using the program SAINT-Plus.[11] All intensity data were scaled and corrected for Lorentz-polarisation and absorption effects using the program SADABS.[11] The crystal system and space group were suggested by the program XPREP[11] and confirmed by visual inspection of the reciprocal lattice in LAYER.[12] Structure solution was achieved using SHELXS (direct methods) or SHELXT (intrinsic phasing), whilst refinement proceeded with SHELXL.[13] XSeed[14] and OLEX2[15] were used as graphical interfaces to the SHELX suite of programs, whilst X-Seed and Mercury[16] were used to generate POV-Ray pictures,[17]

PLATON[18] was used to estimate the electron count for desolvated structures and list the intermolecular interactions.

2.3.2 Powder X-ray Diffraction

Powder X-ray diffraction (PXRD) involves the X-ray irradiation of a polycrystalline sample and is a fast and powerful technique that can be used for various purposes. In this project it was mainly used as a fingerprinting technique and more specifically to:

- confirm that the experimental PXRD pattern of a sample of ground crystals from a successful MOF synthesis agreed with that of the calculated PXRD pattern generated from the single crystal X-ray structure. This was to confirm that the selected single crystal for SCXRD was representative of the bulk sample. In addition, the success and phase purity of subsequent crystallizations needed for other analyses were also established in this manner.
- compare the experimental PXRD patterns to attempts of MOF synthesis by LAG with that of the starting materials. If the PXRD patterns of the ground material were different to that of the superposition of the PXRD patterns of the starting materials, the syntheses were deemed successful.
- establish whether the changes in the structures of MOFs occurred upon desolvation. MOFs need to be desolvated in order to create space for the sorption of other molecules into their matrices. Desolvation was achieved by variable-temperature PXRD (VT-PXRD) experiments, with the selection of temperatures guided by results from thermogravimetric analysis.
- In situ rehydration studies were performed on the dehydrated Cd-based MOF to establish whether the original structure was regained. In this instance, a modified sample chamber was used where the sample was located next to wells containing water, whilst the whole stage was covered with Mylar film.[19]

PXRD and VT-PXRD measurements were performed using a Bruker D8 Advance diffractometer equipped with a Lynxeye detector using CuKα radiation (λ = 1.5406 Å), X-rays were generated with a current flow of 40 mA and voltage of 30 kV. Samples from solvothermal synthesis were removed from the mother liquor, dried on filter paper and gently ground in an agate mortar before placing it on a zero-background sample holder. LAG samples were put directly on the sample holder as they were ground during the attempted syntheses. Scans were performed over a 2θ range of 4-40° with step size and integration times (ranged between 0.250 s and 0.500 s per step) chosen depending on the sample. Calculated PXRD patterns were generated by Mercury using fully refined single crystal X-ray structures. All PXRD patterns were plotted with the software Excel and XmGrace.

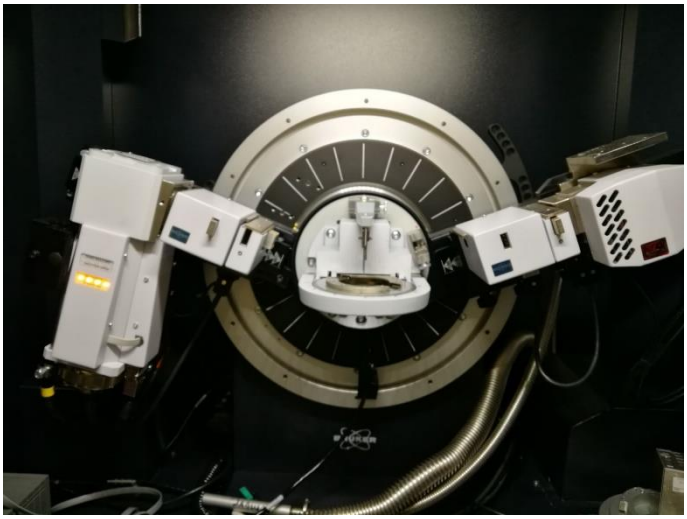

Figure 2.4 Bruker D8 Advance diffractometer

2.4 Thermal Analysis

Hot stage microscopy (HSM), differential scanning calorimetry (DSC) and thermogravimetric analysis (TGA) were employed to establish the samples behaviour upon heating.

2.4.1 Hot Stage Microscopy

HSM allows for the visualization of thermal events such as desolvation, decomposition or changes in colour. This kind of analysis is mostly qualitative and may show temperature differences in the onset of thermal events when compared to DSC and TGA due to differences in the geometries of the experimental setups. HSM was performed by placing the sample on a cover slip which was placed on a Linkam THMS600 hot stage connected to a Linkam TP92 temperature control unit. A Nikon SMZ-10 stereoscopic microscope and a Sony Digital Hyper HAD colour video camera were used to record the images visualized through the Soft Imaging System program analysis.[20] Generally, samples were covered by silicone oil, which allow the detection of desolvation as indicated by the evolution of bubbles. Samples were heated at a rate of 10 °C min^{-1} and up to temperatures where decomposition was indicated by samples turning brown.

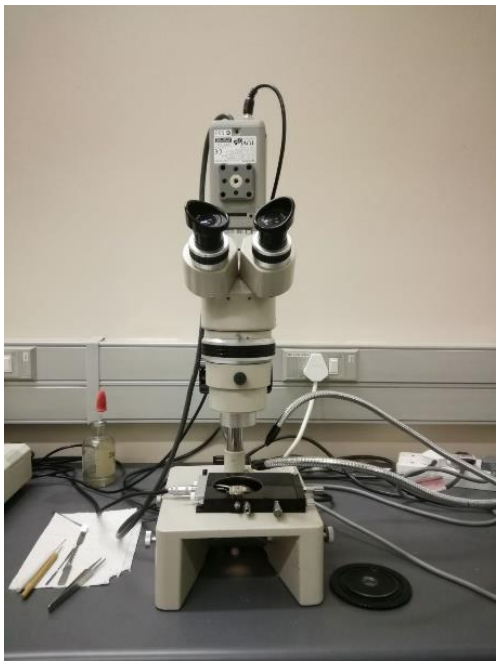

Figure 2.5 HSM instrumentation

2.4.2 Differential Scanning Calorimetry

DSC measures the amount of heat required to increase the temperature of a sample and a reference, plotting the difference in heat input as a function of temperature. The enthalpy of different thermal events, such as melting and solvent loss, can be measured using this technique. A small amount, ~2 mg, of filter paper dried sample was placed in a pan with a pierced lid, which allowed ventilation. The sample pan and references pans are heated together, with exothermic and endothermic events detected due to differences in required heat inputs in order to maintain the same rate of temperature change. Analyses were performed with a DSC25 from Thermal Instruments, with heating rates of 10°C min^{-1}, whilst purge gas flow at a fixed rate of 60 ml min^{-1}. Results were processed with TA Universal software.

Figure 2.6 DSC25 used for DSC analyses

2.4.3 Thermogravimetric Analysis

TGA measures the mass loss of the sample during heating, under a controlled atmosphere. The thermogravimetric data collected is usually compiled into a plot of percentage of initial mass on the y axis versus temperature on the x-axis. Various phenomena, such as

desolvation and thermal decomposition, can be observed. Measurements were performed on a TGA Q500 from TA Instruments. Filter paper dried samples, varying in mass between 2-5 mg, were placed in an open pan attached to a balance and heated at a rate of 10 °C min^{-1} (20 °C min^{-1} when used to prepare dehydrated compounds) under a nitrogen purge flow of 60 ml min^{-1}. Results were processed with TA Universal software.

Figure 2.7 TGA Q500 used for TGA analyses

2.5 Dehydration and Rehydration Studies

A qualitative investigation of dehydration and rehydration properties was conducted on one compound. A sample of a few milligrams (~10 mg) was dehydrated on the TGA instrument, a second analysis was run immediately after the former to ensure the complete dehydration of the compound. Dehydrated compound was firstly ground then placed in small vial, left open, set in a bigger one, closed and half filled with water. This was done to saturate the atmosphere with water vapour. PXRD was conducted on the compound after one and two days of exposure. A final TGA analysis was run to evaluate the amount of water vapour absorbed by the compound.

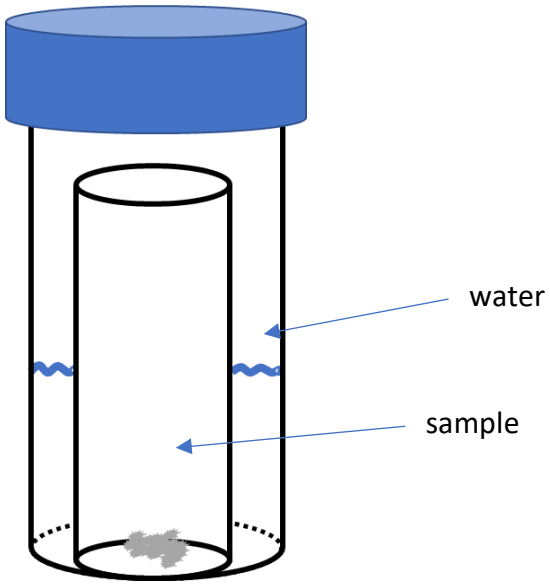

Figure 2.12 Schematic representation of the set-up for rehydration studies

2.6 Additional Software Packages

ConQuest was used to access to the Cambridge Structural Database[21] (CSD) which allowed the assessment of the novelty of the synthesized MOFs. Potential void spaces in the frameworks were calculated and plotted using Mercury (using probe radius of 1.2 Å and grid spacing of 0.7 Å).

2.7 References

1 B.-C. Tzeng, H.-T. Yeh, T.-Y. Chang and G.-H. Lee, Novel Coordinated-Solvent Induced Assembly of Cd(II) Coordination Polymers Containing 4,4′-Dipyridylsulfide, *Cryst. Growth Des.*, 2009, **9**, 2552–2555.

2 E. Tynan, P. Jensen, P. E. Kruger and A. C. Lees, Solvent templated synthesis of metal-organic frameworks: Structural characterisation and properties of the 3D network isomers {[Mn(dcbp)]·1/2DMF}n and {[Mn(dcbp)]·2H2O}n, *Chem. Commun.*, 2004, **10**, 776–777.

3 X. Y. Wang, L. Wang, Z. M. Wang and S. Gao, Solvent-tuned azido-bridged Co2+ layers: Square, honeycomb, and Kagomé, *J. Am. Chem. Soc.*, 2006, **128**, 674–675.

4 C.-P. Li and M. Du, Role of solvents in coordination supramolecular systems, *Chem. Commun.*, 2011, **47**, 5958.

5 K. Akhbari and A. Morsali, Effect of the guest solvent molecules on preparation of different morphologies of ZnO nanomaterials from the $[Zn_2(1,4\text{-bdc})_2(dabco)]$ metal-organic framework, *J. Coord. Chem.*, 2011, **64**, 3521–3530.

6 P. S. Mukherjee, D. Ghoshal, E. Zangrando, T. Mallah and N. R. Chaudhuri, Use of different unsaturated dicarboxylates toward the design of new 3D and 2D networks of copper(II), *Eur. J. Inorg. Chem.*, 2004, 4675–4680.

7 R. Seetharaj, P. V. Vandana, P. Arya and S. Mathew, Dependence of solvents, pH, molar ratio and temperature in tuning metal organic framework architecture, *Arab. J. Chem.*, , DOI:10.1016/j.arabjc.2016.01.003.

8 Y. R. Lee, J. Kim and W. S. Ahn, *Korean J. Chem. Eng.*, 2013, 30.

9 T. Friščić, D. G. Reid, I. Halasz, R. S. Stein, R. E. Dinnebier and M. J. Duer, Ion- and Liquid-Assisted Grinding: Improved Mechanochemical Synthesis of Metal-Organic Frameworks Reveals Salt Inclusion and Anion Templating, Angew. Chemie Int. Ed., 2010, **122**, 724–727.

10 S. L. James, C. J. Adams, C. Bolm, D. Braga, P. Collier, T. Friščić, F. Grepioni, K. D. M. Harris, G. Hyett, W. Jones, A. Krebs, J. Mack, L. Maini, A. G. Orpen, I. P. Parkin, W. C. Shearouse, J. W. Steed and D. C. Waddell, Mechanochemistry: opportunities for new and cleaner synthesis, *Chem. Soc. Rev.*, 2012, **41**, 413–447.

11 Bruker, *Apex II*, 2009, Bruker AXS Inc., Madison, Wisconsin, USA.

12 L. J. Barbour, LAYER - A computer program for the graphic display of intensity data as simulated precession photographs, *J. Appl. Crystallogr.*, 1999, **32**, 351–352.

13 G. M. Sheldrick, A short history of SHELX, *Acta Crystallogr. Sect. A Found. Crystallogr.*, 2007, **64**, 112–122.

14 L. J. Barbour, X-Seed — A Software Tool for Supramolecular Crystallography, *J. Supramol. Chem.*, 2001, **1**, 189–191.

15 O. V Dolomanov, L. J. Bourhis, R. J. Gildea, J. A. K. Howard and H. Puschmann, {\it OLEX2}: a complete structure solution, refinement and analysis program, *J. Appl. Crystallogr.*, 2009, **42**, 339–341.

16 C. F. Macrae, P. R. Edgington, P. McCabe, E. Pidcock, G. P. Shields, R. Taylor, M. Towler and J. van de Streek, {\it Mercury}: visualization and analysis of crystal structures, *J. Appl. Crystallogr.*, 2006, **39**, 453–457.

17 Persistence of Vision Pty. Ltd., 2004.

18 A. L. Spek, Structure validation in chemical crystallography, *Acta Crystallogr. Sect. D Biol. Crystallogr.*, 2009, **65**, 148–155.

19 N. M. Sykes, H. Su, E. Weber, S. A. Bourne and L. R. Nassimbeni, Crystallisation temperature control of stoichiometry and selectivity in host–guest compounds, *CrystEngComm*, 2017, **19**, 5892–5896.

20 Soft Imaging System GmbH, .

21 C. R. Groom, I. J. Bruno, M. P. Lightfoot and S. C. Ward, The Cambridge structural database, *Acta Crystallogr. Sect. B Struct. Sci. Cryst. Eng. Mater.*, 2016, **72**, 171–179.

Chapter 3: Manganese and Cobalt Mixed-Ligand Metal-Organic Frameworks

Different heteroleptic MOFs deriving from the combination of carboxylic and pyridine-based ligands have been isolated and structurally characterized. Three 2D Mn-based mixed-ligand MOFs were prepared using $Mn(NO_3)_2{\cdot}4H_2O$, H_2nipa or H_3btc and bipy. Metal salts were dissolved in water and the ligands in either DMF or DMA. The first MOF (**1**) is largely isostructural to a previously reported MOF in the literature (CSD code: EDAZEQ),[1] however differ in solvent content, and is thus a new compound. The second MOF (**2**) has been previously discovered in the research group of Dr Clive Oliver by interns Juliette Gilbert and Mathieu Dibone (unpublished result) but has now been further analyzed in this project. The third Mn-based MOF (**3**) synthesized is novel, with framework connectivity similar to that of **2** and hosting a different solvent molecule. The fourth mixed-ligand MOF (**4**) was prepared using $Co(NO_3)_2{\cdot}6H_2O$, H_2nipa and bipy and is novel.

3.1 Synthesis

3.1.1 $\{[Mn(nipa)(bipy)]0.5DMF{\cdot}H_2O\}_n$ (1)

$Mn(NO_3)_2{\cdot}4H_2O$ (30 mg, 0.12 mmol) was dissolved in 2 ml of water, whilst the ligands 5-nitro-1,3-benzenedicarboxylic acid (50 mg, 0.24 mmol) and 4,4'-bipyridine (38 mg, 0.24 mmol) were dissolved in 4 ml of DMF. The two solutions were stirred prior to and after mixing, after which the combined solutions were placed in a vial in an oven at 90°C for 72 h. This was followed by cooling at a rate of 10 °C h^{-1}. Yellow crystals formed once the solution reached room temperature. The method of preparation differs from the literature preparation which used $Mn(ClO_4)_2{\cdot}6H_2O$ as the metal salt and used a layering method involving DMF and methanol solutions. The literature MOF is formulated as $\{[Mn(NO_2\text{-ip})(bpy)]0.5DMF{\cdot}0.5MeOH\}_n$ where NO_2-ip and bpy are the equivalent abbreviations for the nipa and bipy abbreviations, respectively, used in this dissertation.

3.1.2 {[Mn(HBTC)(bipy)]0.5DMF·H_2O}$_n$ (2)

$Mn(NO_3)_2 \cdot 4H_2O$ (30 mg, 0.12 mmol) was dissolved in 2 ml of water, whilst benzene-1,3,5-tricarboxylic acid (25 mg, 0.12 mmol) and 4,4'-bipyridine (19 mg, 0.12 mmol) were dissolved in 4 ml of DMF. The two solutions were stirred prior to and after mixing, after which the combined solution was placed in a vial in an oven at 90 °C for 72 h then cooled down at a rate of 10 °C h^{-1}. Small colourless crystals were collected, which were found to be crystals of formic acid, a hydrolysis product of the DMF.[2] The synthesis was then repeated following the one previously used in the research group; the same amount of reagents as before were dissolved in less solvent (2 ml water and 2 ml DMF) and heated at the same temperature, but for a shorter time (48 h), after the cooling only a few vials showed small needle-shape yellow crystals but each had a lot of white precipitate. Crystals grew in the next week, whilst the precipitate redissolved. Complete conversion occurred over two to three weeks.

3.1.3 {[Mn(HBTC)(bipy)]0.5DMA·H_2O}$_n$ (3)

This method was the same as the modified procedure for the preparation of **2**, with the exception that DMA, instead of DMF, was used as a solvent. Blocks of flat yellow crystals formed after the solutions were cooled.

3.1.4 {[Co(nipa)(bipy)]0.5DMF}$_n$ (4)

$Co(NO_3)_2 \cdot 6H_2O$ (17 mg, 0.06 mmol), 5-nitro-1,3-benzenedicarboxylic acid (13 mg, 0.06 mmol) and 4,4'-bipyridine (10 mg, 0.06 mmol) were dissolved in a mixture of DMF (3 ml), H_2O (4 ml) and EtOH (1 ml). The resulting solution was stirred and set in the oven at 90 °C for 72 h. Then the solution was cooled to room temperature at the rate of 10 °C h^{-1}. Small red crystals were collected.

3.2 Structures

3.2.1 {[Mn(nipa)(bipy)]0.5DMF·H_2O}$_n$ (1)

MOF **1** crystallizes in the triclinic crystal system in the space group *P*-1. The asymmetric unit consists of one Mn(II) ion, one fully deprotonated, bridging 5-nitroisophthalate ligand and one pillaring 4,4'-bipyridine ligand. Mn1 has a distorted, octahedral coordination environment (Fig 3.1) with coordination bond distances that range from 2.104(2) to 2.295(2) Å. The equatorial positions are occupied by O1, O2, O3 and O4 of three different nipa ligands while the axial positions are occupied by N2 and N3 of different bipy ligands. The residual electron density maps seem to indicate that solvent molecules are present, but this could not be reliably modelled as DMF or water. Thus, the SQUEEZE routine in PLATON was used to remove the solvent contribution for final structure refinement. However, 0.5 DMF and 1 water molecule have been formulated per ASU based on thermogravimetric analysis. The coordination polymer extends in two dimensions via the nipa and bipy ligands. In the [010] direction the coordination extends via the carboxylate ligands of the nipa ligand. The O1 and O2 atoms of one carboxylate group link two metal ions into a pair via bridging, bidentate coordination, whilst the O3 and O4 atoms of the second carboxylate group link neighbouring pairs of metal ions via bidentate coordination (Fig. 3.2(a)). The bipy ligands extend the coordination in the [-101] direction and are also located in pairs in close vicinity to each other. Fig. 3.2(b) illustrates the 2D coordination sheets stacked along the [101] direction and are laterally shifted with respect to each other with their carboxylate ligands interdigitated.

PLATON identified no classical hydrogen bonds, however six C-H···O hydrogen bonds were found, three of which are between the 2D sheets (Table 3.2). In two of these inter-sheet hydrogen bonds the O5 atom of the nipa nitro group acts as bifurcated hydrogen bond acceptor of two pyridyl hydrogen atoms (C12-H12···O5 and C13-H13···O5), whilst the third inter-sheet hydrogen bond is between a pyridyl hydrogen atom and an oxygen atom of a carboxylate group (C15-H15···O4). The intra-sheet hydrogen bonds contribute to stabilizing the relative conformations of the ligands within the sheets.

Asymmetric unit formula	$C_{18}H_{11}MnN_3O_6$
Formula weight	420.24
Temperature/K	173.15
Crystal system	triclinic
Space group	*P*-1
a/Å	9.8397(17)
b/Å	10.2407(17)
c/Å	10.6151(18)
α/°	78.306(4)
β/°	68.951(4)
γ/°	81.954(4)
Volume/Å^3	974.9(3)
Z	2
ρ_{calc}g/cm^3	1.432
μ/mm^{-1}	0.715
F(000)	426.0
Crystal size/mm^3	0.28 × 0.26 × 0.2
Radiation	MoKα (λ = 0.71073)
2Θ range for data collection/°	4.072 to 57.316
Index ranges	-13 ≤ h ≤ 13, -13 ≤ k ≤ 13, -14 ≤ l ≤ 14
Reflections collected	21751
Independent reflections	4907 [R_{int} = 0.0501, R_{sigma} = 0.0475]
Data/restraints/parameters	4907/0/257
Goodness-of-fit on F^2	1.058
Final R indexes [I>=2σ (I)]	R_1 = 0.0422, wR_2 = 0.1070
Final R indexes [all data]	R_1 = 0.0520, wR_2 = 0.1123
Largest diff. peak/hole / e Å^{-3}	0.78/-0.86

Table 3.1 Crystal data and refinement parameters of **1**

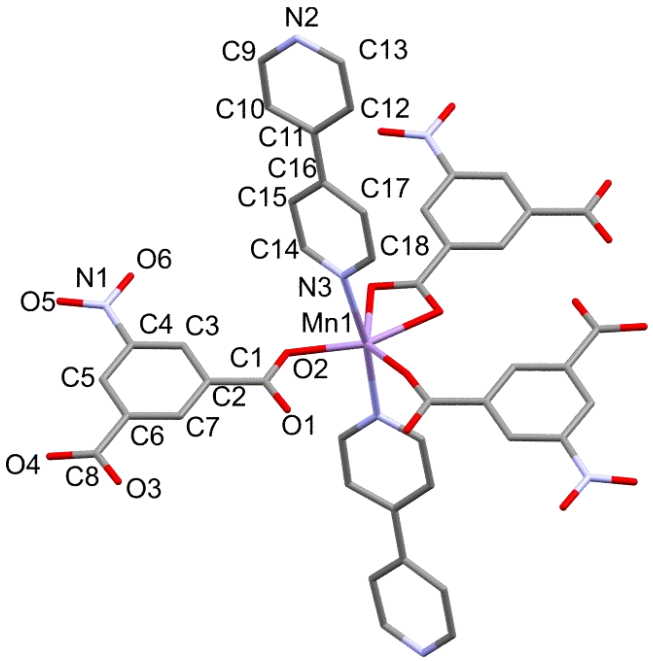

Figure 3.1 Coordination sphere of the unique manganese atom of **1**. Hydrogen atoms omitted for clarity. Solvent molecules were not modelled.

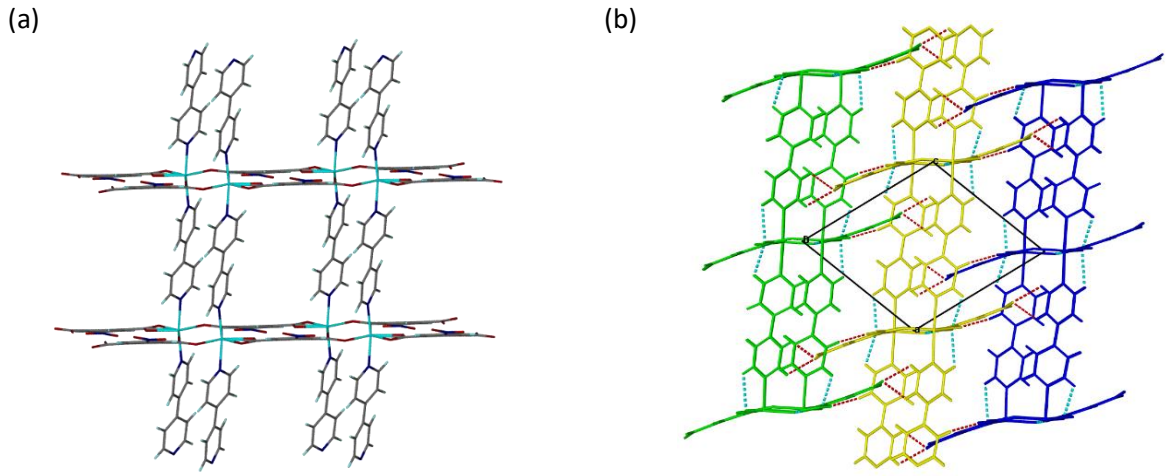

Figure 3.2 (a) shows the basic motif for the coordination polymer extension. Mn^{2+} ions are bridged by nipa and bipy ligands (b) View of 2D sheets (colour-coded down the *b*-axis stacking along the [101] direction with nipa ligands interdigitated and with intra-sheet C-H···O hydrogen bonds shown in turquoise and inter-sheet hydrogen bonds shown in red

Donor(D)–H···Acceptor(A)	D-H (Å)	H···A(Å)	D···A (Å)	D – H···A (°)	Symmetry code
C7-H7···O1	0.84	2.56	2.850(3)	102	x, y, z
C9-H9···O2	0.95	2.56	3.127(3)	119	2-x, 1-y, -z
C12-H12···O5	0.95	2.36	2.998(4)	124	2-x, -y, 1-z
C13-H13···O5	0.95	2.47	3.059(4)	120	2-x, -y, 1-z
C14-H14···O2	0.95	2.51	3.067(3)	117	1-x, 1-y, 1-z
C15-H15···O4	0.95	2.47	3.392(3)	164	-1+x,1+y, z

Table 3.2 Hydrogen bonding interactions as identified by PLATON for **1**

3.2.2 {[Mn(HBTC)(bipy)]0.5DMF·H_2O}$_n$ (2)

MOF **2** is largely isostructural to **1**, also crystallizing in the triclinic crystal system in space group *P*-1. The asymmetric unit is composed of a Mn(II) ion, a bridging, partially deprotonated benzene-1,3,5-tricarboxylic acid ligand (the O3 hydroxyl group is not deprotonated) and a pillaring 4,4'-bipyridine ligand (Fig 3.3). Mn1 has a distorted, octahedral environment, with coordination bond distances that range from 2.128(2) to 2.340(2) Å. The equatorial positions are occupied by O1, O2, O5 and O6 of three different HBTC ligands while the axial positions are occupied by N1 and N2 of different bipy ligands. One half of a DMF molecule, modelled about a centre of inversion, and one water molecule was located in the structure. The position of the carbonyl oxygen atom, and thus the orientation of the DMF molecule, was rationalized based on the proximity of the oxygen atom of the water molecule within hydrogen bonding distance (2.891 Å). The coordination polymer extends in the same fashion as for **1** with the carboxylate oxygen and bipyridyl nitrogen atoms involved in ligation to the metal centres (Fig. 3.4(a)).

PLATON identified three classical O-H···O hydrogen bonds, two being between water and a carboxylate (O1W-H1WB···O2), as well as a carboxylic acid group (O3-H3···O1W) of a 2D sheet, whilst the third O-H···O hydrogen bond is between a water and a DMF solvent molecule (O1W-H1WA···O7). The remaining hydrogen bonds are two intra-sheet C-H···O hydrogen bonds (C16-H16···O5 and C19-H19···O5) and two inter-sheet C-H···O hydrogen bonds (C14-H14···O4 and C15-H15···O4) between the 2D sheets (Table 3.2). The latter two C-H···O hydrogen bonds as for **1**, involve hydrogen bonding of pyridyl hydrogen atoms to a non-coordination oxygen atom.

Asymmetric unit formula	$C_{20.5}H_{17.5}Mn_{2.5}O_{7.5}$
Formula weight	473.81
Temperature/K	173.15
Crystal system	triclinic
Space group	*P*-1
***a*/Å**	10.1938(8)
***b*/Å**	10.3186(8)
***c*/Å**	10.9003(11)
α/°	66.186(2)
β/°	75.093(3)
γ/°	85.935(2)
Volume/Å^3	1012.93(15)
Z	2
ρ_{calc}g/cm^3	1.553
μ/mm^{-1}	0.703
F(000)	486.0
Crystal size/mm^3	0.36 × 0.12 × 0.10
Radiation	MoKα (λ = 0.71073)
2Θ range for data collection/°	4.138 to 61.444
Index ranges	-14 ≤ h ≤ 14, -14 ≤ k ≤ 14, -15 ≤ l ≤ 15
Reflections collected	13599
Independent reflections	6235 [R_{int} = 0.0346, R_{sigma} = 0.0503]
Data/restraints/parameters	6235/0/316
Goodness-of-fit on F^2	1.079
Final R indexes [I>=2σ (I)]	R_1 = 0.0549, wR_2 = 0.1395
Final R indexes [all data]	R_1 = 0.0714, wR_2 = 0.1494
Largest diff. peak/hole / e Å^{-3}	1.48/-0.59

Table 3.3 Crystal data and refinement parameters of **2**

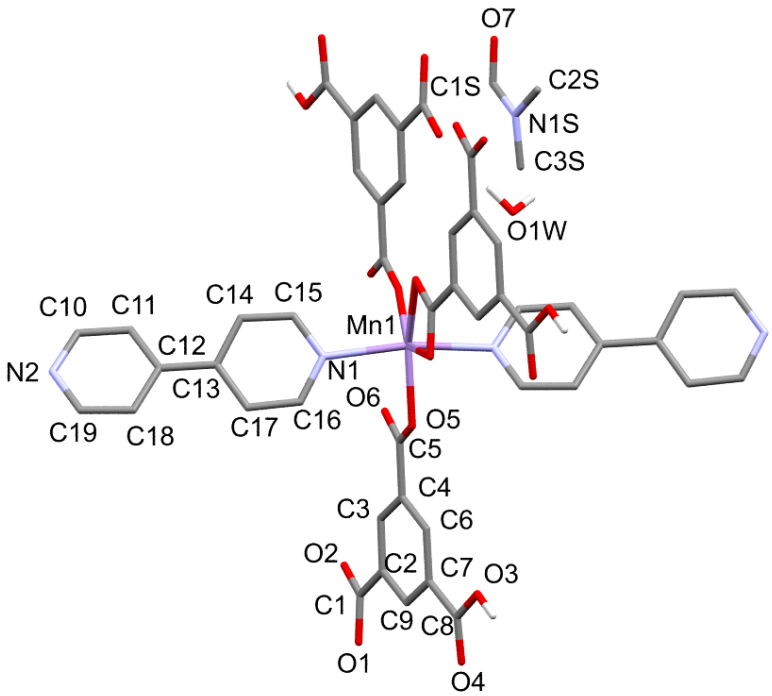

Figure 3.3 Coordination sphere of the unique manganese ion in **2**. Hydrogen atoms, except for those of water molecule and -COOH unit, omitted for clarity.

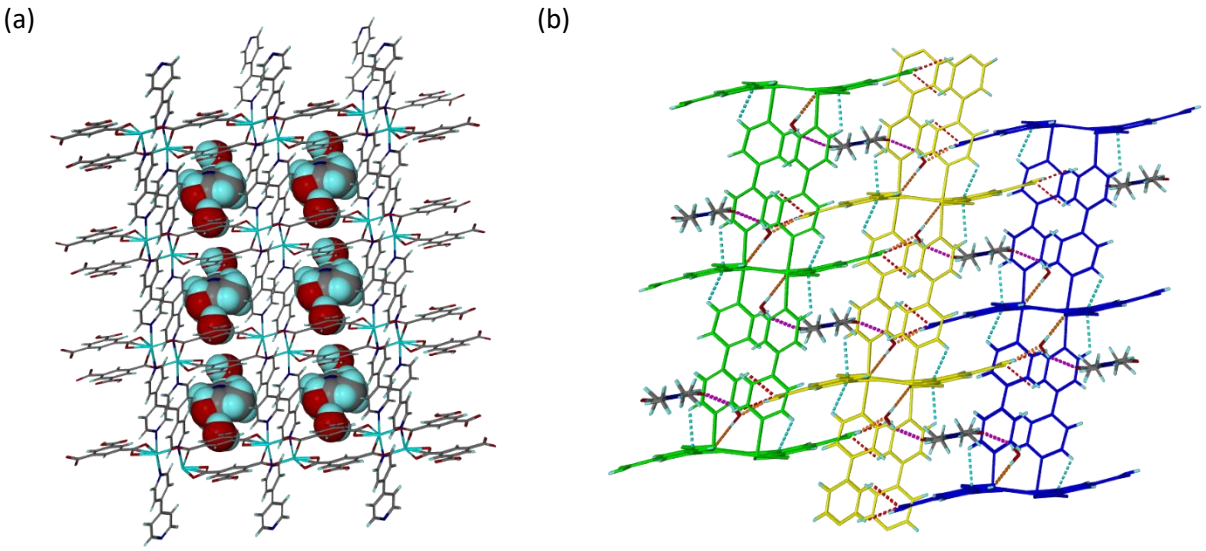

Figure 3.4 (a) **2** shows the same basic motif of the 2D coordination polymer as for **1** with included DMF and water solvent molecules shown in space-filling mode (b) View of 2D sheets (colour-coded) down the *a* axis and stacking along the [011] direction. Intra- and inter-sheet C-H···O hydrogen bonds are shown in turquoise and red respectively; inter-solvent O-H···O hydrogen bonds are shown in purple; water···sheet O-H···O and C-H···O hydrogen bonds are shown in orange.

Donor(D)–H···Acceptor(A)	D-H (Å)	H···A(Å)	D···A (Å)	D – H···A (°)	Symmetry code
O1W-H1WA···O7	0.83	2.23	2.891(1)	137	-x, 3-y, -1-z
O1W-H1WB···O2	0.85	2.00	2.843(4)	174	-x, 4-y, -1-z
O3-H3···O1W	0.84	1.80	2.625(4)	165	-x, 4-y, -z
C14-H14···O4	0.95	2.45	3.011(4)	118	x, -1+y, z
C15-H15···O4	0.95	2.36	2.985(4)	123	x, -1+y, z
C16-H16···O5	0.95	2.59	3.121(4)	116	-1+x, -1+y, 1+z
C19-H19···O5	0.95	2.56	3.083(4)	115	-1+x, y, z

Table 3.4 Hydrogen bonding interactions as identified by PLATON for **2**

3.2.3 {[Mn(HBTC)(bipy)]0.5DMA·H_2O}$_n$ (3)

3 crystallizes in the monoclinic crystal system in the space group *C2/c*. The ASU, is similar to that of **2**, consisting of one Mn(II) ion with a distorted, octahedral environment, one deprotonated, bridging HBTC ligand (the O3 hydroxyl oxygen atom is not deprotonated) and a bipy pillaring ligand. The coordination bond distances range from 2.135(2) to 2.320(2) Å with the equatorial positions occupied by O1, O2, O5 and O6 of three different HBTC ligands while axial positions are occupied by N1 and N2 of two different bipy ligands. In the ASU there is one full molecule of water and half of a DMA molecule located about an inversion centre. Refinement constraints were applied to the DMA molecule based on mode values for bonded and non-bonded distances for non-ligated DMA molecules on the CSD.[3]The position of the carbonyl oxygen atom, and thus the orientation of the DMA molecule, was rationalized based on the proximity of the oxygen atom of the water molecule within hydrogen bonding distance (2.937 Å). The coordination polymer extends in the same fashion as for **1** and **2** (Fig. 3.6) with the non-coordinating carboxylic acid group of the HBTC ligand alternating between an 'up' and 'down' orientation along the *c* direction of the 2D sheet.

PLATON identified three classical O-H···O hydrogen bonds, one being between water and the DMA molecule (O1W-H1WA···O1S), with the other two being between water and a carboxylate oxygen atom (O1W-H1WB···O6), and water and a carboxylic acid hydrogen atom (O3-H3···O1W) of a 2D sheet. The remaining hydrogen bonds are one C-H···O hydrogen bond between the water and a DMA molecule (C3S-H3SA···O1W), three inter-sheet C-H···O hydrogen bonds (C14-H14···O4, C15-H15···O4 and C17-H17···O5) and one intra-sheet C-H···O hydrogen bond (C16-H16···O2).

Asymmetric unit formula	$C_{10.5}H_{9.25}Mn_{0.5}N_{1.25}O_{3.75}$
Formula weight	240.41
Temperature/K	100.09
Crystal system	monoclinic
Space group	*C*2/*c*
***a*/Å**	18.001(5)
***b*/Å**	11.609(3)
***c*/Å**	20.301(5)
α/°	90
β/°	103.396(5)
γ/°	90
Volume/Å^3	4126.8(18)
Z	16
ρ_{calc}g/cm^3	1.548
μ/mm^{-1}	0.691
F(000)	1976.0
Crystal size/mm^3	0.20 × 0.14 × 0.10
Radiation	MoKα (λ = 0.71073)
2Θ range for data collection/°	4.124 to 56.746
Index ranges	$-23 \leq h \leq 24$, $-15 \leq k \leq 15$, $-27 \leq l \leq 27$
Reflections collected	62665
Independent reflections	5176 [R_{int} = 0.0868, R_{sigma} = 0.0411]
Data/restraints/parameters	5176/11/290
Goodness-of-fit on F^2	1.060
Final R indexes [I>=2σ (I)]	R_1 = 0.0541, wR_2 = 0.1347
Final R indexes [all data]	R_1 = 0.0751, wR_2 = 0.1476
Largest diff. peak/hole / e Å^{-3}	1.68/-1.18

Table 3.5 Crystal data and refinement parameters of **3**

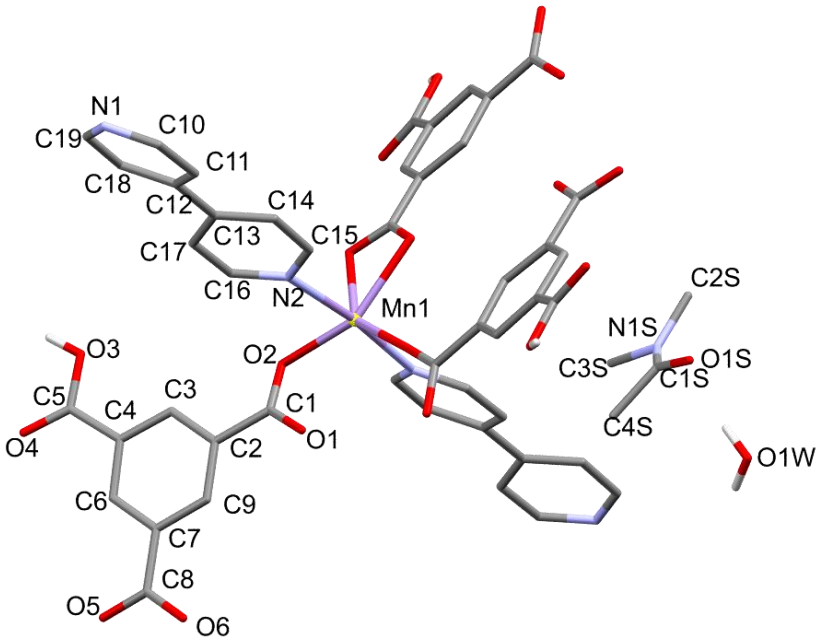

Figure 3.5 Coordination sphere of the unique manganese ion of **3**. Hydrogen, except for those belonging to the water molecule and the -COOH units, omitted for clarity

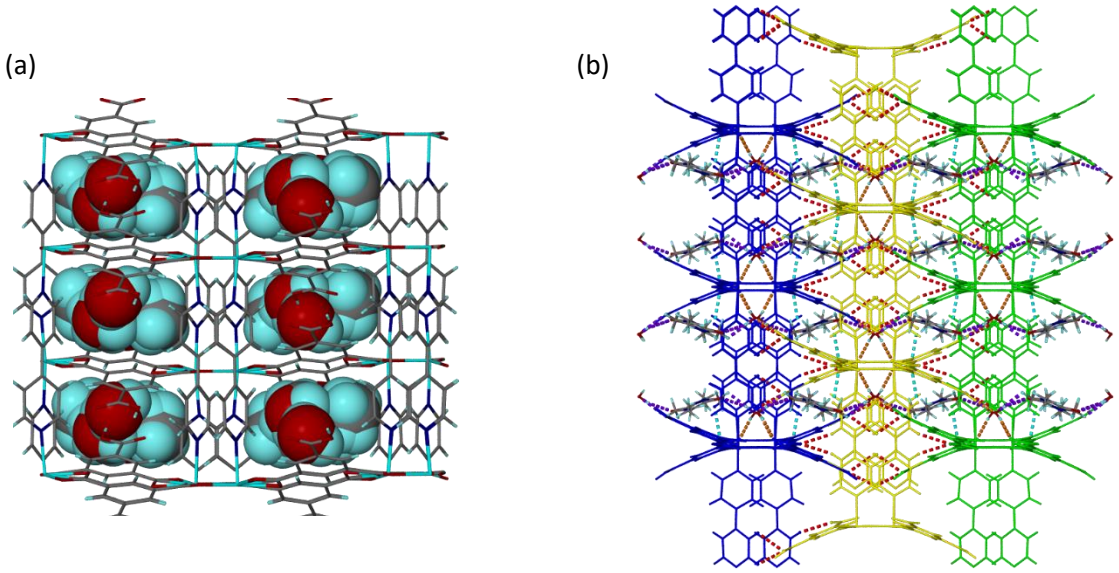

Figure 3.6 (a) shows the same basic motif of the 2D coordination polymer as for **1** and **2**. DMA and water solvent molecules are shown in space-filling mode (b) View of 2D sheets (colour-coded) down the *c*-axis and stacking along the [100] direction. Intra- and inter-sheet C-H···O hydrogen bonds are shown in turquoise and red, respectively; inter-solvent O-H···O and C-H···O hydrogen bonds are shown in purple; water···sheet O-H···O and C-H···O hydrogen bonds are shown in orange.

Donor(D) – H···Acceptor(A)	D-H (Å)	H···A(Å)	D···A (Å)	D – H···A (°)	Symmetry code
O1W-H1WA···O1S	0.87	2.07	2.915(7)	164	x, y, z
O1W-H1WB···O6	0.87	2.01	2.857(5)	163	1/2-x, 3/2-y, 1-z
O3-H3···O1W	0.84	1.76	2.604(4)	176	1-x, 1-y, 1-z
C3S-H3SA···O1W	0.98	2.5	3.020(1)	113	1/2-x, 3/2-y, 1-z
C14-H14···O4	0.95	2.46	3.021(4)	117	1/2-x, 3/2-y, 1-z
C15-H15···O4	0.95	2.32	2.960(4)	125	1/2-x, 3/2-y, 1-z
C16-H16···O2	0.95	2.55	3.101(4)	117	-x, 1+y, 1/2-z
C17-H17···O5	0.95	2.60	3.518(4)	163	-1/2+x, 3/2-y, -1/2+z

Table 3.6 Hydrogen bonding interactions as identified by PLATON for **3**

3.2.4 {[Co(nipa)(bipy)]0.5DMF}$_n$ (4)

MOF **4** is largely isostructural to **1**, also crystallizing in the triclinic crystal system in space group *P*-1. The asymmetric unit is composed of a Co(II) ion, a fully deprotonated, bridging 5-nitroisophthalate ligand and one pillaring 4,4'-bipyridine ligand. Co1 has a distorted, octahedral coordination environment (Fig 3.7) with coordination bonds that range from 2.029(2) to 2.232(3) Å. The equatorial positions are occupied by O1, O2, O3 and O4 of three different nipa ligands while the axial positions are occupied by N1 and N2 of different bipy ligands. One of the bipy pyridyl rings were found to exhibit rotational disorder about the C11-C12 bond with atoms C9, C10, C17 and C18 disorder over two positions. The major component (labelled A) refined to a site occupancy factor (sof) of 0.63. The residual electron density maps after modelling the disorder indicated the possible presence of a DMF molecule. One half of a DMF molecule was modelled in the ASU about an inversion centre. A high residual density peak of 3.47 e Å^{-3} was deemed to be too close to the DMF molecule to be modelled as a water molecule and was not supported by thermogravimetric analysis. This peak could indicate more disordered positions of the DMF molecule but additional positions could not be reliably modelled.

PLATON identified no classical hydrogen bonds but seven C-H···O hydrogen bonds were listed. Four of these involve intra-sheet hydrogen bonds, whilst the three inter-sheet hydrogen bonds are between the same atoms as found in the case of **1**. No hydrogen bonds were identified between the solvent and the 2D sheets.

Asymmetric unit formula	$C_{19.5}H_{14.5}CoN_{3.5}O_{6.5}$
Formula weight	460.78
Temperature/K	100.15
Crystal system	triclinic
Space group	*P*-1
***a*/Å**	10.101(2)
***b*/Å**	10.185(2)
***c*/Å**	10.672(2)
α/°	65.813(3)
β/°	76.134(4)
γ/°	79.304(4)
Volume/Å^3	967.6(3)
Z	2
ρ_{calc}g/cm^3	1.582
μ/mm^{-1}	0.935
F(000)	470.0
Crystal size/mm^3	0.3 × 0.14 × 0.07
Radiation	MoKα (λ = 0.71073)
2Θ range for data collection/°	4.174 to 56.69
Index ranges	-13 ≤ h ≤ 13, -13 ≤ k ≤ 13, -14 ≤ l ≤ 14
Reflections collected	18723
Independent reflections	4824 [R_{int} = 0.0511, R_{sigma} = 0.0542]
Data/restraints/parameters	4824/55/332
Goodness-of-fit on F^2	1.034
Final R indexes [I>=2σ (I)]	R_1 = 0.0596, wR_2 = 0.1593
Final R indexes [all data]	R_1 = 0.0783, wR_2 = 0.1721
Largest diff. peak/hole / e Å^{-3}	3.47/-0.77

Table 3.7 Crystal data and refinement parameters of **4**

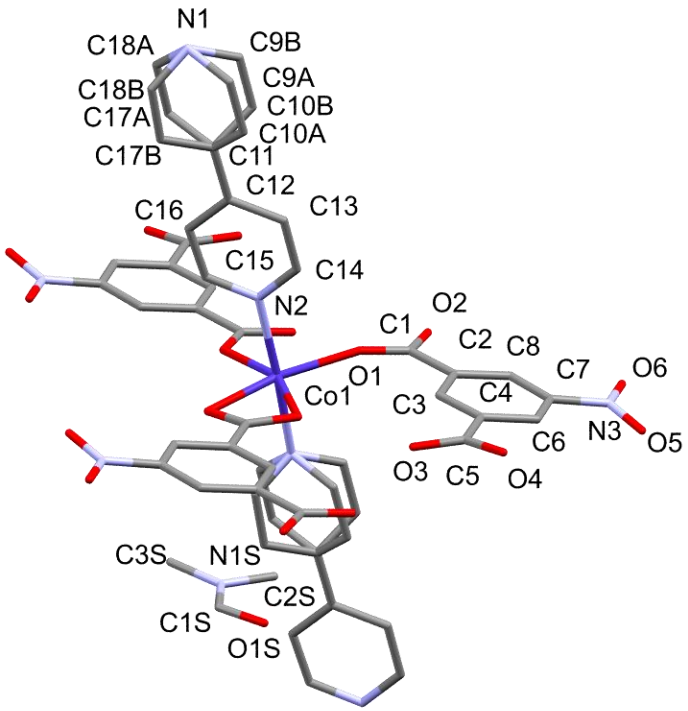

Figure 3.7 Coordination sphere of the unique cobalt ion in **4**. Hydrogen atoms omitted for clarity.

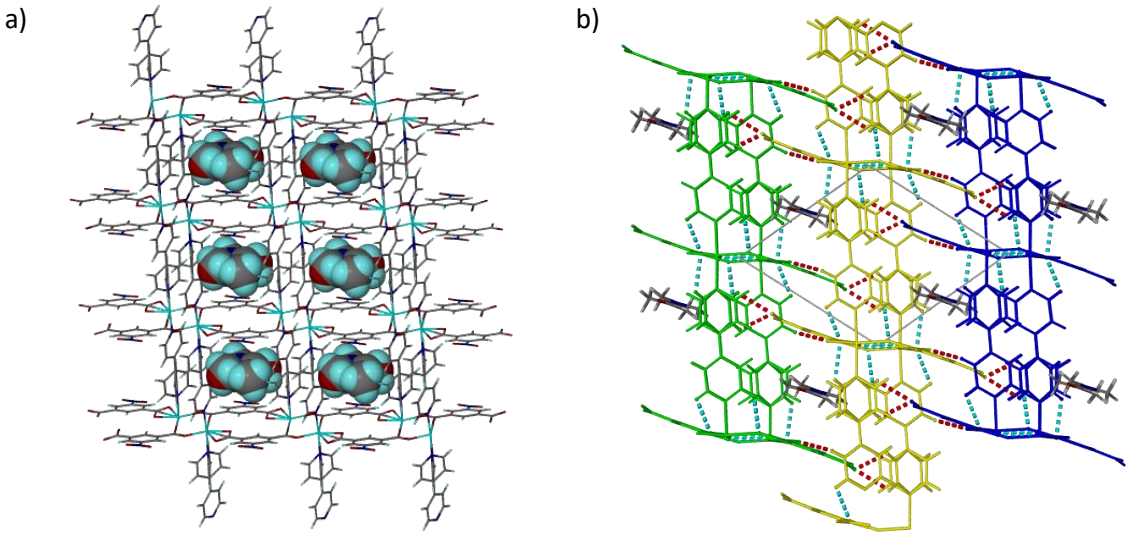

Figure 3.8 (a) shows the same basic motif of the 2D coordination polymer as for **1** with Co^{2+} ions replacing the Mn^{2+} ions. DMF solvent molecules shown in space-filling mode (b) 2D sheets (colour-coded) stacking along the [011] direction. Intra- and inter-sheet C-H···O hydrogen bonds are shown in turquoise and red, respectively.

Donor(D)–H···Acceptor(A)	D-H (Å)	H···A(Å)	D···A (Å)	D – H···A (°)	Symmetry code
C3-H3···O3	0.95	2.47	3.373(5)	158	-x, 2-y, -z
C9A-H9A···O5	0.95	2.58	3.026(8)	109	-x, 2-y, 1-z
C10A-H10A···O5	0.95	2.33	2.888(9)	117	-x, 2-y, 1-z
C14-H14···O1	0.95	2.56	3.064(5)	114	x, -1+y, 1+z
C15-H15···O2	0.95	2.5	2.981(5)	111	1-x, 1-y, 1-z
C16-H16···O4	0.95	2.45	3.380(5)	165	1+x, -1+y, z
C18A-H18A···O2	0.95	2.47	3.028(7)	118	1-x, 2-y, -z

Table 3.8 Hydrogen bonding interactions as identified by PLATON for **4**.

3.3 Crystal Packing and Void Space Comparison

Each MOF discussed here has the same metal-ligand connectivities in their respective frameworks. Mn/Co-btc/nipa mono-dimensional chains pillared by 4,4'-bipyridine, lead to the formation of 2D MOFs with empty cavities that host solvent molecules (Figs. 3.9-3.13). Mercury was used in order to calculate and visually show the void spaces in the structures, after solvent coordinates were deleted (Figs. 3.14-3.17). Each structure shows a different percentage and shape of the void spaces. In **1**, the voids are discrete, in **2** and **4** they are straight channels, with wider and narrower portions, that run through the framework all with the same orientation while in **3** the channels orientations alternated. **1**, **2** and **4** have similar parallel orientations of their acid ligands whilst **3** shows an alternating 'up/down' orientation of its acid ligand. The void space data for **1**-**4** are presented in Table 3.9.

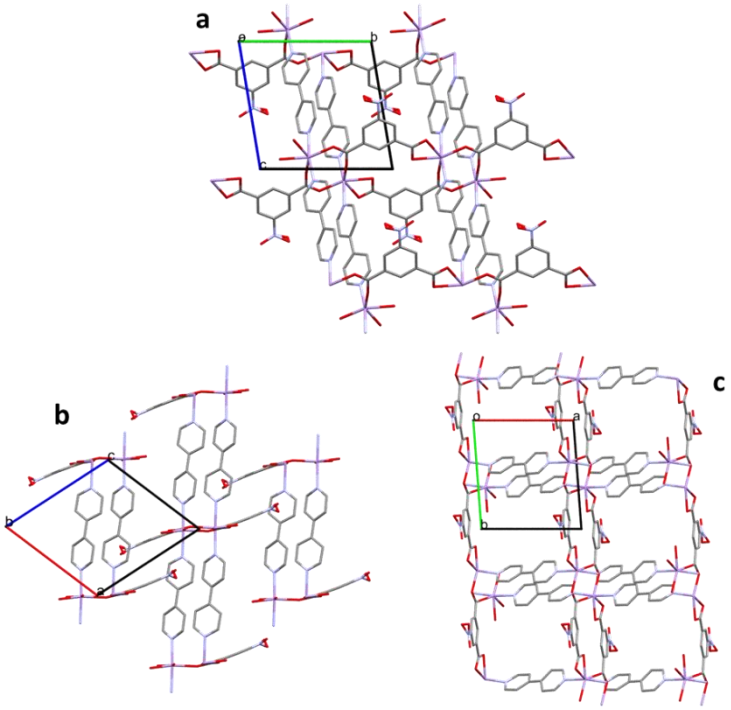

Figure 3.9 View of **1** along the three axes: axis *a* (a), axis *b* (b) and axis *c* (c). Unit cell is portrayed in every view and each axis is associated to a colour: red (*a*), green (*b*) and blue (*c*).

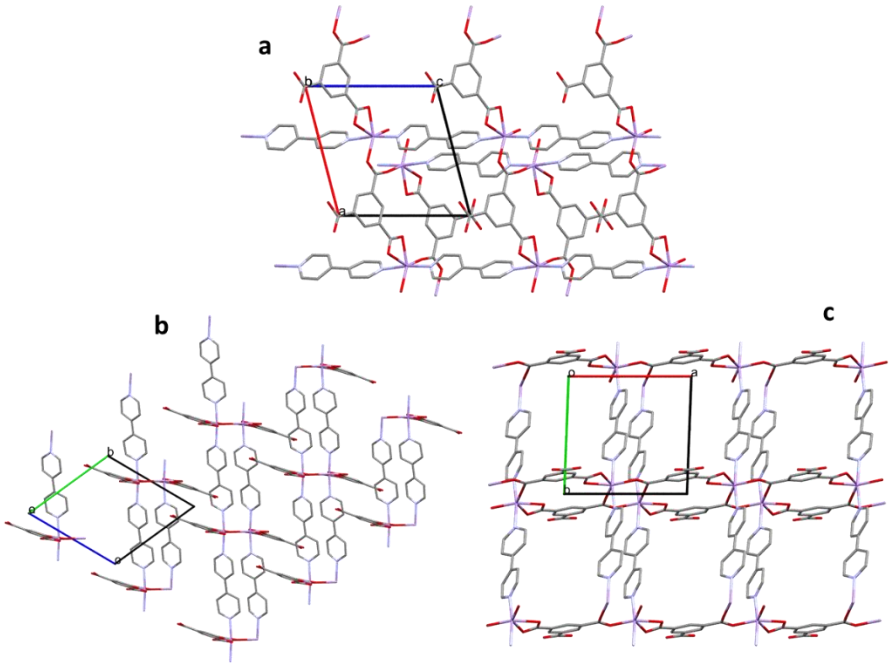

Figure 3.10 View of **2** along the three axes: axis *b* (a), axis *a* (b) and axis *c* (c). Unit cell is portrayed in every view and each axis is associated to a colour: red (*a*), green (*b*) and blue (*c*).

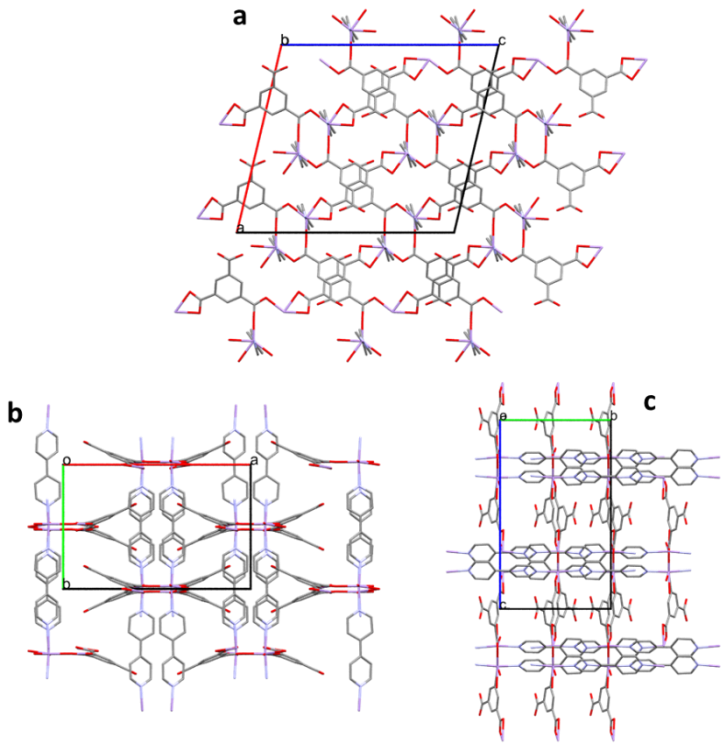

Figure 3. 11 View of **3** along the three axes: axis *b* (a), axis *c* (b) and axis *a* (c). Unit cell is portrayed in every view and each axis is associated to a colour: red (*a*), green (*b*) and blue (*c*).

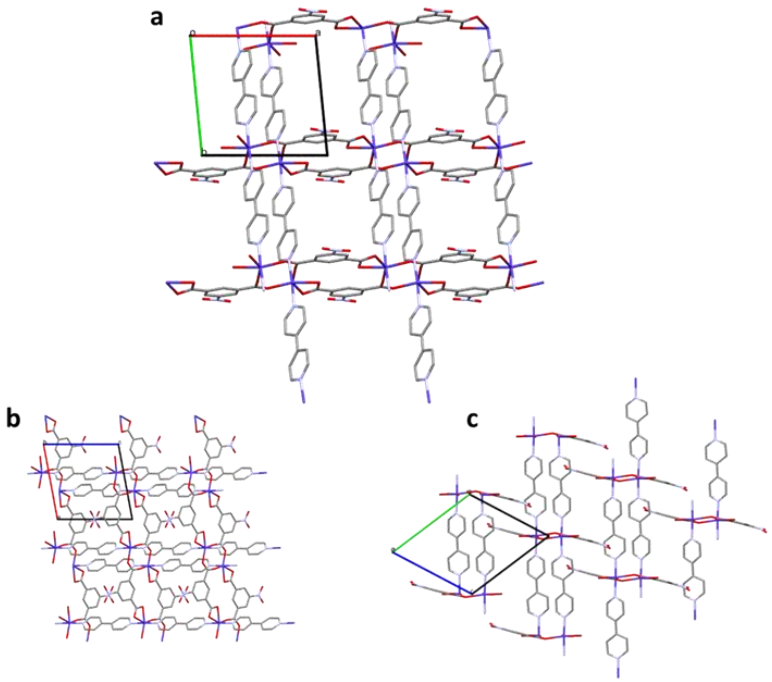

Figure 3.12 View of **4** along axes *c* (a), *b* (b) and *a* (c). Unit cell is portrayed in every view and each axis is associated to a colour: red (*a*), green (*b*) and blue (*c*).

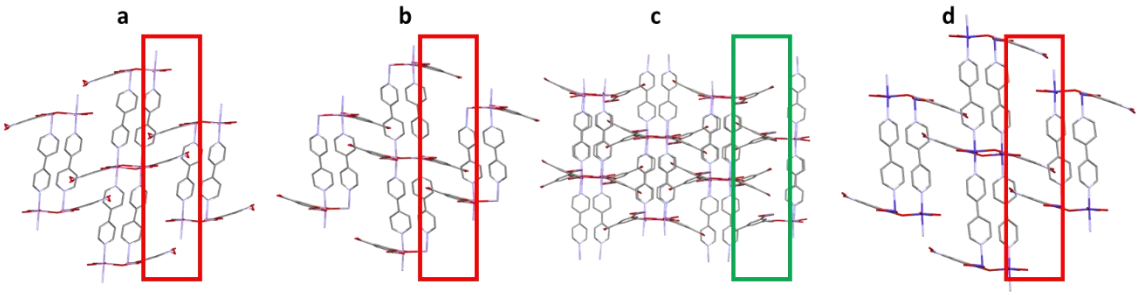

Figure 3.13 View of **1(a)**, **2(b)**, **3(c)** and **4(d)** along axes *b*, *a*, *c* and *a*, respectively. The extremities not involved in any kind of bonds (nitro group for **1** and **4**, carboxylic group for **2** and **3**) are highlighted by red rectangles, green for **3**. The different orientation of these extremities constitutes the main difference between the three structures.

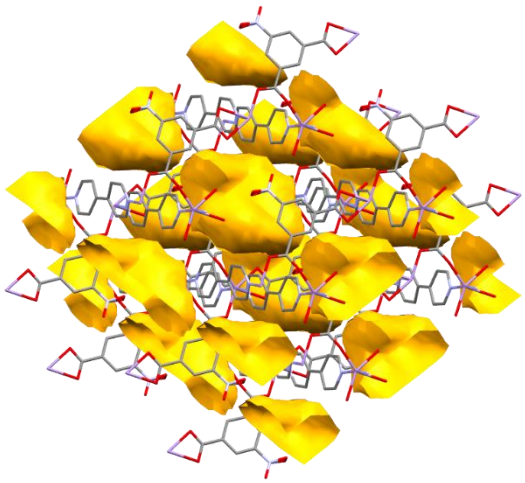

Figure 3.14 Crystal packing of **1** showing isolated voids.

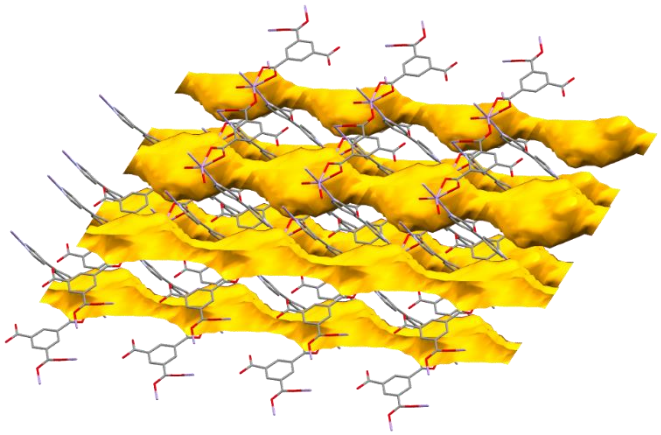

Figure 3.15 Crystal packing of **2** showing corrugated void channels throughout the structure all with the same orientation.

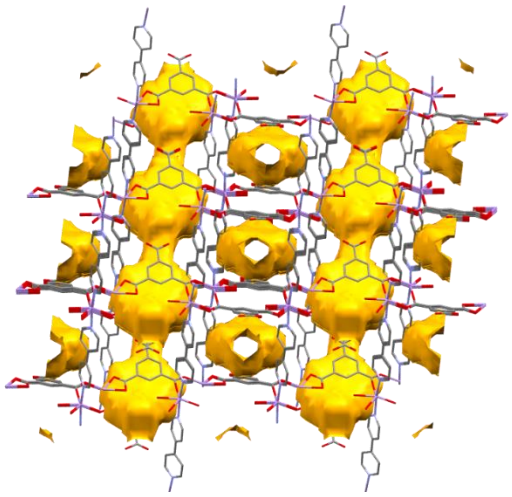

Figure 3.16 Crystal packing of **3** showing void channels throughout the structure with alternating orientations.

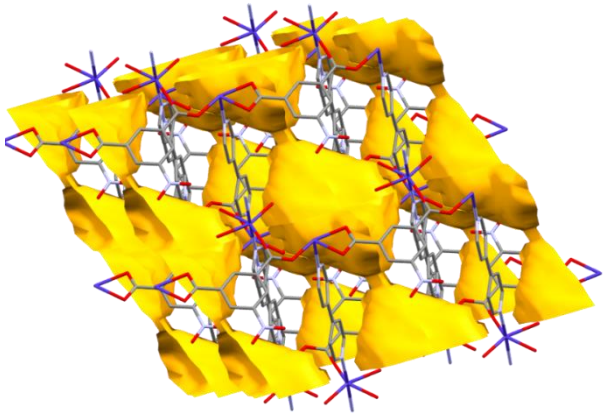

Figure 3.17 Crystal packing of **4** showing voids connected by small channels.

	Unit Cell Volume (Å^3)	Void Volume (Å^3)	%
(1)	974.9	152.73	15.7
(2)	1012.9	160.94	15.9
(3)	4126.8	727.63	17.6
(4)	967.6	163.41	16.9

Table 3.9 Void volumes for each structure, calculated in Mercury using a probe radius of 1.2 Å and grid spacing of 0.7 Å

3.4 Thermal Analysis

Hot Stage Microscopy, Differential Scanning Calorimetry and Thermal Gravimetric Analysis

{[Mn(nipa)(bipy)]0.5DMF·H_2O}$_n$ (1): HSM pictures show that bubbling starts at 137 °C, pointing to thermally induced crystal desolvation, with bubbling continuing during decomposition (Fig. 3.18). Loss of solvent is concomitant with the opacification of the crystals. Correspondingly, the DSC thermogram shows three endothermic peaks (Fig. 3.19). The first one is small and broad, centred around 60 °C, and probably corresponds to the loss of water, whilst the second peak, strongly asymmetric and very prominent from 120 °C to 280 °C, probably corresponds to the loss of DMF. The last endothermic peak, around 336 °C, is associated with decomposition of the MOF. The TGA trace shows that mass loss starts around 40 °C, and proceeds up to 300 °C, with the biggest loss, probably due to desolvation of DMF, occurring in the interval 180-280 °C.

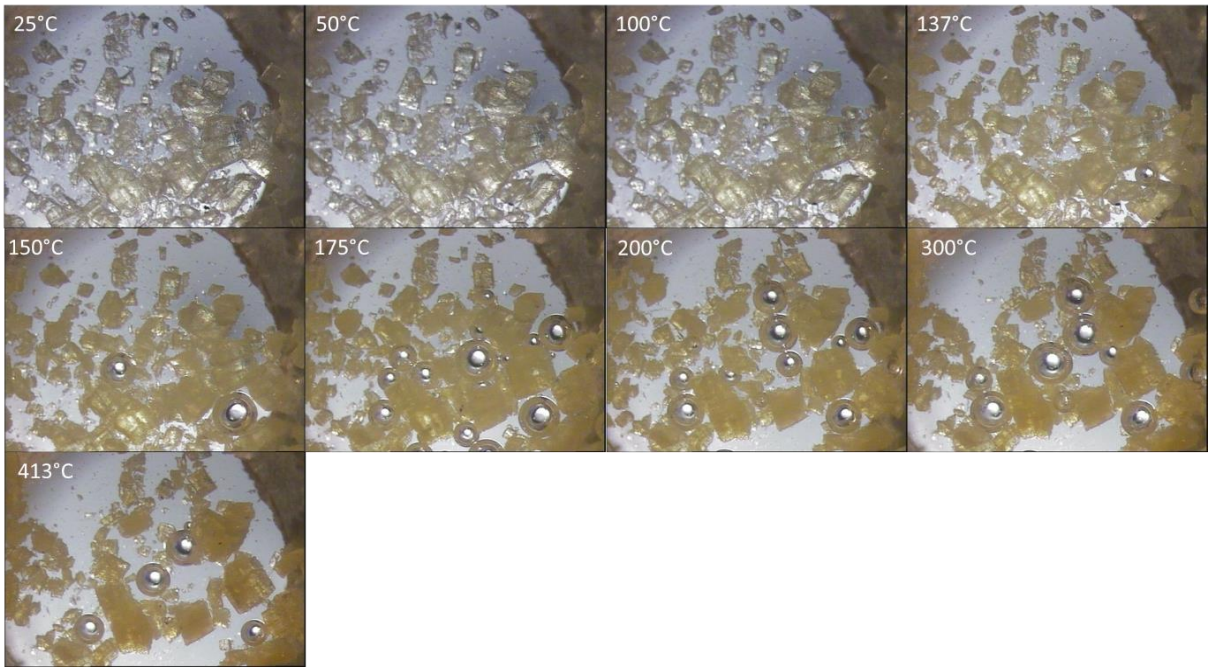

Figure 3.18 Representative HSM images of **1**.

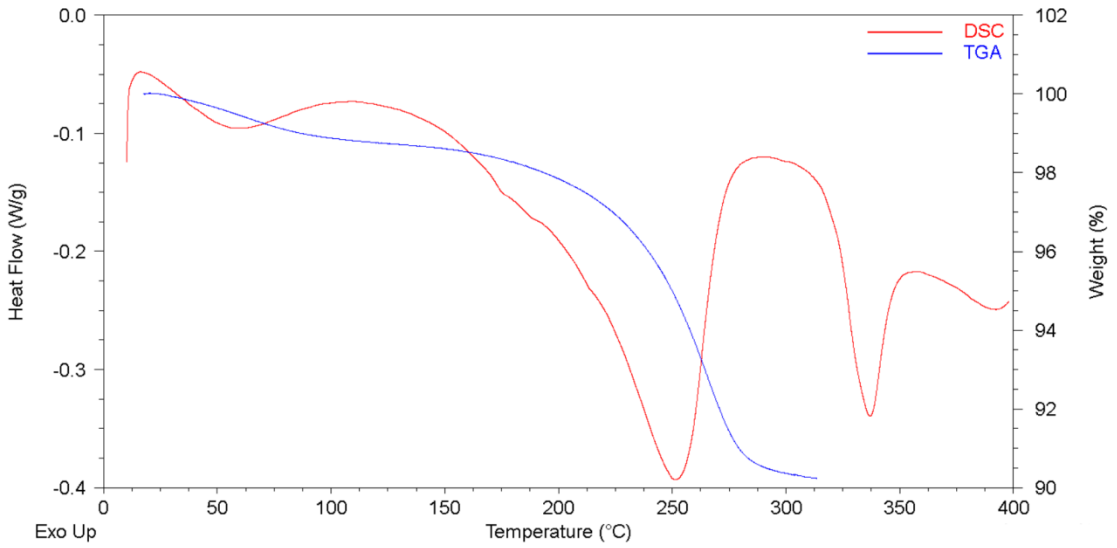

Figure 3.19 Overlay of DSC (red) and TGA (blue) of **1**.

{[Mn(HBTC)(bipy)]0.5DMF·H_2O}$_n$ (2): HSM pictures show the appearance of bubbles from 75 °C until decomposition, which occurs at ~400 °C (Fig. 3.20). Also here opacification of the crystals is evident during the solvent loss. DSC thermogram shows a first asymmetric peak centred at 90°C then a very broad peak in the interval 120-250 °C and finally a small peak at 276 °C with a shoulder at 283 °C (Fig. 3.21). The first endothermic peak overlaps with the first significant mass loss in the TGA thermogram, corresponding to a 3.7% mass loss (Fig 3.21). The second broad peak instead overlaps with the large mass loss observed in the TGA trace from 100 to 300 °C. These two peaks can then be attributed to desolvation. The last endothermic peak is not related to a mass loss and it may then be related to a low energy barrier phase transition (not further investigated), which precedes the framework decomposition near to 400 °C.

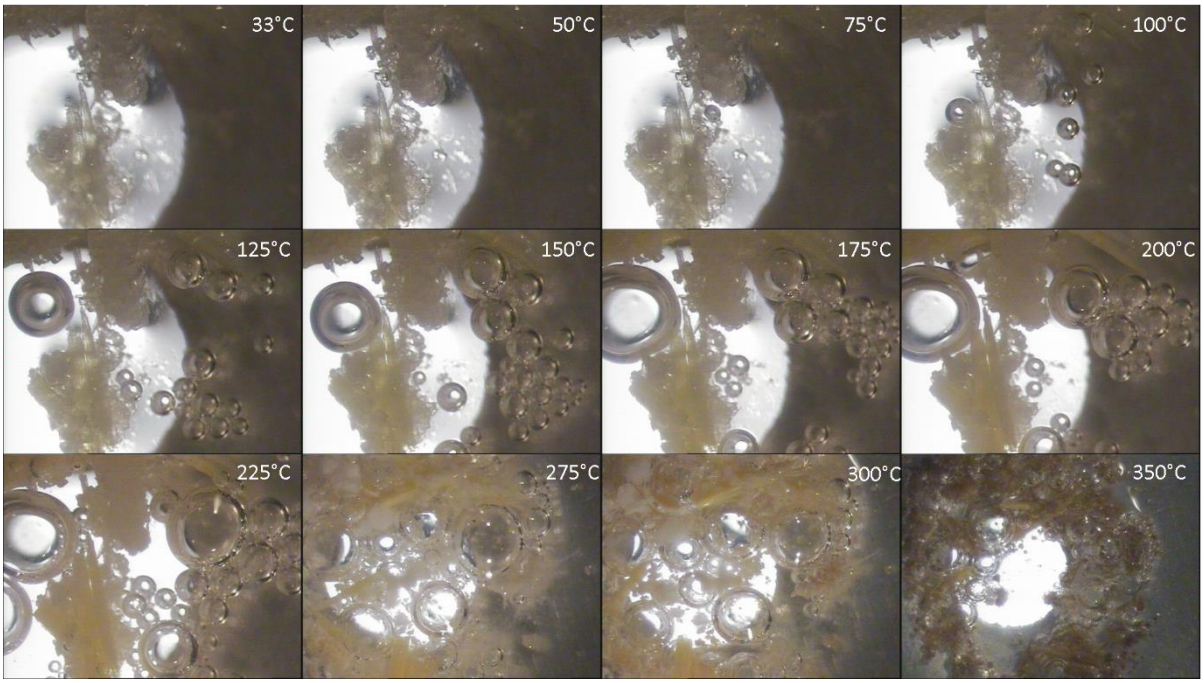

Figure 3.20 Representative HSM images of **2.**

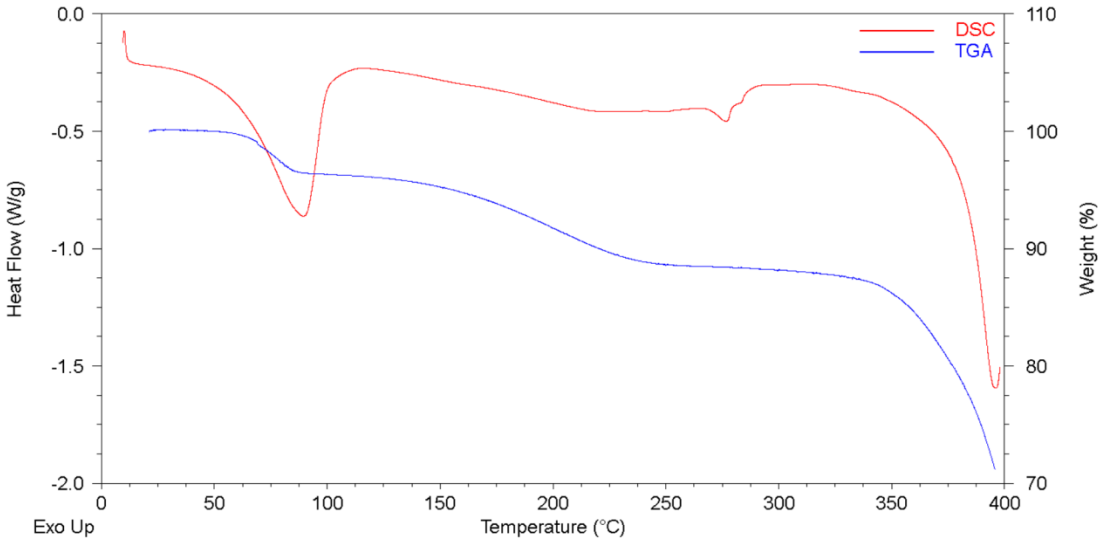

Figure 3.21 Overlay of DSC (red) and TGA (blue) thermogram of **2**.

{[Mn(HBTC)(bipy)]0.5DMA·H_2O}$_n$ (3): HSM pictures highlight that solvent loss starts at around 90 °C and ends at 300 °C (Fig 3.22). Some bubbles also appear as the crystals start turning brown, it is a sign of decomposition, probably due to decarboxylation of the COO groups. Both DSC and TGA thermograms (Fig 3.23) indicate desolvation events similar to that of **2**, with an endothermic peak centred at 116 °C, a very broad peak centred around 250 °C and a small, sharp peak at 295 °C with a little shoulder at 301 °C. As was the case for **2**, the first two could be related to the solvent loss even if these are not perfectly overlapped with the mass loss showed in the TGA thermogram.

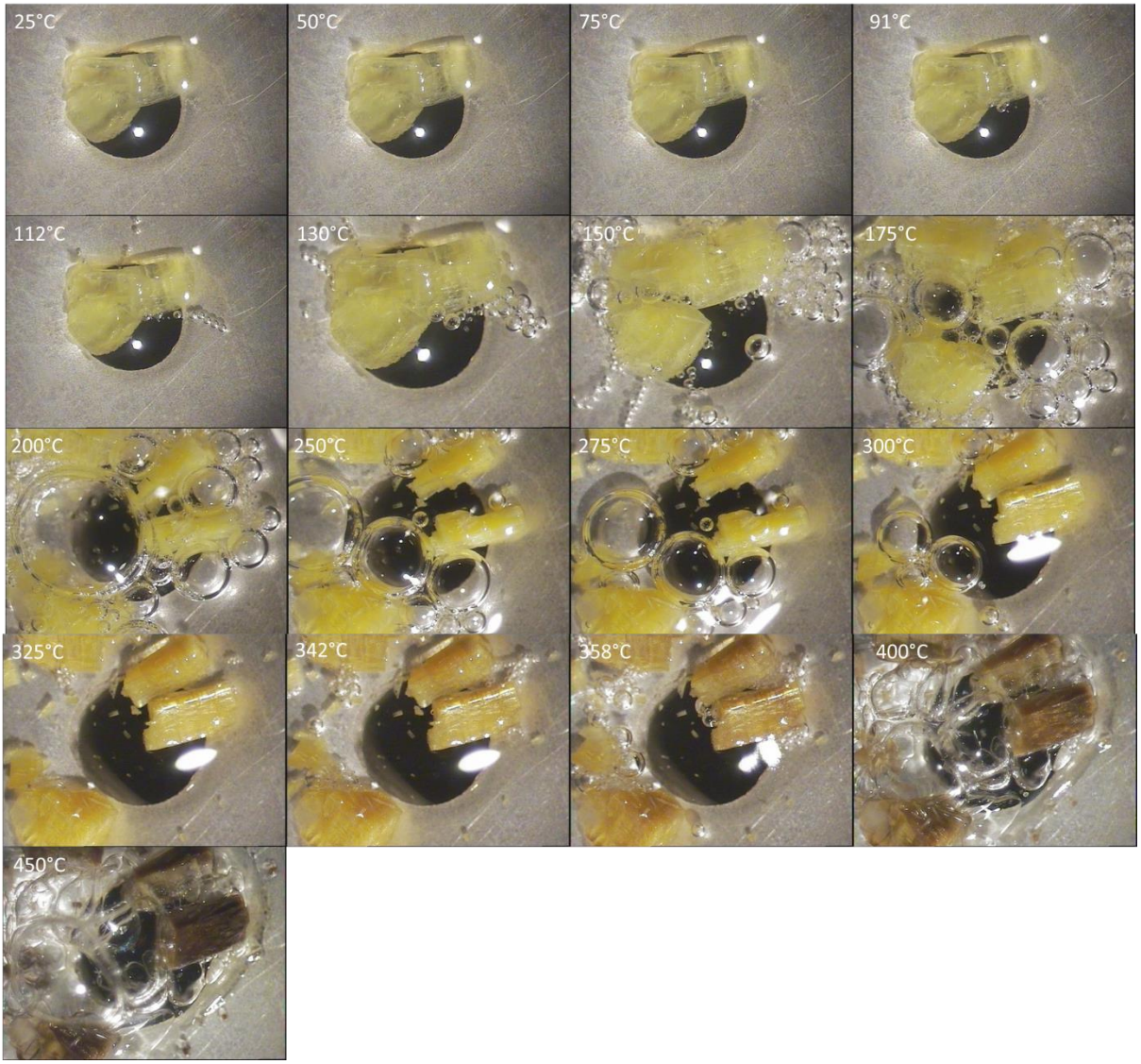

Figure 3.22 HSM images of **3**. Clear yellow crystals of **3** become first opaque (loss of solvent) and then brownish after 300 °C owing to decomposition.

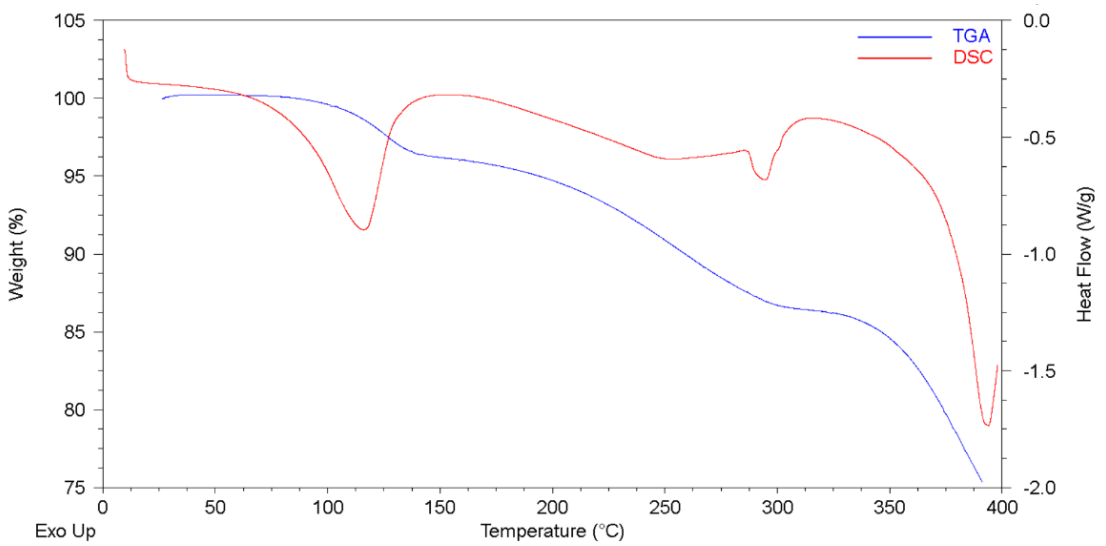

Figure 3.23 Overlay of DSC (red) and TGA (blue) thermograms of **3**.

{[Co(nipa)(bipy)]0.5DMF}$_n$ (4): In the HSM analysis, the crystals, covered by silicon oil, were heated from 25 to 450 °C, with a temperature ramp rate of 10°C min^{-1} (Fig 3.24). As may be inferred from Fig. 3.24, it seems that no solvent is lost during heating, although the DSC thermogram shows a wide and asymmetric endothermic peak centred at 210 °C and TGA thermogram indicates 8% mass loss between 100 and 250°C (Fig. 3.25). An endothermic peak centred at 305°C could be related to a phase transition, which however was not further investigated. The darkening of the crystals observed at temperatures higher than 350°C is ascribed to thermal decomposition.

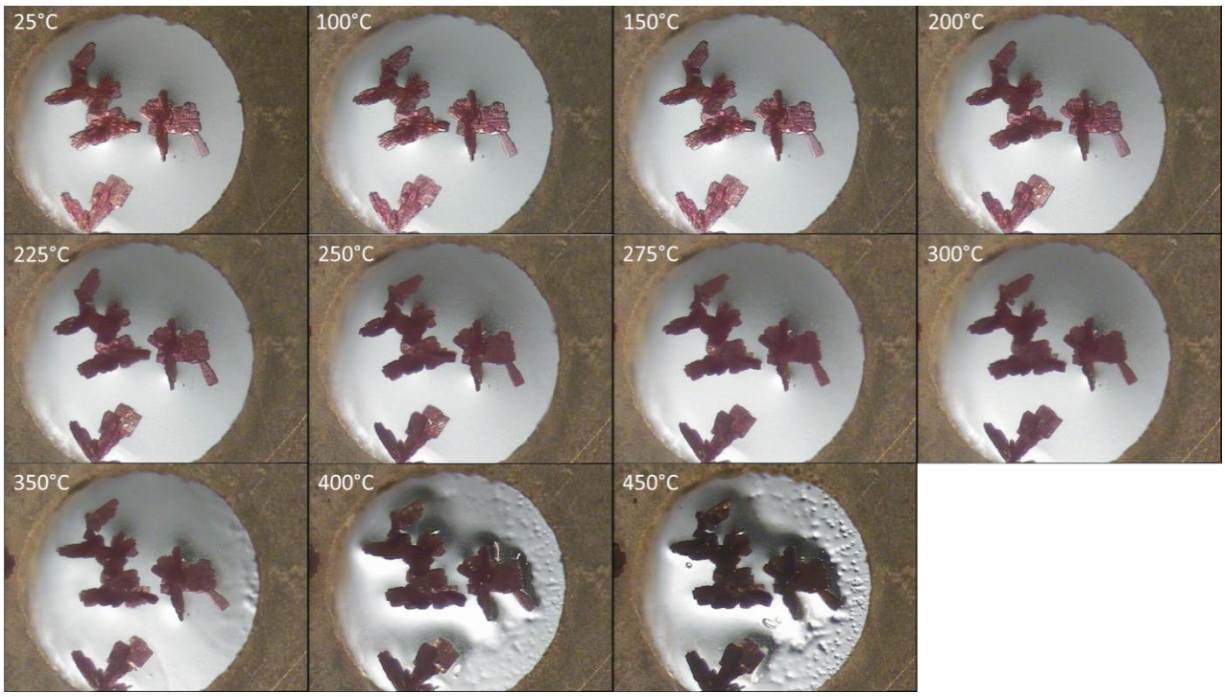

Figure 3.24 HSM images of **4**, the only visible events were the opacification of crystals and their decomposition.

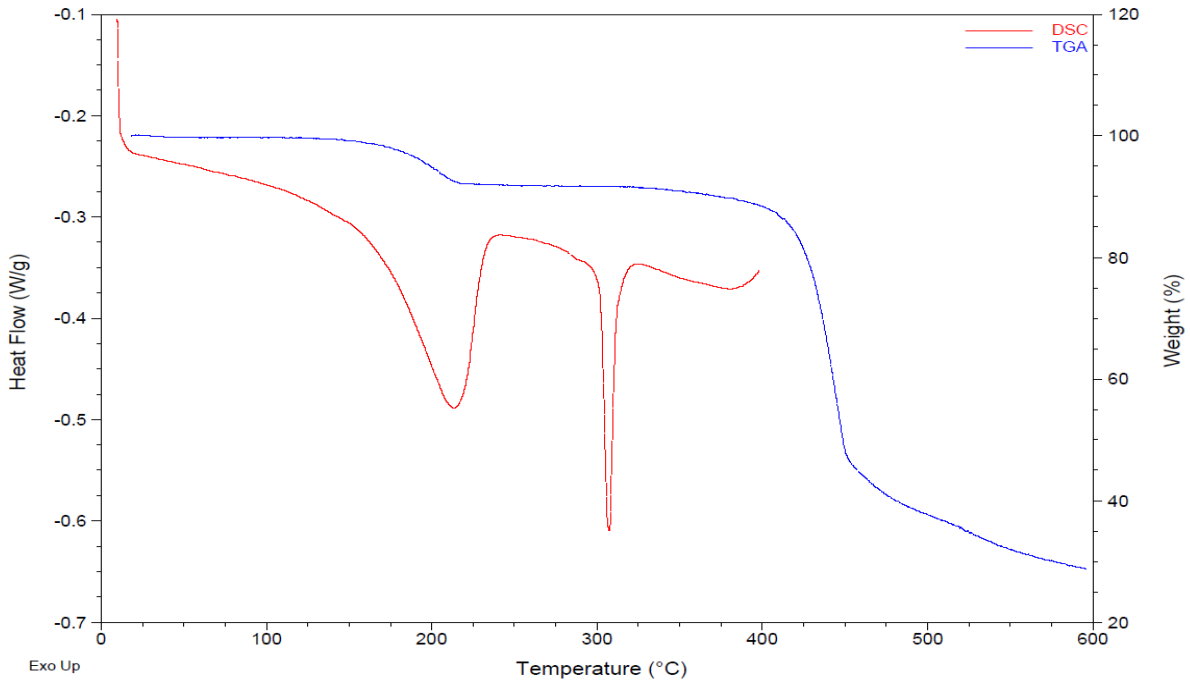

Figure 3.25 Overlay of DSC (red) and TGA (blue) thermogram of **4**.

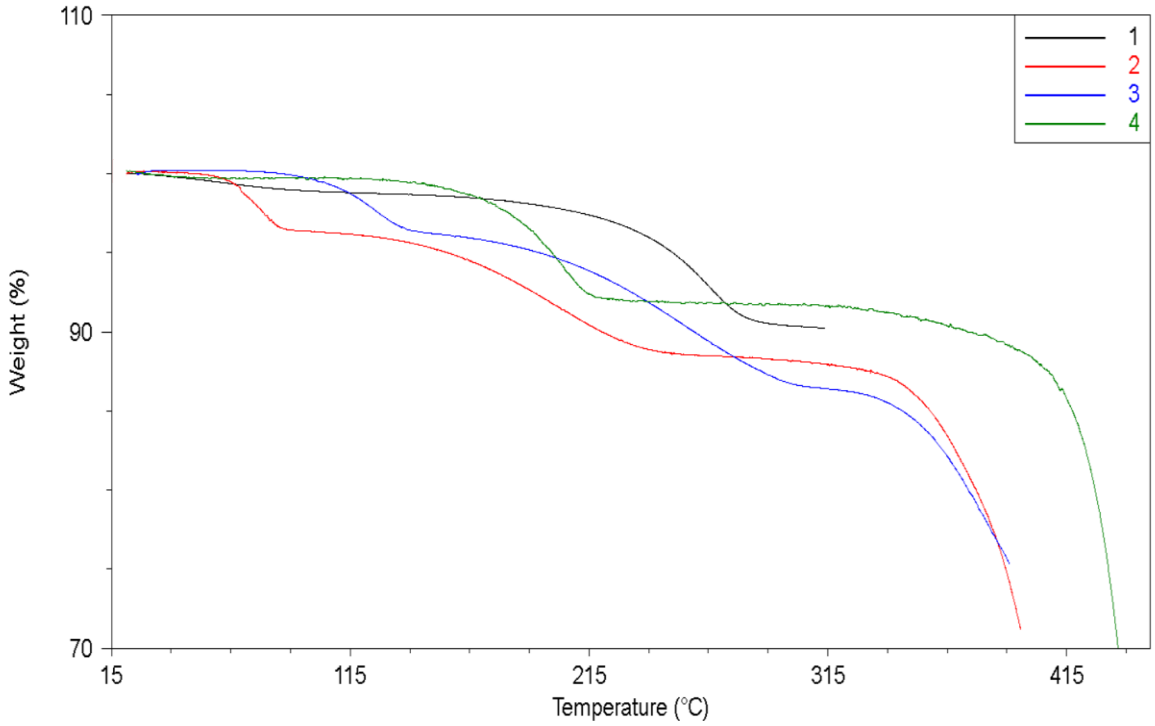

Figure 3.26 Overlay of TGA thermograms of **1**,**2**, **3** and **4** reported in black, red, blue and green.

An attempt to describe the thermal behaviour could be achieved by relating the overlay of TGA thermograms presented above (Fig. 3.26) to the intermolecular interactions and crystal packing described under headings **3.2** and **3.3**. The identified hydrogen bonds did not offer a straightforward correlation; however, it was found that the potential void space in each structure (generated by deleting the solvent coordinates where these were modelled) may offer an explanation to the observed desolvation trends. No conclusions can be made for **1** based on hydrogen bonds because solvent molecules were not modelled, however, a possible explanation for the higher temperature solvent loss (with regards to DMF) could be ascribed to the absence of channels between void spaces in the structure as shown in Figure 3.14. This could indicate that it is energetically more difficult for solvent molecules to evacuate as conformational changes in the MOF would have to occur in order to allow passage of the solvent molecules. Both **2** and **4** have modelled DMF molecules, the latter shows a higher temperature solvent loss even if intermolecular interactions involving DMF in either structure were not indicated. This could be related to void shapes (Figs. 3.15 and

3.17) in a similar way to **1**, as the channels in **4** seems more constricted when compared to those of **2**. The observed disorder for one of the pyridyl rings in **4** may indicate that desolvation is facilitated through rotation of this ring, making this MOF a candidate for future single-crystal-to-single-crystal desolvation studies. The thermal behaviour of **3** is analogous to **2** but solvent loss is shifted to a higher temperature. This could be due to DMA being involved in hydrogen bonding in **3** (Table 3.6), unlike DMF in **2** which is not involved in any hydrogen bonding (Table 3.4).

It is possible to calculate the percentage of mass loss associated with solvent considering the molecular weight of each ASU and the corresponding solvent. Each percentage was calculated with the following equation (ASU here is to be intended without solvent hosted in the cavities):

$$\frac{Mw_{Solvent}}{Mw_{ASU} + Mw_{Solvent\ A} + Mw_{Solvent\ B}} * 100 = XX\%$$

	ASU	ASU + Solvent(s)		H_2O (%)	DMF or DMA	Total
(1) + ½ DMF + 1 H_2O	420.25	474.81	Calculated	3.79	7.70	11.49
			Experimental	1.76	9.90	11.66
(2) + ½ DMF + 1 H_2O	419.26	473.82	Calculated	3.80	7.71	11.52
			Experimental	3.65	7.75	11.39
(3) + ½ DMA + 1 H_2O	419.26	471.83	Calculated	3.75	9.06	12.81
			Experimental	3.49	9.15	12.64
(4) + ½ DMF	424.23	460.78	Calculated	/	7.93	7.93
			Experimental	/	8.15	8.15

Table 3.10 Results obtained from the equation reported above for solvents that are probably hosted in the frameworks, compared to the percentage of mass loss achieved from TGA.

The results reported in Table 3.10 show a good match with the experimental TGA data. Each MOF exhibits a two-step mass loss with the first related to water loss and the latter to DMF/DMA loss, except for **4** that exhibits only one mass loss associated to DMF removal. The discrepancy in individual calculated and experimental mass losses for water and DMF in **1** is explained by its TGA (Fig. 3.19) showing that these two masses losses may be overlapped. The total calculated and experimental mass losses are in good agreement.

3.5 Powder X-Ray Diffraction

Crystals formed under solvothermal conditions were gently ground prior to being subjected to PXRD analysis. The room temperature PXRD patterns confirmed the purity of the bulk materials with these patterns having good agreement with those calculated from the respective single crystal structures (Fig. 3.27). Differences in relative peak heights in the experimental patterns can be ascribed to preferred orientation effects.

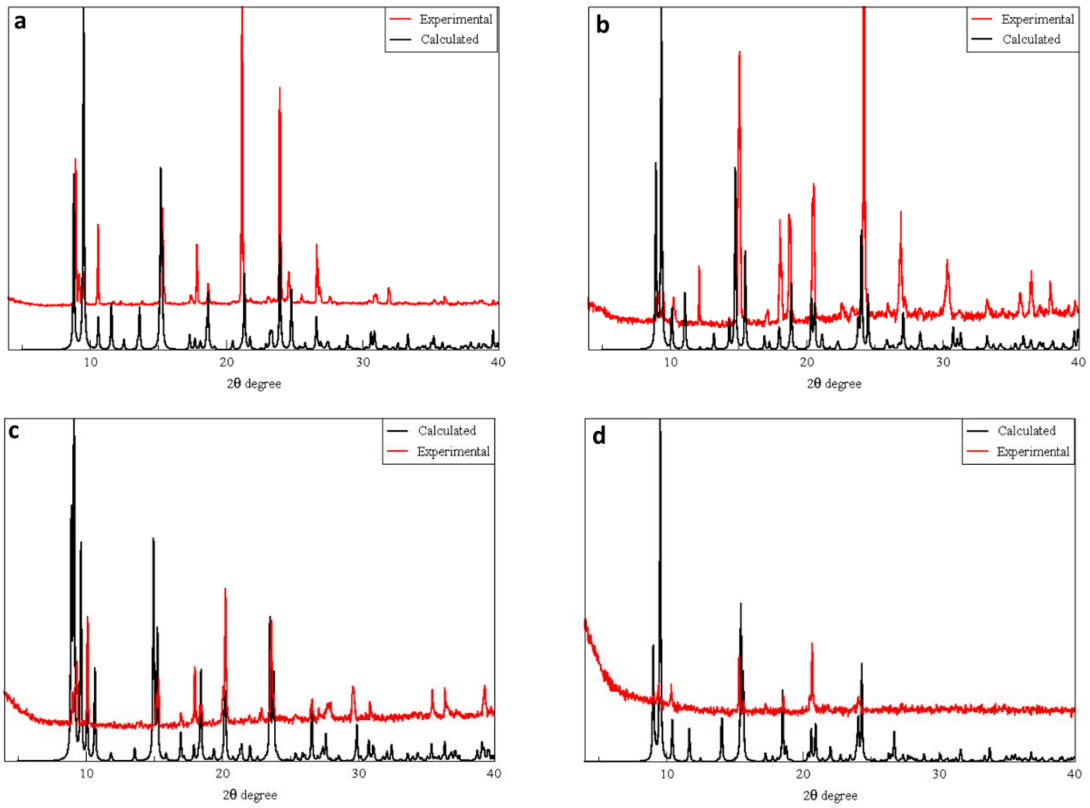

Figure 3.27 Overlay of experimental and calculated PXRD patterns for **1** (**a**), **2** (**b**), **3** (**c**) and **4** (**d**)

3.6 Mechanochemical synthesis: Liquid-assisted grinding (LAG experiment)

Liquid-assisted grinding (LAG) experiments were conducted to assess whether it was possible to synthesize **1** and **2** *via* this method, which could have the advantage of high yields and fast synthesis, as well as ease of preparation. $Mn(NO_3)_2 \cdot 4H_2O$, 4,4'-bipyridine and 5-nitro-1,3-benzenedicarboxylic acid (**mixture A**) or benzene-1,3,5-tricarboxylic acid (**mixture B**) was mixed together with a drop of water and ground manually with mortar and pestle. PXRD patterns were recorded every 15 minutes of grinding. In both cases, intense peaks, not related to starting materials, appeared just after 15 minutes of grinding. Longer reaction times did not modify the PXRD traces in the case of **mixture A**, while in the case of **mixture B** the maximum intensity of the peaks was reached after 30 minutes of grinding. As reported in Fig. 3.27, LAG experiment patterns do not match those of the calculated patterns and are neither a superposition of the reagent PXRD patterns. Therefore, it is possible that different MOFs were produced but these were not further investigated.

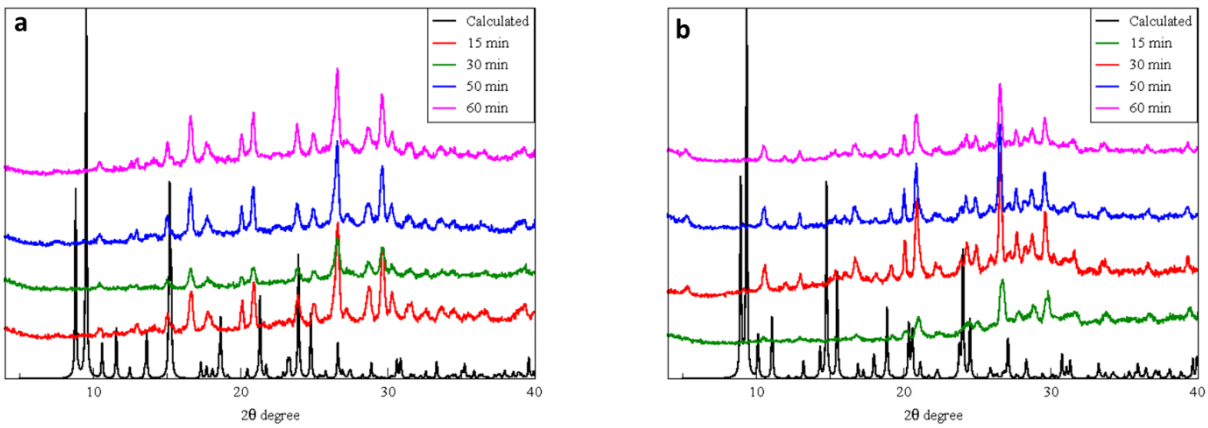

Figure 3.28 PXRD patterns recorded on **mixture A** (**a**) and **mixture B** (**b**) for different times of grinding and compared to the calculated PXRD pattern of **1** and **2** respectively

3.7 References

1 T. Fukushima, S. Horike, H. Kobayashi, M. Tsujimoto, S. Isoda, M. L. Foo, Y. Kubota, M. Takata and S. Kitagawa, Modular design of domain assembly in porous coordination polymer crystals via reactivity-directed crystallization process, *J. Am. Chem. Soc.*, 2012, **134**, 13341–13347.

2 C. Jinxi, O. Masaaki and K. Susumu, Two New Coordination Polymers Based on Hexanuclear Metal Cluster Cores, *Chem. Lett.*, 2006, **35**, 526–527.

3 C. R. Groom, I. J. Bruno, M. P. Lightfoot and S. C. Ward, The Cambridge structural database, *Acta Crystallogr. Sect. B Struct. Sci. Cryst. Eng. Mater.*, 2016, **72**, 171–179.

Chapter 4: Cadmium Coordination Polymer

A novel 2D CP was prepared using $CdBr_2$ and benzene-1,3,5-tricarboxylic acid (H_3BTC) as starting materials. The 2D CP has a molecular formula of $\{[Cd_{1.5}(btc)(H_2O)_{4.5}]\cdot H_2O\}_n$ (**5**) and has been characterized by X-Ray diffraction (SCXRD, PXRD, VTPXRD) and thermal analysis (HSM, DSC, TGA). Dehydration and rehydration studies have been successfully performed combining PXRD and TGA.

4.1 Synthesis

$CdBr_2$ (49 mg, 0.18 mmol), benzene-1,3,5-tricarboxylic acid (13 mg, 0.06 mmol) and 2,3-di(4-pyridyl)-2,3-butanediol (15 mg, 0.06 mmol) were dissolved in DMF (3 ml), H_2O (2 ml), ethanol (1 ml), the solution was stirred to aid dissolution and afterwards heated in an oven at 90 °C for 48 hours. The solution was cooled down at a rate of 10 °C h^{-1} after which flat, colourless crystals appeared. The 2,3-di(4-pyridyl)-2,3-butanediol is not present in the structure so samples without it were prepared, they still gave rise to the same crystal but physically mixed with by-products that make impossible to separate them.

4.2 Structure

5 crystallizes in the monoclinic crystal system in the space group *C*2/*c*. The asymmetric unit consists of one and a half cadmium(II) ions, one fully deprotonated, bridging benzene-1,3,5-tricarboxylate (BTC) anion, four and a half coordinated water molecules and one uncoordinated water molecule. Cd1 is located on a 2-fold axis with a trigonal bipyramidal coordination environment with coordination bonds that range from 2.250 to 2.738 Å. The two axial positions are occupied by the O1 atoms of two different BTC anions (related by the 2-fold axis), whilst three water molecules occupy the equatorial positions (O7 is located on the 2-fold axis, whilst two O8 atoms, related by the 2-fold axis, complete the coordination sphere). In addition, the O8 water molecule is disordered over two positions, labelled A and B, respectively, with site occupancy factors (sof) of 0.70 and 0.30, respectively. Cd2 has a pentagonal bipyramidal coordination environment; the axial positions being occupied by

oxygen atoms O9 (disordered over two positions with sofs of 0.70 (A) and 0.30 (B)) and O11 from two water molecules, whilst the equatorial positions are occupied by O10 of water molecule, two oxygen atoms (O3 and O4) from one carboxylate group and two oxygen atoms (O5 and O6) from a second carboxylate group. In addition, the O6 oxygen atom is disordered over two positions, labelled A and B, respectively, with sofs of 0.76 and 0.24, respectively. The uncoordinated water molecule (O12) is bonded *via* hydrogen bonds to a coordinated carboxylate oxygen atom (O3) and a coordinated water molecule oxygen atom (O11).

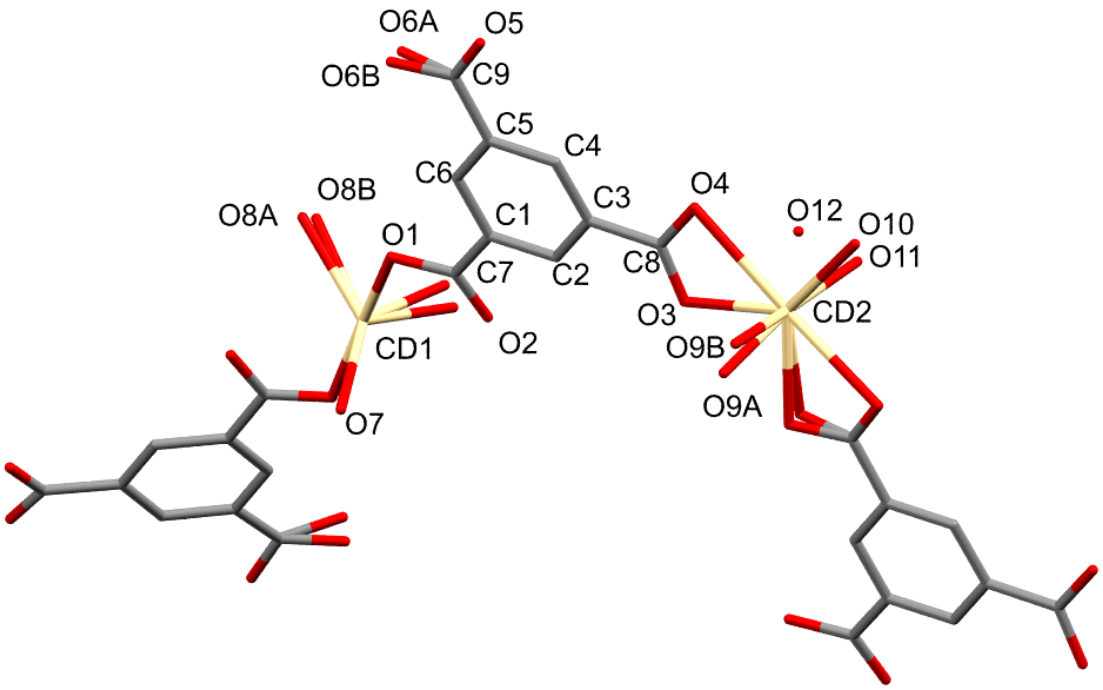

Figure 4.1 Coordination spheres of the unique cadmium ions in **5**. Hydrogen atoms omitted for clarity.

Asymmetric unit formula	$C_9H_{14}Cd_{1.5}O_{11.5}$
Formula weight	474.80
Temperature(K)	100
Crystal system	monoclinic
Space group	*C*2/*c*
***a* (Å)**	19.0101(16)
***b* (Å)**	7.3447(7)
***c* (Å)**	20.4158(17)
***α* (°)**	90
***β* (°)**	97.281(2)
***γ* (°)**	90
Volume (Å^3)	2827.5(4)
Z	8
Calculated density ρ_{calc} (g/cm^3)	2.231
μ (mm^{-1})	2.336
F(000)	1856.0
Crystal size (mm^3)	0.10 × 0.10 × 0.10
Radiation	MoKα (λ = 0.71073)
2Θ range for data collection (°)	4.022 to 61.348
Index ranges	$-27 \leq h \leq 27$, $-10 \leq k \leq 10$, $-29 \leq l \leq 29$
Reflections collected	34428
Independent reflections	4388 [R_{int} = 0.0367, R_{sigma} = 0.0206]
Data/restraints/parameters	4388/0/218
Goodness-of-fit on F^2	1.051
Final R indexes [I>=2σ (I)]	R_1 = 0.0224, wR_2 = 0.0536
Final R indexes [all data]	R_1 = 0.0244, wR_2 = 0.0549
Largest diff. peak/hole (e Å^{-3})	2.11/-1.68

Table 4.1 Crystal data and refinement parameters of **5.**

4.3 Crystal Packing

The coordination bonds of **5** effect a two-dimensional CP (Fig 4.2), which is constituted from two one-dimensional chains made by Cd2, with its pentagonal bipyramidal environment, and Cd1, the latter connecting the Cd2 'chains'. The two 'chains' have a relative orientation which differ by an angle of ~33.5° (Fig. 4.3). Each 2D framework is interdigitated with two neighbours on either side, as shown in Fig. 4.4. Voids in this structure could not be calculated by Mercury (based on a 1.2 Å probe radius) even when the coordinates of the uncoordinated water molecules were deleted, an indication of its tight fit in the structure.

.

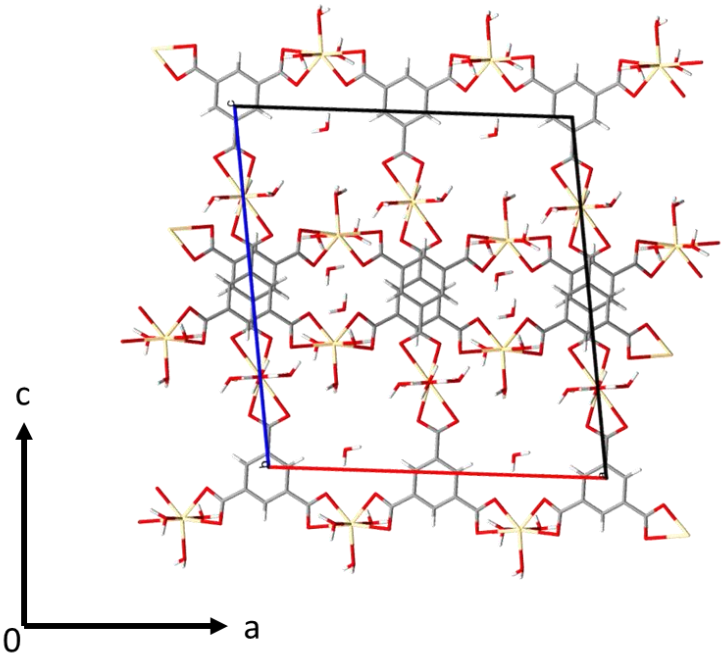

Figure 4.2 View of **5** along *b*-axis.

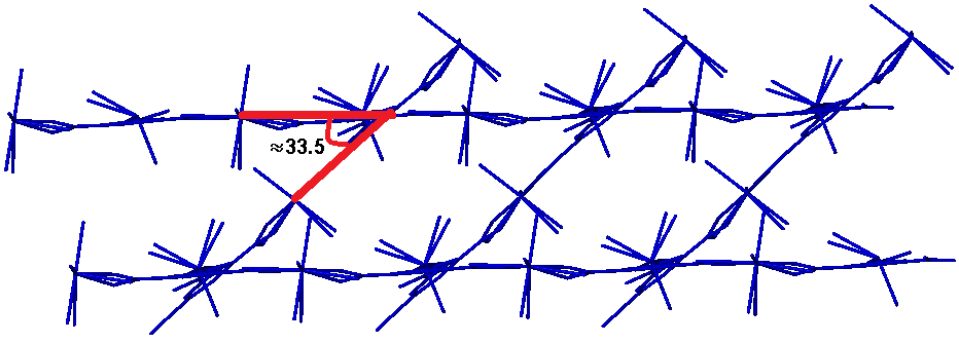

Figure 4.3 View along *c*-axis showing the 1D chains and the angle between them.

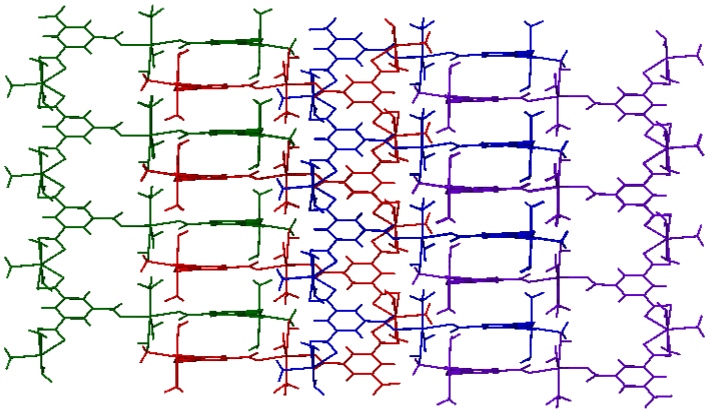

Figure 4.4 Crystal packing of **5** showing the interdigitated arrangement of neigbouring 2D CPs, highlighted in different colours.

4.4 Thermal analysis

4.4.1 Hot Stage Microscopy

A few drops of silicon oil were placed over selected crystals which were heated from 25 to 450 °C at a heating rate of 10 °C min^{-1}. The appearance of bubbles at 80 °C, even when it only becomes evident at 120°C, indicates the start of the loss of solvent with concomitant opacification of the crystals indicating that monocrystallinity was not retained; however, the VT-PXRD analysis indicated that a change to another crystalline phase had occurred.

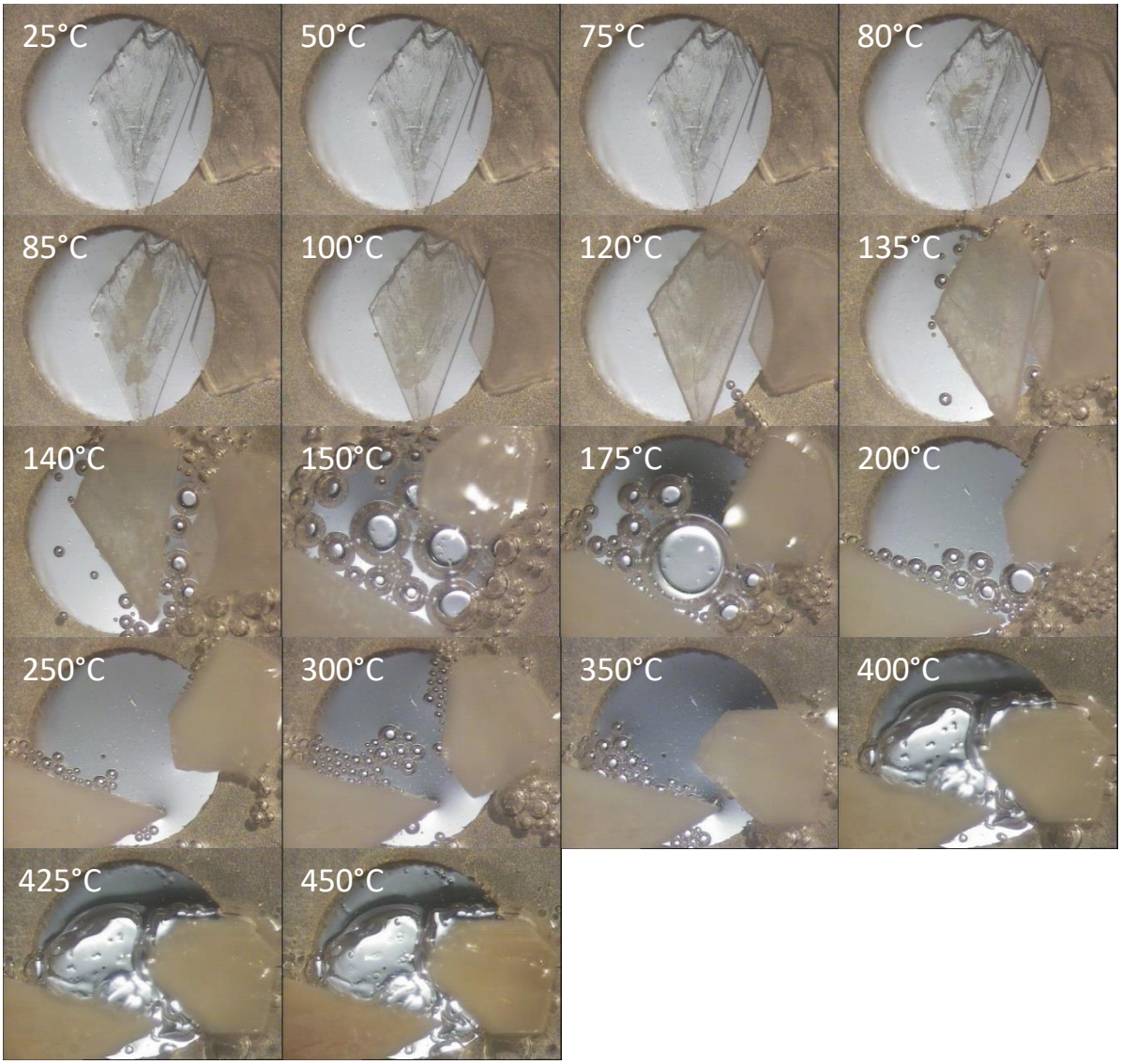

Figure 4.5 Pictures recorded during hot stage microscopy showing the loss of solvent upon heating.

4.4.2 Differential Scanning Calorimetry and Thermal Gravimetric Analysis

The DSC thermogram (Fig. 4.6) shows two overlapping endotherms between 50-100 °C, which probably corresponds to the concomitant release of uncoordinated and coordinated water molecules. Two other endothermic bands appear around 185 °C and 305 °C, which probably correspond to additional solvent loss as indicated by TGA (Fig 4.6). The TGA thermogram indicates that the mass loss starts at ~50 °C with a rapid mass loss occurring between 70 and 100°C, the amount of mass loss in this interval is 13.45%. There after the mass loss steadily decreases up 400 °C by another 7.63%, with a total of 21.16% before the drastic mass loss of ~70% that indicates decomposition of the coordination compound. The molecular weight of the ASU is 474.80 amu while for water molecule is 18.02 amu so compared to the ASU it is 3.80%. Table 4.2 presents the amount of water loss for each section of the thermogram.

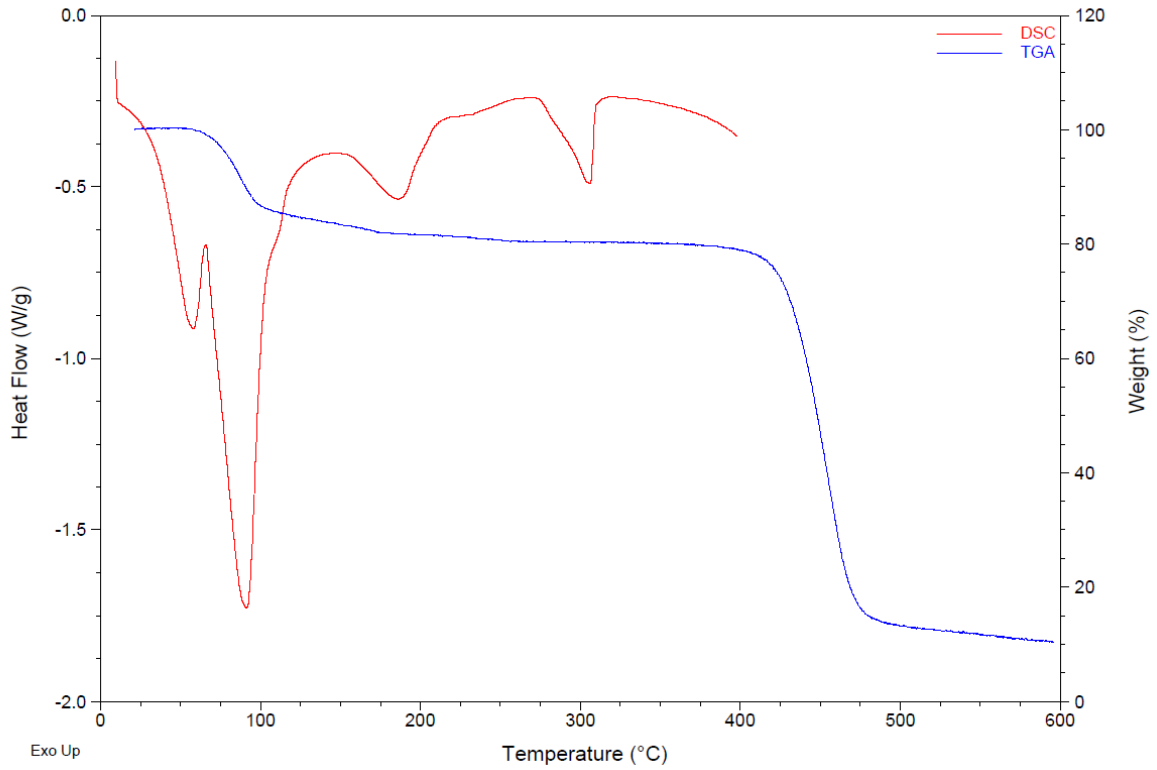

Figure 4.6 Overlay of DSC (red) and TGA (blue) thermograms of **5**. The DSC thermogram was recorded from 20 to 400°C with the heating rate of 10 °C min^{-1} while the TGA was recorded from 20 to 600 °C with the heating rate of 10 °C min^{-1}.

	Thermogram section		
	50-100°C	100-400°C	Total
Exp. Mass loss (%)	13.43	7.63	21.06
H_2O molecule(s)	3.54	2.00	5.54
Calc. Mass loss (%)	-	-	20.87
H_2O molecules modelled	-	-	5.5

Table 4.2 TGA data obtained for **5**, first line reports the experimental percentage of mass loss while the second line the hypothetical water molecules associated calculated with the formula reported in the previous chapter.

4.5 Powder X-Ray Diffraction

Crystals made *via* the solvothermal method were gently ground with a mortar and pestle in preparation for PXRD and VTPXRD analysis (Fig 4.7 and 4.8). The room temperature PXRD pattern confirms the purity of the bulk material. The variable-temperature PXRD shows that the material undergoes a phase change (crystallinity is retained) as it is heated over the temperature range of solvent loss. For example, at 50°C, a prominent peak appears at 10.5° 2θ and remains up to 300 °C and also when the sample is cooled back to 30 °C.

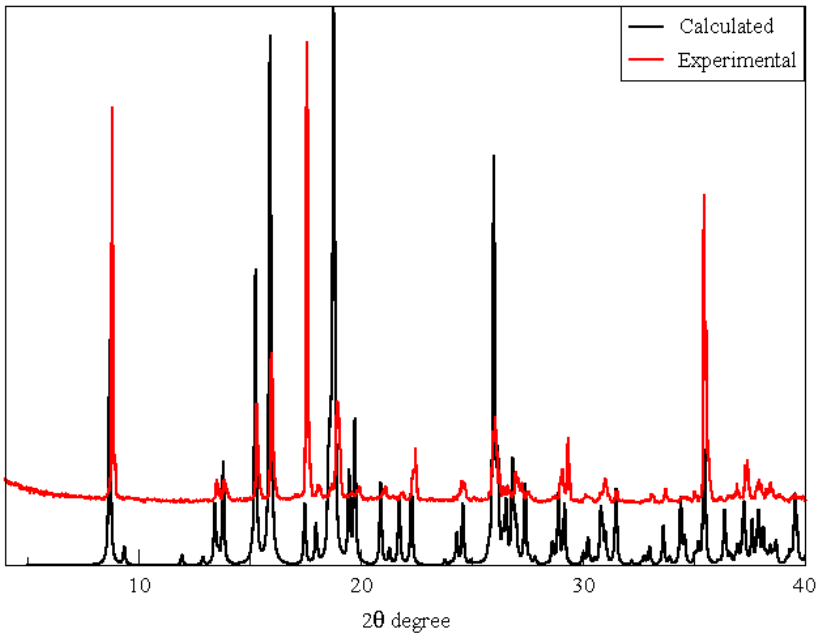

Figure 4.7 Overlay of experimental PXRD pattern of **5** with the calculated pattern.

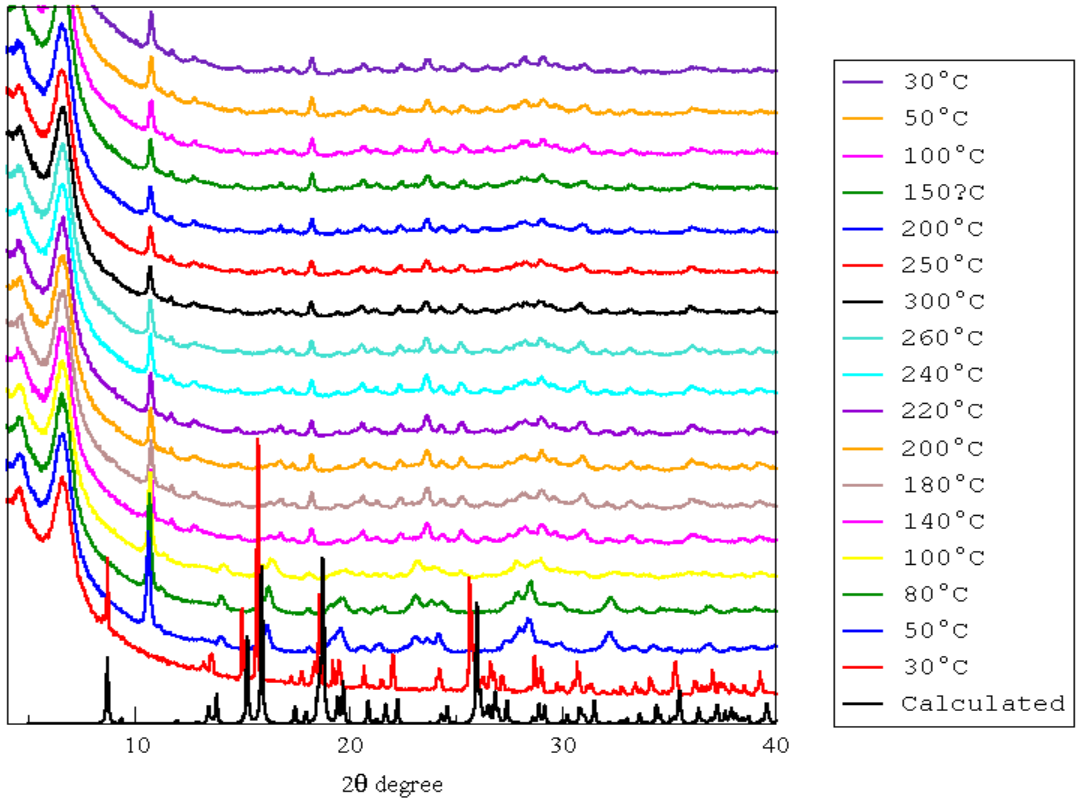

Figure 4.8 VT-PXRD of **5** from 30°C to 300°C and cooling to 30°C.

4.6 Dehydration and Rehydration Studies

These studies were performed to test whether the dehydrated sample (involving the loss of coordinated water molecules) can re-adsorb water from the atmosphere since the metal sites would be unsaturated. A PXRD pattern was recorded on freshly ground sample, before heating, in order to verify the structure of the material. Subsequently, the sample was heated on the TGA equipment to 200 °C (black curve in Fig. 4.9a), followed by immediate reheating to verify that no further mass loss occurred (red curve Fig. 4.9a). The same sample was then exposed to a water vapour atmosphere (a small sample vial was placed inside a bigger, capped vial with water). After two days, the TGA analysis confirmed that nearly all water molecules lost initially were regained through this experiment (green curve in Fig. 4.9a). At each corresponding step a PXRD pattern was recorded confirming: firstly, that after heating

the structure of the material changed (according to the VT-PXRD patterns in Fig. 4.8) and, secondly, that the original structure of the hydrated framework was regained (Fig 4.9**b**).

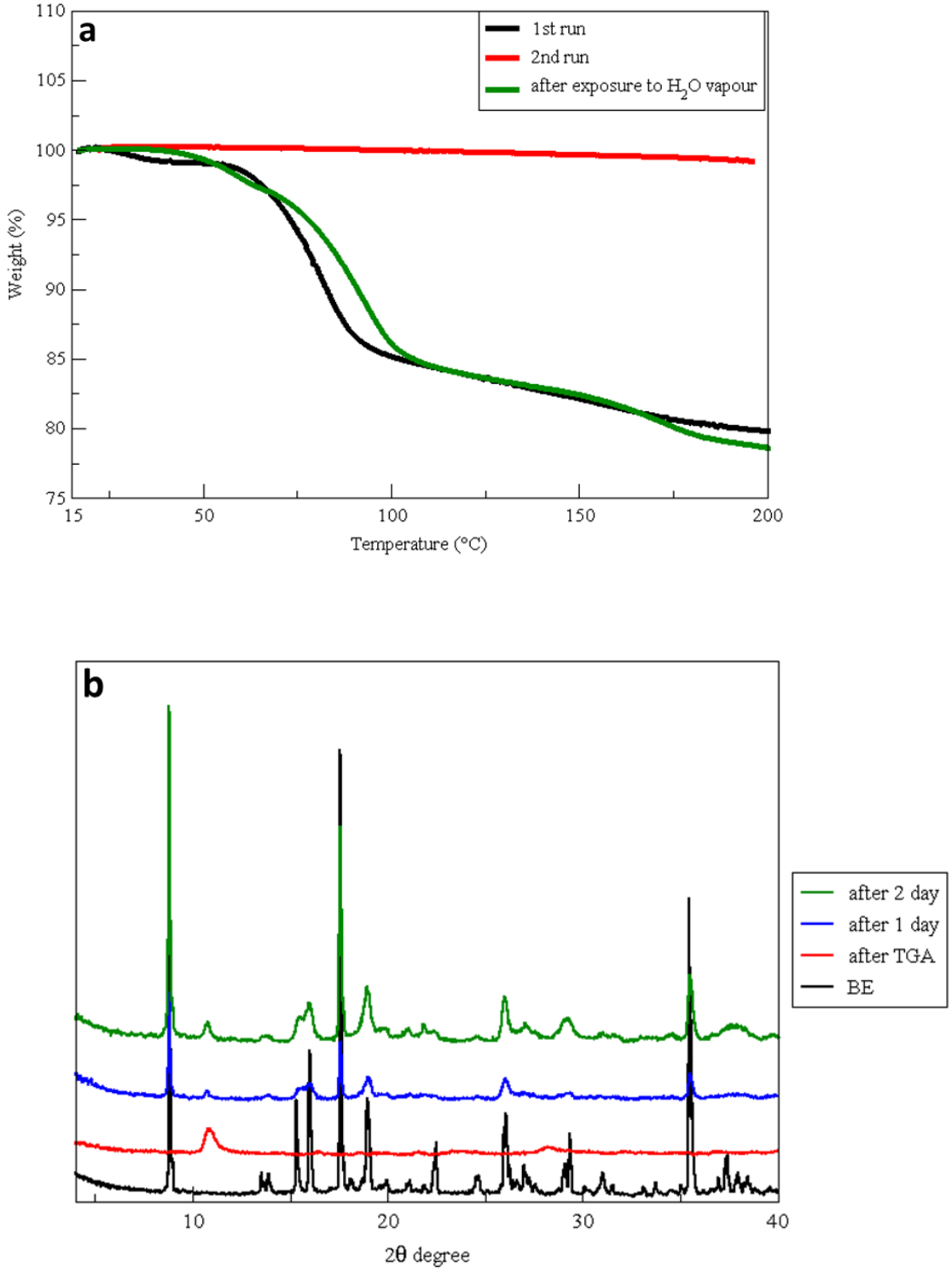

Figure 4.9 TGA (**a**) and associated PXRD patterns (**b**) of dehydration and rehydration studies of **5.**

4.7 Mechanochemistry Experiment

A liquid-assisted grinding (LAG) experiment was conducted to assess whether it was possible to synthesize **5** *via* this method, which could have the advantage of high yields and fast synthesis, as well as ease of preparation. $CdBr_2$ and benzene-1,3,5-tricarboxylic acid were mixed together with a drop of water and ground manually with mortar and pestle. PXRD patterns were recorded for different times of grinding and the resulting powder was exposed to water vapour as shown in paragraph 3.5. Fig. 4.10 indicates that crystallinity increased with the time of grinding, however, peaks height only significantly increased when the longest-ground material was exposed to water vapour (light green in Fig. 4.10). This pattern shows significant differences to that obtained by the solvothermal method, indicating that it is a different crystalline phase. The LAG experiment PXRD pattern is not in good agreement with either the one obtained from solvothermal synthesis or the calculated pattern, however, a good match was found with the PXRD pattern of trimesic acid (Fig. 4.11).

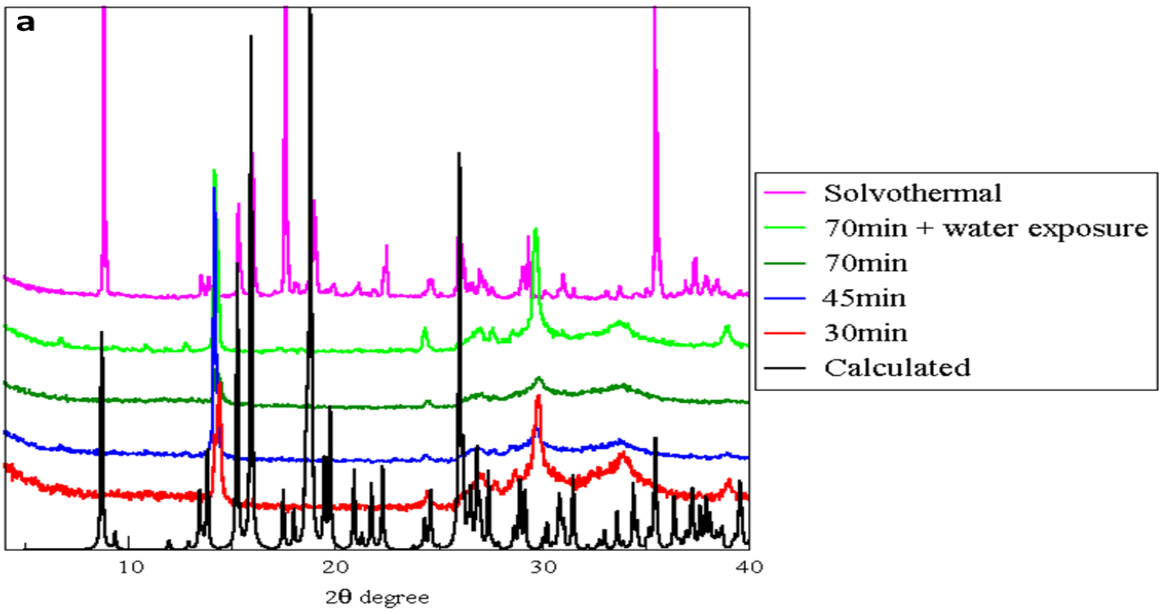

Figure 4.10 PXRD patterns recorded on a mixture of $CdBr_2$, trimesic acid and H_2O for different times of grinding (red, blue and dark green). After 70 minutes of grinding the powder was exposed to water vapour for two days (light green). Calculated pattern (black) and diffractogram of crystals prepared under solvothermal conditions (purple) are added in order to facilitate comparison.

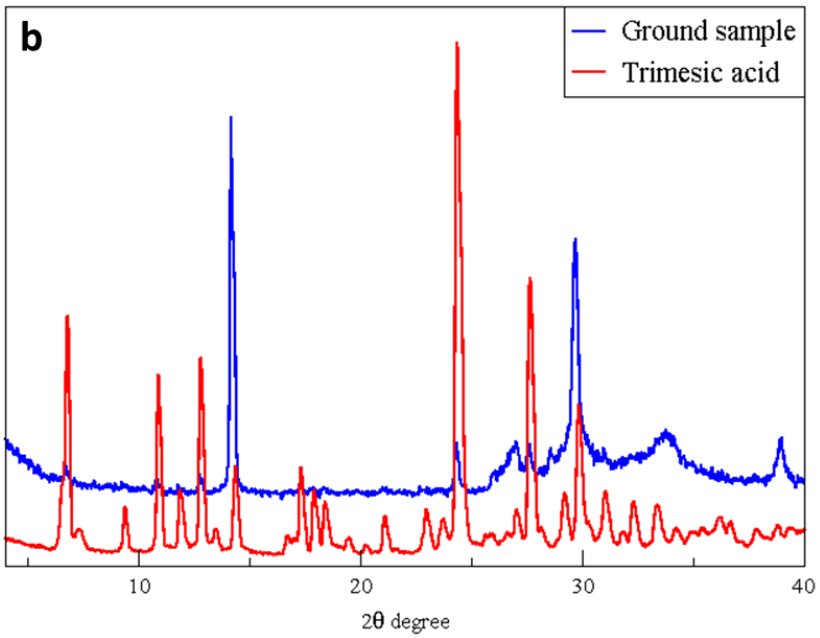

Figure 4.11 Overlay of PXRD diffractogram of the ground sample (blue) and trimesic acid (red). The blue pattern corresponds to the light green of Figure 4.10. The most intense peaks of the ground mixture overlay with the most prominent peaks of the trimesic acid.

4.8 *In situ* rehydration study

In addition, a rehydration study was also performed *in situ* on the PXRD equipment using a modified stage which consisted of water wells next to the sample.[1] The sample was heated to 300 °C (mainted for 30 minutes) and cooled back to room temperature (~25 °C) before commencement of the *in situ* experiment. Diffractograms were recorded over a period of 14 hours but after 3 hours and 15 minutes no further changes in the patterns were observed. Each diffractogram was recorderd over ~15 minutes in the scan range of 4-40° 2θ (Fig.4.12). The different amount of time necessary for the complete rehydration of **5** with respect to the experiment reported previously is probably due to the different conditions of exposure to water vapour that occurs during these two different experiments. In both experiments it seems that the compound reverts to its previous structure upon rehydration (Fig 4.13).

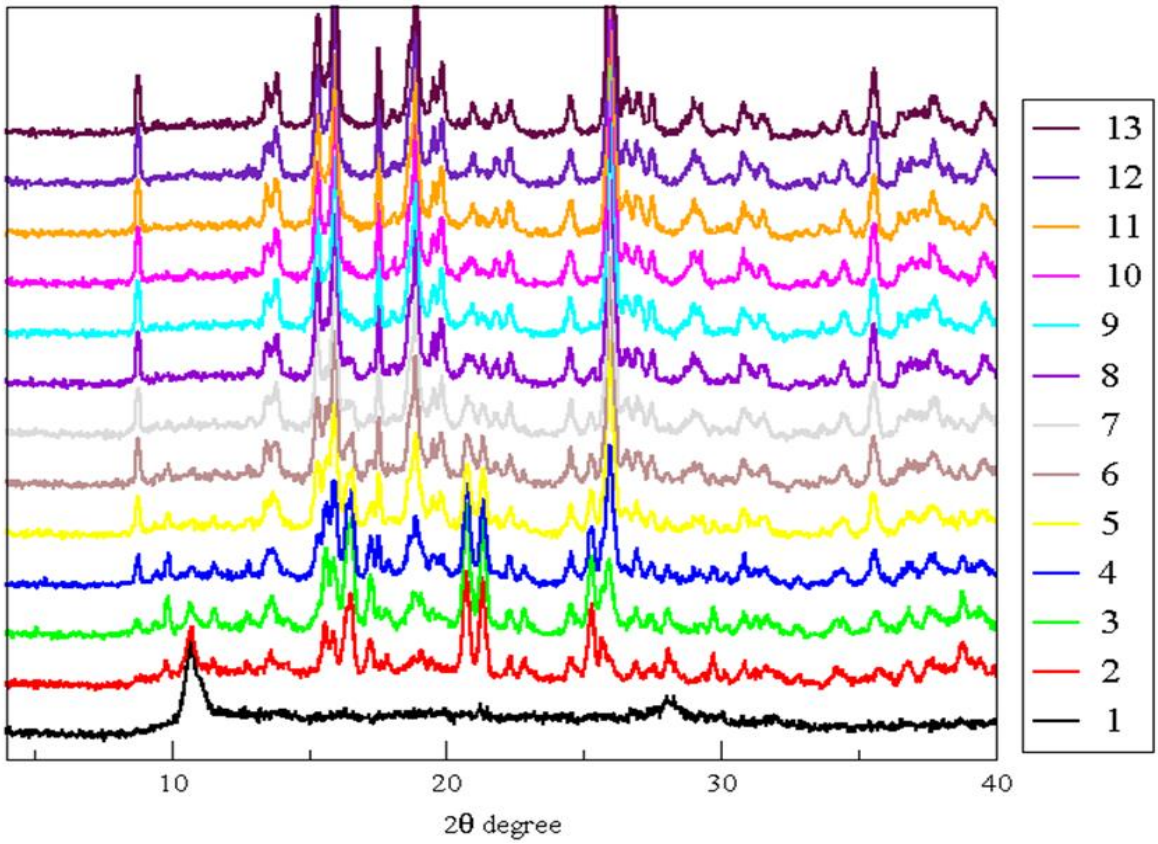

Figure 4.12 Evolution of PXRD diffractograms of dehydrated **5** during water vapour exposure. Each step corresponds to 15 minutes. No patterns recorded after 3h and 15 minutes are shown as these were not different with respect to pattern 13.

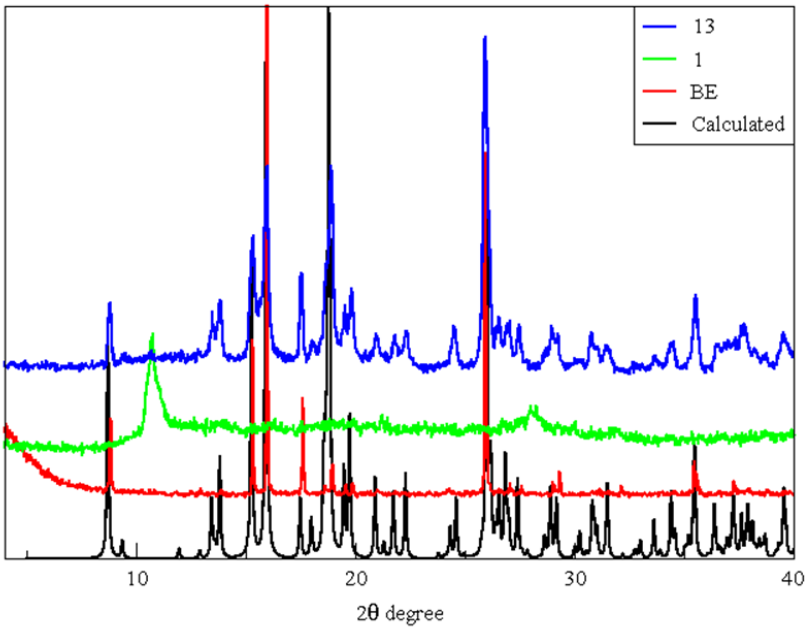

Figure 4.13 Comparison between different patterns of **5**, from bottom: calculated (black), PXRD recorded before in situ rehydration study (red) and the first (light green) and the last (blue) significant diffractograms recorded during the *in situ* experiment. BE = before experiment.

4.9 Reference

1 N. M. Sykes, H. Su, E. Weber, S. A. Bourne and L. R. Nassimbeni, Crystallisation temperature control of stoichiometry and selectivity in host–guest compounds, *CrystEngComm*, 2017, **19**, 5892–5896.

Chapter 5: Conclusion

This chapter provides a summary of the results obtained for this research project. Many crystals were synthesized but only five of them were chosen for investigating in detail, employing X-ray diffraction and thermoanalytical techniques. Four were previously unknown, namely a 2D cadmium-based CP and three mixed-ligand 2D MOFs. Two of the mixed-ligand MOFs were based on manganese and the third on cobalt.

5.1 Summary

The table below presents all the crystals obtained during this project with their corresponding starting materials and preparation conditions.

Carboxylic acid	**Bipyridyl**	**Metal Salts**	**Solvent(s)**	**Conditions**	**Comment**
2,5-pyridinedicarboxylic acid	1,2-bis(4-pyridyl)ethane	$Co(NO_3)\cdot 6H_2O$	DMF/H_2O	Solvothermal, 90 °C, 48 h	Known [1]
2,5-pyridinedicarboxylic acid	1,2-bis(4-pyridyl)ethane	$Co(NO_3)\cdot 6H_2O$	DMF/H_2O	Solvothermal, 90 °C, 48 h	Known [2]
2,6-pyridinedicarboxylic acid	1,2-bis(4-pyridyl)ethane	$Co(NO_3)\cdot 6H_2O$	H_2O/MeOH	Slow Diffusion	Known [3]
2,6-pyridinedicarboxylic acid	1,2-bis(4-pyridyl)ethane	$Cu(NO_3)\cdot 3H_2O$	DMF/H_2O	Solvothermal, 90 °C, 48 h	Previously discovered in Dr. Oliver's research group
1,3,5-benzenetricarboxylic acid	2,3-di(4-pyridyl)-2,3-butanediol	$Co(NO_3)\cdot 6H_2O$	DMF/H_2O	Solvothermal, 90 °C, 72 h	Known [4]
1,3,5-benzenetricarboxylic acid	2,3-di(4-pyridyl)-2,3-butanediol	$CdBr_2$	DMF/H_2O-EtOH	Solvothermal, 90 °C, 48 h	**5**
1,3,5-benzenetricarboxylic acid	2,3-di(4-pyridyl)-2,3-butanediol	$Mn(NO_3)\cdot 4H_2O$	DMF/H_2O-EtOH	Solvothermal, 90 °C, 48 h	Known [5]
1,3,5-benzenetricarboxylic acid	2,3-di(4-pyridyl)-2,3-butanediol	$Mn(NO_3)\cdot 4H_2O$	H_2O/EtOH	Solvothermal, 90 °C, 48 h	Known [6]
1,3,5-benzenetricarboxylic acid	2,3-di(4-pyridyl)-2,3-butanediol	$Pb(NO_3)$	DMF/H_2O-EtOH	Solvothermal, 90 °C 72 h	No single crystal
1,3,5-benzenetricarboxylic acid	4,4'-bipyridine	$Co(NO_3)\cdot 6H_2O$	DMF/H_2O-EtOH	Solvothermal, 90 °C 72 h	Previously discovered in Dr. Oliver's research group
1,3,5-benzenetricarboxylic acid	4,4'-bipyridine	$Mn(NO_3)\cdot 4H_2O$	DMF/H_2O	Solvothermal, 90 °C, 48 h	**2**
1,3,5-benzenetricarboxylic acid	4,4'-bipyridine	$Mn(NO_3)\cdot 4H_2O$	DMA/H_2O	Solvothermal, 90 °C, 48h	**3**

5-nitroisophthalic acid	4,4'-bipyridine	$Mn(NO_3)\cdot 4H_2O$	DMF/H_2O	Solvothermal, 90 °C, 72h	**1**
5-nitroisophthalic acid	4,4'-bipyridine	$Mn(NO_3)\cdot 4H_2O$	DMA/H_2O	Solvothermal, 90 °C, 48h	**3**
5-nitroisophthalic acid	4,4'-bipyridine	$Co(NO_3)\cdot 6H_2O$	DMF/H_2O-EtOH	Solvothermal, 90 °C, 72h	**X, same cell of 4 but different solvent. Not investigated**

Table 5.1 Crystals resulting from various starting materials and synthetic methods. Compounds treated in this dissertation are indicated with the associated numbers used in previous chapters.

5.1.1 Manganese and Cobalt Mixed-Ligand Metal-Organic Frameworks (1-4)

Different 2D mixed-ligand MOFs deriving from the combination of carboxylic and pyridine base ligands were synthesized under solvothermal conditions and fully characterised by X-ray diffraction and thermal analysis. Three, based on manganese, were prepared using $Mn(NO_3)_2\cdot 4H_2O$, H_2nipa or H_3btc and bipy. The first MOF (**1**) is largely isoskeletal to a previously reported MOF in the literature (CSD code: EDAZEQ),[7] however differs in solvent content and is thus a different compound. The second MOF (**2**) has been previously discovered in the research group of Dr Clive Oliver (unpublished results) but was characterized in much further detail in this dissertation. The third Mn-based MOF (**3**) synthesized is novel, albeit with the same metal-ligand connectivity as **2** and contains a different solvent molecule. The fourth mixed-ligand MOF (**4**) was prepared using $Co(NO_3)_2\cdot 6H_2O$, H_2nipa and bipy and is novel. All four MOFs were characterized by SCXRD, PXRD, HSM, TGA and DSC. **1**, **2** and **4** crystallize in the triclinic crystal system in the space group *P*-1, while **3** crystallizes in the monoclinic crystal system in the space group *C*2/*c.* Crystal packings in all the structures are very similar, with the carboxylate ligands giving rise to 1D arrays pillared by the bipyridine ligands. However, **3** shows a difference with respect to **1** and **2:** its carboxylic extremities not involved in coordination bonding are not all oriented in the same way but alternate up and down (depending on the point of view) along their direction of ligation. Mercury was used to show that all the structures contain potential cavities. These were isolated in **1**, connected by channels in **2**, **3** and **4**. The geometrical

features of these void spaces provided a possible explanation for the observed relative order of desolvation temperatures for the different structures. The presence of these potential void spaces in the frameworks also makes all these compounds candidates for gas sorption experiments especially for CO_2 due to the possible interactions with the uncoordinated carboxylic and nitro moieties. Starting materials of **1** and **2** were also subject to LAG experiments but the comparison of their PXRD patterns with their corresponding calculated diffractograms showed poor agreement.

5.1.2 Cadmium Coordination Polymer (5)

A novel 2D CP was synthesized under solvothermal conditions starting from $CdBr_2$, 1,3,5-benzenetricarboxylic acid and 2,3-di(4-pyridyl)-2,3-butanediol. The bipyridine, even if not present in the final structure, is necessary to obtain higher yield and avoiding the precipitation of by-products. The compound was characterized using SCXRD, PXRD, VT-PXRD, HSM, TGA and DSC. Dehydration and rehydration studies were successfully performed combining PXRD and TGA analysis. In addition, an *in situ* rehydration study was conducted on PXRD equipment. **5** crystallizes in the monoclinic crystal system in the space group *C2/c*. From VTPXRD and HSM analysis it seems that **5**, when subject to heating, undergoes to a phase change and loses its monocrystallinity. It was not possible to determine the new structure of the compound. The reversibility of this process was highlighted during dehydration/rehydration studies, if exposed to water vapours **5** is able to absorb it, coming back to its initial structure. The structure does not exhibit voids and only one uncoordinated water molecule is hosted in the framework. The loss of around 18% of mass shown by TGA thermogram must be related to the loss of coordinated water molecules that can be readily “re-captured” by the compound. This characteristic makes **5** a promising candidate for water sorption. In addition, an attempt to produce **5** by LAG was performed but from the PXRD diffractogram recorded on the ground sample is clear that LAG does not allow reproduction of the structure.

5.2 Future work

All the compounds presented in this dissertation are candidates for gas sorption studies. The initial focus should be on water vapour sorption of **5** and CO_2 for **1**-**4**. In addition, a LAG experiment could be conducted on **3** and **4** to assess the possibility of producing these compounds by this synthetic technique. Lastly, the observed disorder for one of the pyridyl rings in **4** may indicate that this MOF is a candidate for future single-crystal-to-single-crystal desolvation studies, which may elucidate the mechanism of desolvation.

5.3 References

1 L. F. Song, C. H. Jiang, C. L. Jiao, J. Zhang, L. X. Sun, F. Xu, W. S. You, Z. G. Wang and J. J. Zhao, Two new metal-organic frameworks with mixed ligands of carboxylate and bipyridine: Synthesis, crystal structure, and sensing for methanol, *Cryst. Growth Des.*, 2010, **10**, 5020–5023.

2 G. Tian, G. Zhu, X. Yang, Q. Fang, M. Xue, J. Sun, Y. Wei and S. Qiu, A chiral layered Co(II) coordination polymer with helical chains from achiral materials., *Chem. Commun.*, 2005, **149**, 1396.

3 L. Nathan and T. Mai, Influence of the spectator cation on the structure of anionic pyridine-2,6-dicarboxylato complexes of cobalt(II), nickel(II), and copper(II), *J. Chem. Crystallogr.*, 2000, **30**, 509–518.

4 N. Guillou, C. Livage, J. Marrot and G. Férey, Tetraaquabis(3,5-dicarboxybenzo-ato-O)cobalt(II), *Acta Crystallogr. Sect. C Cryst. Struct. Commun.*, 2000, **56**, 1427–1428.

5 S. S. Y. Chui, S. M. F. Lo, J. P. H. Charmant, a G. Orpen and I. D. Williams, A Chemically Functionalizable Nanoporous Material $[Cu_3(TMA)_2(H_2O)_3]_n$, *Science (80-.).*, 1999, **283**, 1148–1150.

6 C. Jinxi, O. Masaaki and K. Susumu, Two New Coordination Polymers Based on Hexanuclear Metal Cluster Cores, *Chem. Lett.*, 2006, **35**, 526–527.